Universität Rostock

Traditio et Innovatio

Phosphorus-centered radicals and biradicals

Cumulative Dissertation

to acquire the academic degree

Doctor rerum naturalium (Dr. rer. nat.)

of the Faculty of Mathematics and Natural Sciences

at the University of Rostock

submitted by Jan Christoph Lukas Rosenboom, born on 06.06.1997 in Buxtehude

Rostock, 15.08.2024

https://doi.org/10.18453/rosdok_id00005096

The present work was accomplished at the Department of Chemistry at the University of Rostock, at the chair of Inorganic Chemistry in the group of Prof. Dr. Axel Schulz during the period from October 2020 until August 2024.

1. Reviewer: Prof. Dr. Axel Schulz (Universität Rostock)
2. Reviewer: Prof. Dr. Jan Weigand (TU Dresden)
3. Reviewer: Prof. Dr. Christian Müller (FU Berlin)

Date of thesis defence: 03.12.2024

Statement of Authorship

I hereby affirm that I have written this thesis independently and without outside assistance. Except as indicated, no other resources were used. All references as well as verbatim extracts were quoted, and all sources of information were specifically acknowledged.

Ich versichere hiermit an Eides statt, dass ich die vorliegende Arbeit selbstständig angefertigt und ohne fremde Hilfe verfasst habe. Dazu habe ich keine, außer den von mir angegebenen Hilfsmitteln und Quellen verwendet und die den benutzten Werken inhaltlich und wörtlich entnommenen Stellen habe ich als solche kenntlich gemacht.

Rostock, 15.08.2024

Jan Rosenboom

Danksagungen (Acknowledgements)

Die in dieser Arbeit vorgestellten Ergebnisse wären ohne die Unterstützung durch zahlreiche Personen über die gesamte Zeit des Studiums und der Promotion nicht möglich gewesen.

Daher möchte ich zunächst meinen Eltern Sabine und Werner danken! Vielen Dank für das Ermöglichen meines Studiums und meiner Promotion und das viele Vertrauen und die Unterstützung, die man eigentlich nicht in Worte fassen kann.

Mein spezieller Dank gilt Axel Schulz für sein Vertrauen in meine Arbeit an diesem anspruchsvollen, aufregenden Thema, das sich in eine Richtung entwickelt hat, die wohl keiner von uns am Anfang voraussehen konnte. Ich möchte mich für den unkomplizierten Austausch, die zahlreichen Denkanstöße und die Möglichkeit bedanken, gerade auch verrückte und erst einmal wenig erfolgversprechende Ansätze und Ideen verfolgen zu dürfen.

In gleichem Maße möchte ich Jonas Bresien danken. Ich habe viel von dir gelernt, sowohl wissenschaftlich, als auch menschlich. Ohne deine hervorragende Betreuung, die Einführung in das wissenschaftliche Arbeiten die zahlreichen, aufschlussreichen Gespräche und deine Expertise bei den quantenmechanischen Rechnungen wäre diese Arbeit so niemals möglich gewesen. In Zusammenhang mit Letzterem gilt mein Dank außerdem dem HPC-Team des ITMZ für die Bereitstellung und Wartung der Hochleistungsrechner.

Leon Teichmeier möchte ich für seine engagierte Arbeit in seinen Abschlussarbeiten, das Durchhaltevermögen und die tolle Zeit im Labor danken. Auf viele weitere Disbiradikale und Kristalle dann in deiner Promotion!

Dem gesamten Arbeitskreis und der anorganischen Abteilung gilt mein Dank für die angenehme und entspannte Arbeitsatmosphäre und den regen Austausch. Insbesondere möchte ich mich bei Edgar und Liesa für die Hilfe bei vielen Fragestellungen im Labor und um den Arbeitskreis bedanken.

Mein Dank gilt ebenso allen „Ehemaligen“, dabei zunächst Tim für die Betreuung meiner Masterarbeit und die Einführung in die Laborarbeit und auch Henrik, Lilli, Julia, Basti für ihre Ratschläge und Hinweise, sowie die stets gute Zusammenarbeit. Auch meinen aktuellen Kollegen, Jonas S., Yannic, Karsten, Leon, Pascal, Cornelius und Lea möchte ich für die

harmonische und produktive Zusammenarbeit in den verschiedenen Laboren danken. Es hat immer viel Spaß gemacht mit euch zusammenzuarbeiten!

In Bezug auf die komplexe Analytik in dieser Arbeit gilt meine große Dankbarkeit zunächst Florian Taube. Danke für die vielen spannenden EPR-Messungen und Simulationen, danke für die vielen fruchtbaren Diskussionen, danke dass ich immer vorbeikommen und dich mit meinen „komischen“ Molekülen von der Arbeit abhalten durfte! Ebenso gilt mein Dank in diesem Zusammenhang Björn Corzilius für seine hervorragende Expertise im Bereich der EPR-Spektroskopie ohne den dieses Projekt sicherlich ebenfalls nicht möglich gewesen wäre.

Heike Borgwaldt und Dirk Michalik möchte ich für die Durchführung und Berücksichtigung zahlreicher Sondermessungen und –Wünsche in der NMR-Spektroskopie danken sowie für die sehr angenehme Zusammenarbeit.

Isabel Schicht und Alexander Villinger danke ich für die Messung und das Lösen der Kristallstrukturen, gerade bei den schwierigen fehlgeordneten verbrückten Molekülen in dieser Arbeit.

Serhiy Demeshko, Maik Reinhard, Marina Bennatti und Jabor Rabeah danke ich für die Durchführung weiterer EPR- und SQUID-Experimente im Rahmen der verschiedenen Projekte.

Ich danke außerdem der gesamten weiteren analytischen Abteilung, insbesondere Angela Weihs und Jana Pittner für ihr Engagement hinsichtlich der Elementaranalyse.

Des Weiteren gilt mein Dank Nadja Kohlmann, der elektronischen und feinmechanischen Werkstatt, Jörg Harloff und Ronald Wustrack, sowie Paul Goschnick und Jana Unger dafür, dass sie mir auf unterschiedlichste Weise mit Hilfe und Rat zur Seite standen.

Der Konrad-Adenauer-Stiftung möchte ich für die finanzielle und ideelle Unterstützung während meines Studiums und meiner Promotion danken. Ich kann inzwischen sagen, dass die Stiftung mein Leben in den letzten Jahren sehr geprägt und bereichert hat und es ohne die vielen tollen Menschen die ich dort kennenlernen und die vielen schönen Momente, die ich auf den Seminaren erleben durfte, wahrscheinlich ganz anders verlaufen wäre.

Vielen Dank Johannes, Fynn, Florentin, Max, Celestina, Antonia und Chris für die Freundschaft und die vielen inspirierenden Gespräche und in den letzten Jahren!

Danke!

Zusammenfassung

Diese Arbeit beschäftigt sich mit der Synthese, Reaktivität und den spektroskopischen Eigenschaften von P-zentrierten Mono- und Biradikalen. Zunächst wurde mit der Addition von Aldehyden an das Biradikal [•P(μ-NTer)$_2$P•] ein klassischer konzertierter Reaktionsmechanismus detailliert untersucht und aufgeklärt. Im Kontrast dazu konnte mit der Addition von Bromalkanen an [•P(μ-NTer)$_2$P•] erstmalig radikalische Reaktivität für dieses Molekül beobachtet werden. Hieraus folgte die Synthese des persistenten, phosphorzentrierten Monoradikals [•P(μ-NTer)$_2$PEt], welches mittels EPR-Spektroskopie auch als Intermediat im hier vorgeschlagenen radikalischen Reaktionsmechanismus nachgewiesen werden konnte. Basierend auf der Reaktion von [•P(μ-NTer)$_2$P•] mit Bromalkanen konnte mit einem Dibromalkan schließlich die Verbrückung zweier Biradikaleinheiten erreicht werden. Hieraus wurde ein phosphorzentrierte Disbiradikal synthetisiert und seine spezielle elektronische Situation mittles umfangreicher EPR-Experimente und quantenchemischer Rechnungen aufgeklärt.

Summary

This thesis deals with the synthesis, reactivity and spectroscopic properties of P-centered mono- and biradicals. First, the addition of aldehydes to the biradical [•P(μ-NTer)$_2$P•], a classical concerted reaction mechanism, was investigated and elucidated in detail. In contrast, radical reactivity for this molecule was observed during the addition of bromoalkanes to [•P(μ-NTer)$_2$P•]. This led to the synthesis of the persistent, phosphorus-centered monoradical [•P(μ-NTer)$_2$PEt], which could also be detected by EPR spectroscopy as an intermediate during the radical reaction mechanism proposed here. Based on the reaction of [•P(μ-NTer)$_2$P•] with bromoalkanes, the bridging of two biradical units was finally achieved with a dibromoalkane. From this, a phosphorus-centered disbiradical was synthesized and its special electronic situation was elucidated by means of extensive EPR experiments and quantum chemical calculations.

Table of contents

List of Abbreviations

$\Delta E_{S\text{-}T}$	singlet-triplet energy gap
AIBN	azobis(isobutyronitrile)
AO	atomic orbital
approx.	approximately
ca.	circa
calcd.	calculated
CENSO	command line energetic sorting
cf.	compare (lat. conferre)
CREST	conformer-rotamer ensemble sampling tool
DSC	differential scanning calorimetry
DFT	density functional theory
DNP	dynamic nuclear polarization
e.g.	for example (lat. exempli gratia)
EPR	electron paramagnetic resonance
ESR	electron spin resonance, see EPR
et al.	and others (lat. *et alii/aliae)*
FWHM	full width at half maximum
HOMO	highest occupied MO
HONO	highest occupied MO
IR	infrared spectroscopy
LA	Lewis acid
LUMO	lowest unoccupied MO
LUNO	lowest unoccupied NO
m	meta
μ-	bridging group (in formulae)
MEP	minimum energy path
MO	molecular orbital
NO	natural orbital
NBO	natural bond orbital
NMR	nuclear magnetic resonance
o	ortho
p	para
PES	potential energy surface
ref.	reference
RT	room temperature
sim.	simulated
SCXRD	single crystal XRD
SQUID	superconducting quantum interference device
*t*Bu	*tert*-butyl
Ter	terphenyl (2,6-dimesitylphenyl)
THF	tetrahydrofuran
TS	transition state
vdW	van der Waals
XRD	X-ray diffraction
zfs	zero-field-splitting
ZPE	zero-point energy

Units of measurement

The International System of Units (SI) is utilized throughout this work to measure experimental and theoretical quantities. All derived units and their expression in terms of the SI base units are given below:

Quantity	**Unit**	**Name**	**Conversion to SI base units**
Frequency	MHz	Megahertz	$1\ \mathrm{MHz} = 1 \times 10^{6}\ \mathrm{s^{-1}}$
	Hz	Hertz	$1\ \mathrm{Hz} = 1\ \mathrm{s^{-1}}$
Magnetic field strength	G	Gauss	$1\ \mathrm{G} = 1 \times 10^{-4}\ \mathrm{T}$
Length	Å	Ångström	$1\ \text{Å} = 1 \times 10^{-10}\ \mathrm{m}$
Power	mW	Milliwatt	$1\ \mathrm{mW} = 1 \times 10^{-3}\ \mathrm{kg\ m^{2}\ s^{-1}}$
temperature	°C	Degree Celsius	$\vartheta/°\mathrm{C} = T/\mathrm{K} - 273.15$
Volume	mL	Milliliter	$1\ \mathrm{mL} = 1\ \mathrm{cm^{3}} = 1 \times 10^{-6}\ \mathrm{m^{3}}$
Energy	kJ	Kilojoule	$1\ \mathrm{kJ} = 1 \times 10^{3}\ \mathrm{m^{2}\ kg\ s^{-2}}$
Wavenumber	$\mathrm{cm^{-1}}$	Reciprocal centimeter	$1\ \mathrm{cm^{-1}} = 100\ \mathrm{m^{-1}}$
time	d	Day	$1\ \mathrm{d} = 8.64 \times 10^{4}\ \mathrm{s}$
	h	Hour	$1\ \mathrm{h} = 3.6 \times 10^{3}\ \mathrm{s}$
	min	Minute	$1\ \mathrm{min} = 60\ \mathrm{s}$

List of synthesized compounds

Abbr.	Structural formula
Ter	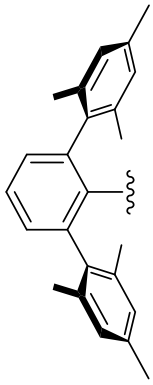
1	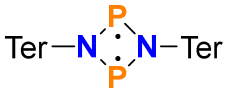
1H (model system)	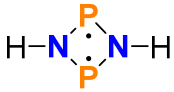
2a	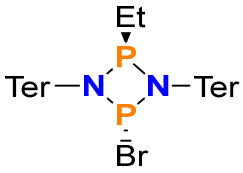
2b	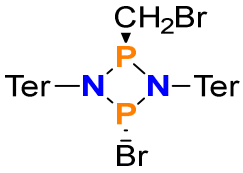
2c	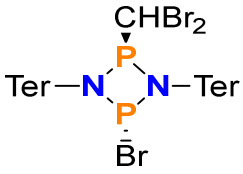
2d	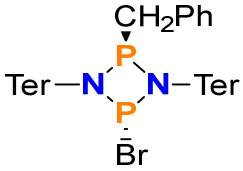

Abbr.	Structural formula
2e	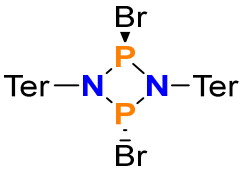
2f	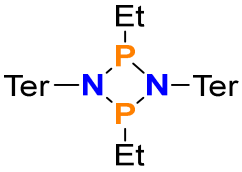
3Et•	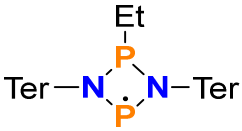
3Br• (calculated intermediate)	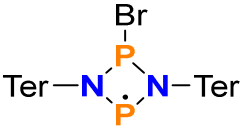
4a	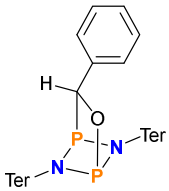
4b	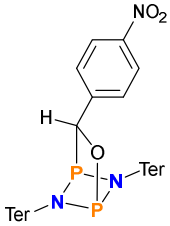
4c	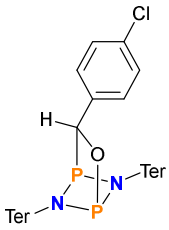
4d	c

Abbr.	Structural formula
5a	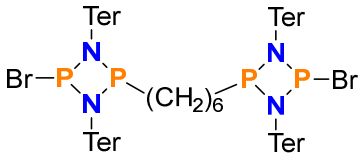
5b	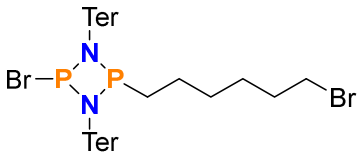

Abbr.	Structural formula
6a	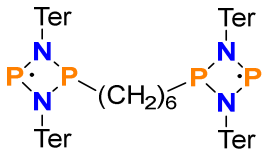
K6b	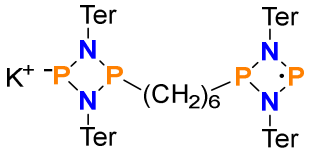

1 Aim

The primary aim of this work was the synthesis of new phosphorus-centered radicals and biradicals derived from the open-shell singlet biradical [•P(μ-NTer)$_2$P•], followed by an examination of their electronic properties and reactivity towards small molecules. A key goal was linking two N_2P_2 units, to form a (dis)-biradical in turn, where the electronic interaction between the spins is controlled by the nature of the linker (Scheme 1).

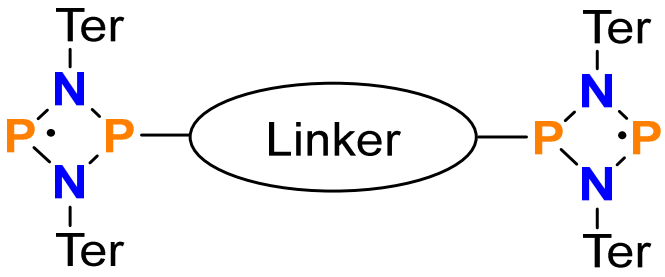

Scheme 1. General concept of linking two N_2P_2 to form a disbiradical (depending on the linker).

Another objective was the investigation of reaction mechanisms of [•P(μ-NTer)$_2$P•] in reactions with different substrates such as bromoalkanes and aldehydes. Although previous studies have demonstrated that [•P(μ-NTer)$_2$P•] reacts with various small molecules (e.g. H_2, alkynes, alkenes) in a concerted closed-shell manner, a detailed exploration of the mechanism – including comparisons of activation barriers and transition states – had not been conducted. Additionally, radical reactivity of [•P(μ-NTer)$_2$P•] had not been described at all prior to this work.

All resulting compounds were to be fully characterized using single crystal X-ray diffraction, NMR spectroscopy when applicable, vibrational spectroscopy (IR and Raman) and especially EPR spectroscopy. EPR experiments were crucial due to the paramagnetic nature of the newly synthesized radical and biradical compounds.

To gain deeper insights into the reactivity and electronic structure of the molecules involved, the experimental work was to be complemented by high-level ab-initio and density functional theory (DFT) calculations.

2 Introduction

2.1 From persistent monoradicals to biradicals

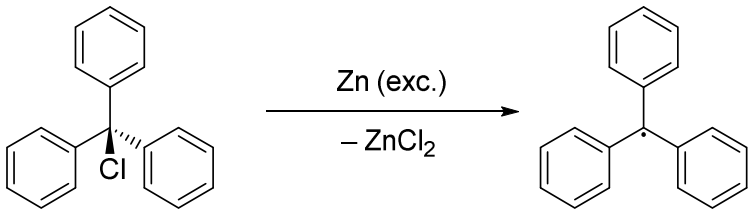

Scheme 2. Synthesis of the first persistent radical by Gomberg.[1]

Historically, the first persistent monoradical (triphenylmethyl) was synthesized by Gomberg in 1900 (Scheme 2),[1] laying the foundation for the whole field of radical and biradical chemistry. However the term "radical" itself as a molecule with an unpaired electron was only coined later and underwent a change towards its modern definition upon the arrival of modern bonding theory (LEWIS, 1916)[2] and quantum mechanics (Heisenberg, 1925).[3,4]

Soon after the discovery of the first monoradicals the synthesis of the first biradicals (molecules with two radical centers that act nearly independently of each other)[5] followed with THIELES (1904)[6] and CHICHIBABINS (1907)[7] hydrocarbons.

The first paramagnetic triplet biradical based on GOMBERG's works was synthesized in 1915 by SCHLENK (Scheme 3).[8]

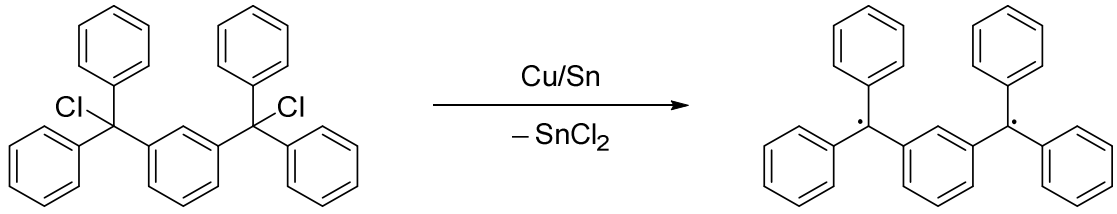

Scheme 3. Synthesis of the first paramagnetic biradical by SCHLENK.[8]

After those first discoveries, the field of biradical chemistry remained relatively dormant until the 1960s. The discovery of bisnitroxides[9–12] and the application of the newly discovered EPR-spectroscopy (ZAVOISKY, 1944)[13] towards biradicals marked milestones of biradical chemistry

during that period. In 1968 a first comprehensive review by Morozova and Dyatkina on biradicals of different types and their spectroscopic properties followed.[14]

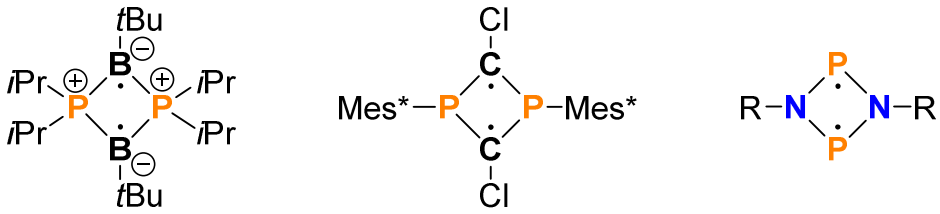

Scheme 4. Some heterocyclobutanediyl biradicals.

Since the 1960s the number of papers on biradical chemistry each year has vastly increased.[4] In the recent decades, based on the pioneering works of NIECKE[15] and BERTRAND[16] various heterocyclobutanediyls (Scheme 4) have been synthesized, laying the foundation for this work.

2.2 Phosphorus-centered monoradicals

While the number of persistent radicals has increased rapidly since GOMBERG'S works and some of them have found widespread application in organic chemistry like TEMPO ((2,2,6,6-tetramethylpiperidin-1-yl)oxyl)[17] the number of known persistent phosphorus-centered radicals is relatively low. An overview of such monoradicals that have been structurally characterized is shown in Scheme 5.

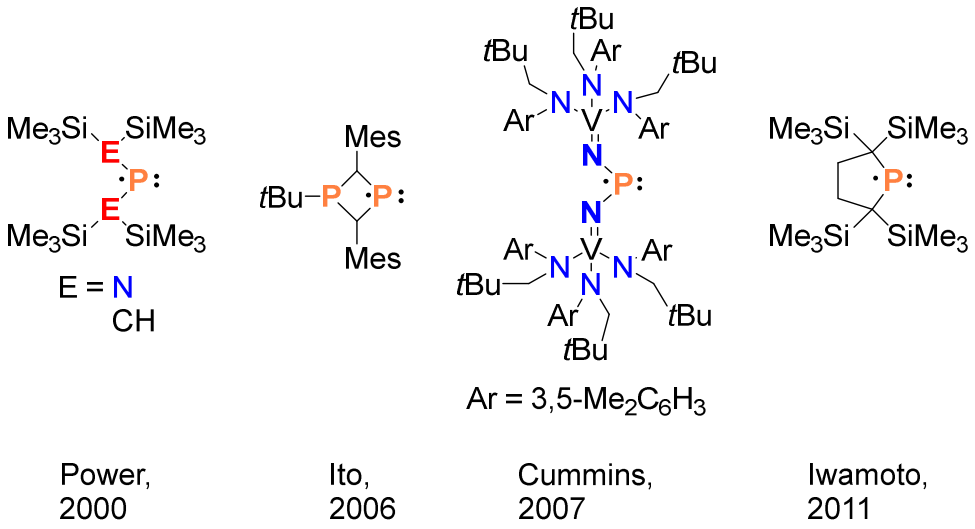

Scheme 5. Selected examples of neutral, persistent, P-centered persistent radicals.[18–21]

Apart from typical radical reactions, P-centered radicals are known to activate various small molecules such as P_4,[22,23] chalcogens,[23,24] CS_2, and CO_2.[25]

2.3 Biradicals – Theory

Biradicals can generally be classified by the interaction between the two unpaired electrons in the molecule. This interaction is quantified by the electron-electron exchange coupling constant *J*. In the case of $J \approx 0$, there is (almost) no interaction between the radical electrons and following the definition of SCHULZ such a species can be called a disbiradical.[26] The resulting molecule is thus a two-doublet species with (nearly) degenerate singlet and triplet states. In the other case, if $J \neq 0$, a biradical(oid) is present. If $J < 0$, the electrons couple antiferromagnetically with each other, resulting in a singlet ground state. If $J > 0$, the electrons couple ferromagnetically and the molecule has a triplet ground state. The transition between all these species is continuous regarding the magnitude of the *J*-coupling.

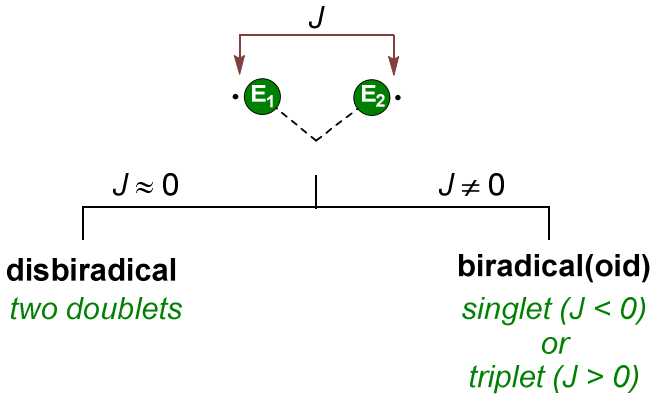

Scheme 6. Classification of biradicals by the electron-electron coupling constant *J* (E = any arbitrary atom bearing an unpaired electron).[27]

2.4 Reactivity of biradicals in general and of [•P(μ-NTer)$_2$P•] in particular

The reactivity of biradicals may range between classical radical and closed-shell reactivity. Typical reaction modes of biradicals generally include dimerization, concerted addition, stepwise radical reactions and redox chemistry.[4,28,29]The reactivity of the open shell singlet biradical [•P(μ-NTer)$_2$P•][30] has been studied extensively in our group since its discovery in 2011. Typical reactivity towards small molecules include concerted pericyclic addition reactions with many molecules such as alkenes or alkynes.[31] With H_2 a concerted addition towards the cis-product occurs that is reversible at higher temperature (>60°C).[32] Carbon monoxide and isonitriles insert into the four-membered N_2P_2-ring and light-switchable five-membered cyclic biradicals are formed.[33] With silver salts as oxidizing agents a radical cation [•P(μ-NTer)$_2$P$^+$] could be synthesized from **1**.[34] An overview over these and more reactions is presented in Scheme 7. Mechanistically, all the addition reactions observed so far are concerted reactions. No radical reactivity of **1** has been described prior to this work.

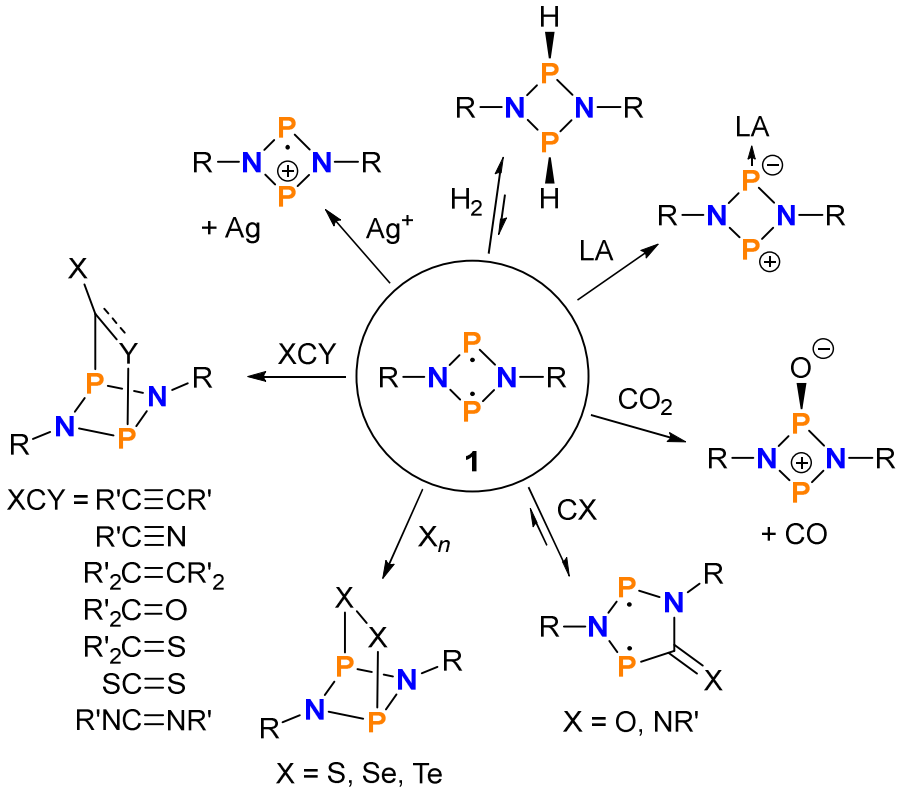

Scheme 7. Reactivity of **1** known prior to this work. Reaction modes include pericyclic addition reactions, oxidation and insertion reactions. Scheme adapted with permission from J. Rosenboom, A. Villinger, A. Schulz, J. Bresien, *Dalton Trans.* **2022**, 51, 13479-13487.

2.5 Disbiradicals from a synthetic point of view

Following the synthesis of the first biradicals (see above), the first species that can be identified as disbiradicals have been synthesized as early as 1928 by Leo and Wittig.[35] The electronic properties of disbiradicals were examined by EPR spectroscopy for the first time in 1956 by Sloan and Vaughan.[36] Heteroatom-centered disbiradicals followed with bisaroxyls (Müller[37] 1958, **I** in Scheme 8) and the groundbreaking synthesis of bisnitroxides (**II** in Scheme 8), independently discovered from one another by Roxantsev and coworkers [9,10] and Lemair and coworkers in 1965.[11,12] Other classes of disbiradicals that have been extensively worked on include trityl[38](**III**)- and verdazyl[39](**IV**)-based biradicals. In the recent years countless new derivatives have been synthesized and found application as polarizing agents in DNP-NMR spectroscopy. With that application in mind even disbiradicals combining two different radical centers have been generated. [38,40–42] To the best of my knowledge phosphorus-centered disbiradicals did not exist before this work.

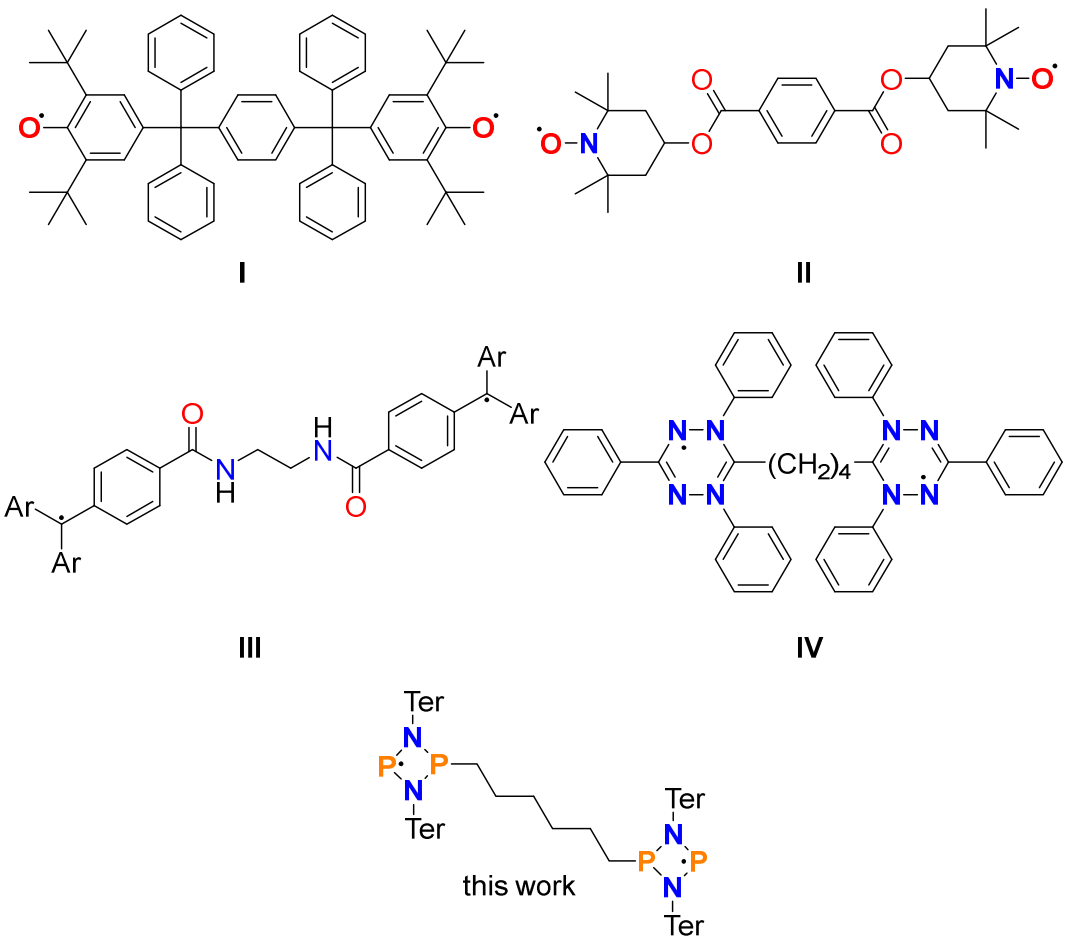

Scheme 8. Aroxyl-(**I**)-, nitroxide-(**II**), trityl-(**III**) and verdazyl-(**IV**) based disbiradicals and the disbiradical synthesized in this work.

2.6 EPR spectroscopy of biradicals

Due to the presence of unpaired electrons in such molecules, EPR spectroscopy is one of the key analytical methods during the examination of biradical species. It can be especially useful to distinguish between the different types of biradicals (see section 2.3) as the presence and type of their EPR signals depend on the spin state they are in.[28] Open-shell singlet biradicals like [•P(μ-NTer)$_2$P•][30] are EPR silent as their spin density is zero. Even in the presence of a strong external magnetic field only one energy level exists and no resonance signal is observed.[28]

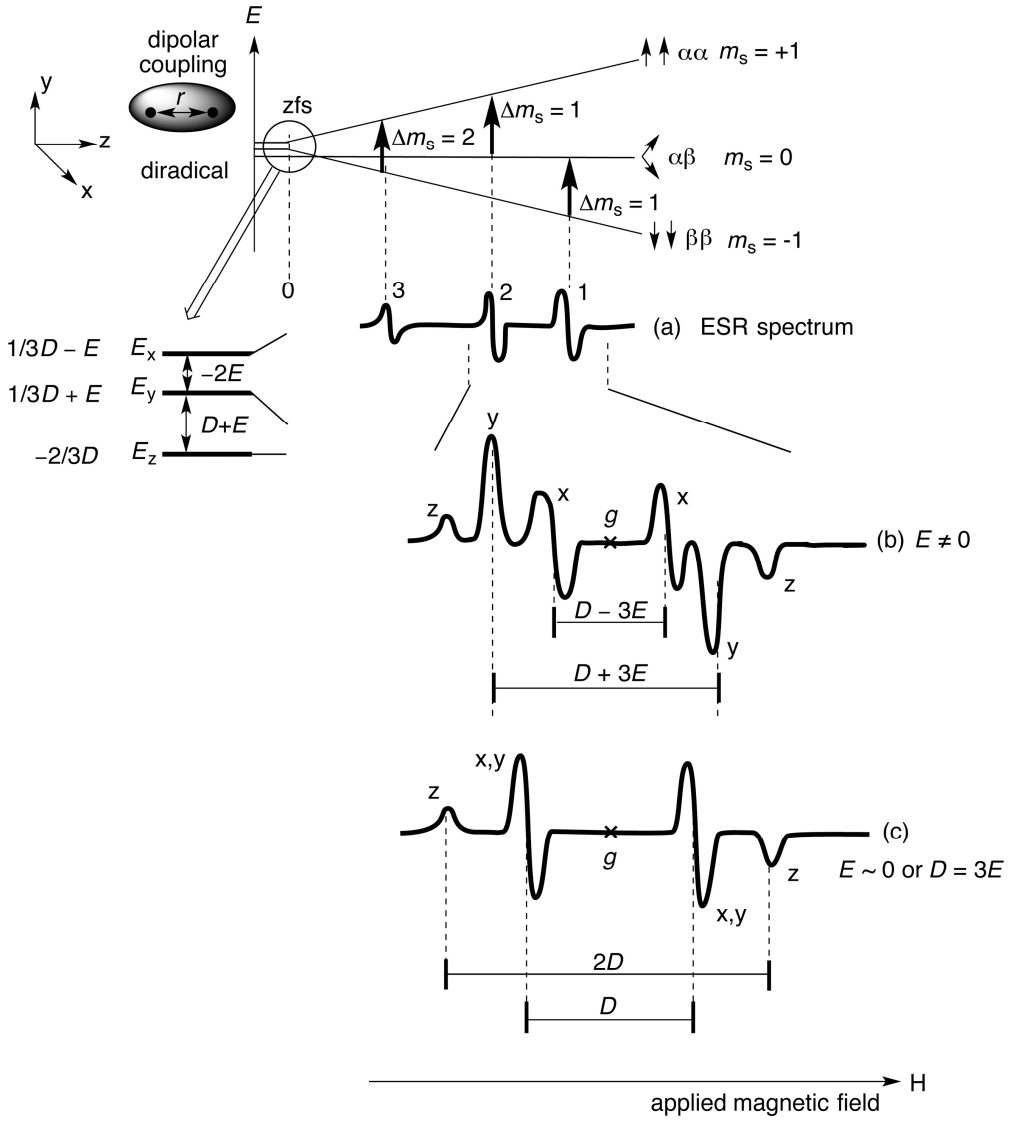

Figure 1. Typical EPR spectra of triplet biradicals in the solid state. Signal splitting determined by the zfs parameters *D* and *E*. (a) simplified spectrum with two allowed Δm_S = 1 transitions (1,2) and forbidden transition (3), (b) allowed transitions in a real spectrum considering magnetic axes x,y,z ($E \neq 0$), (c) allowed transitions when $E \sim 0$ or $D = 3E$, energy levels E_x and E_y become degenerate .[28] Figure reprinted with permission from M. Abe, *Chem. Rev.* **2013**, *113*, 7011–7088.

Triplet biradicals and disbiradicals on the other hand show distinct EPR spectra. Triplet biradicals are S = 1 species and have three energy levels ($m_S = -1, 0, +1$). The dipolar coupling of the two electronic spins generates an internal magnetic field causing a splitting of the energy levels into the three levels even without an external magnetic field (also see Figure 1). This splitting is called zero-field-splitting (zfs) and is characterized by the two zfs parameters *D* and *E*.[28] When an external magnetic field is applied during an EPR measurement the two transitions of the three different energy levels in a triplet state ($-1 \rightarrow 0, 0 \rightarrow +1$) are thus observed at different fields. Additionally, in a typical triplet EPR spectrum oftentimes a weak $\Delta m_S = 2$ line can be observed at half the magnetic field of the center of the $\Delta m_S = 1$ signal. The observation of this "forbidden" transition over two energy levels can be considered strong evidence for a triplet biradical.[4] In real triplet EPR spectra the two allowed transitions would normally appear as six lines in total due to the three magnetic axes x,y and z ((b) in Figure 1). In a structure with 3-fold or higher symmetry the energy levels E_x and E_y become degenerate and 4 lines are observed for the allowed transitions ((c) in Figure 1).[28]

What is also worth noting is that in solution the zfs is generally averaged out. Therefore, to determine D and E or to observe the half-field signals one must work in a rigid matrix, i.e. frozen solution.

In a disbiradical, where the singlet and triplet state are (nearly) degenerate, the EPR spectrum depends on the ratio between the electron-electron exchange coupling constant *J* of the two nearly independent electron spins and the hyperfine coupling constant *A*. Various such ratios and the resulting EPR spectra for a symmetrical disbiradical with the unpaired electrons centered at *I* = ½ nuclei (in this case ^{31}P) are depicted in Figure 2.

In the limiting case of a very small |*J*| / *A* ratio, a "perfect" disbiradical is present (no interaction between the two electron spins, $J \approx 0$) and the EPR signal is indistinguishable from that of a monoradical where just the coupling to the nucleus bearing the unpaired electron is causing signal splitting. In case of a large |*J*| / *A* ratio a three-line signal is visible due to spectroscopically significant coupling between the unpaired electrons. In the case of $J \approx A$ complex coupling patterns may arise as visible in the simulated spectra in the middle of Figure 2.

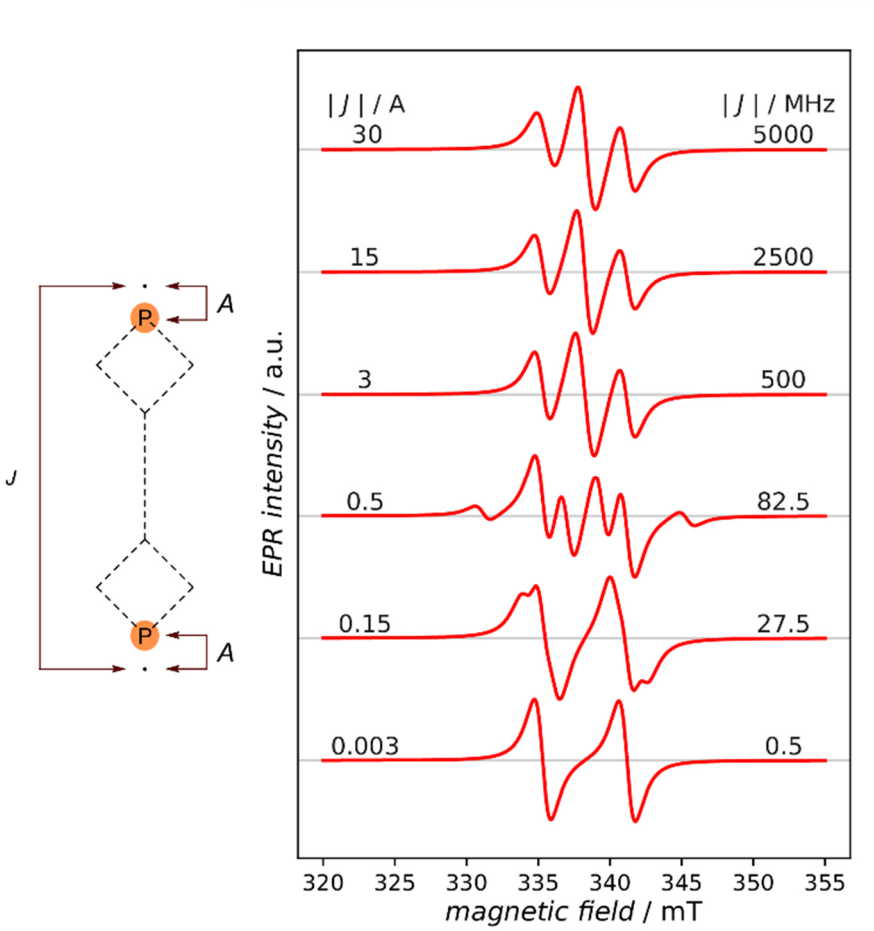

Figure 2. Comparison of simulated EPR signals arising from a symmetric P-centered disbiradical depending on the $|J|$ / A ratio (g_{iso} = 2.0023, $A_{iso}(^{31}P)$ = 165 MHz, S = 1/2, lw = 2 mT (100% LORENTZIAN, FWHM), $\omega_{\mu w}$ = 9.48 GHz).[27]

It is worth noting that the strength of the *J*-coupling cannot be determined from EPR spectroscopy alone at large $|J|$ / A ratios above $|J|$ / A > ~ 3. A molecule with such parameters is better described an effective spin S = 1 system, coupling with $A/2$ to two, in this specific case, equivalent nuclei without specification of the value of the *J*–coupling. This phenomenon was first described in copper acetate and also in other systems such as TSCHITSCHIBABIN type biradicals.[43,44] This also explains the difference between the EPR spectra of a biradical whose radical electrons are centered at I = ½ nuclei with significant *J*-coupling and a monoradical coupling to two equivalent I = ½ nuclei. The spectra in both cases would be 1:2:1 three-line signals, however the coupling constant in the monoradical would be twice as large as the one in the biradical case, allowing to distinguish one from the other (assuming A is equivalent in both cases).

3 Results and Discussion

Many biradical reactions follow a classic "closed-shell" like, concerted reaction pathway.[4,28,45,46] This was also the case for all addition reactions to **1** investigated prior to this work. No radical mechanism for a reaction of **1** had been described so far.[30,47,48] Also, while the structures of the addition products of the concerted addition reactions to **1** had been confirmed by SCXRD and some individual DFT calculations had been done, no comprehensive study comparing activation barriers etc. of different addition reactions had yet been performed. Thus, a first step of this work was to investigate the mechanism of the concerted addition of small molecules to **1** further.

3.1 Additions of aldehydes to [•P(μ-NTer)$_2$P•]

(J. Rosenboom, A. Villinger, A. Schulz, J. Bresien, *Dalton Trans.* **2022**, *51*, 13479-13487)

While the addition of various small molecules (H_2, alkenes, alkynes) and also ketones to **1** was already known,[49] the reaction of aldehydes with **1** or in fact to the best of my knowledge with any other formal hetero-cyclobutanediyl had not yet been investigated prior to this work.

We chose to investigate the addition of aldehydes to **1** due to the calculated very low activation barrier, making it a perfect example for concerted addition reactions to biradicals. Together with a comprehensive computational study including other typical substrates for biradical reactions, it was the goal of this study to shed light on the nature of the mechanism of concerted additions to biradicals. As shown in Scheme 8, four different aldehydes (**4a-4c**) with different substitutions and thus different electronic situations were chosen.

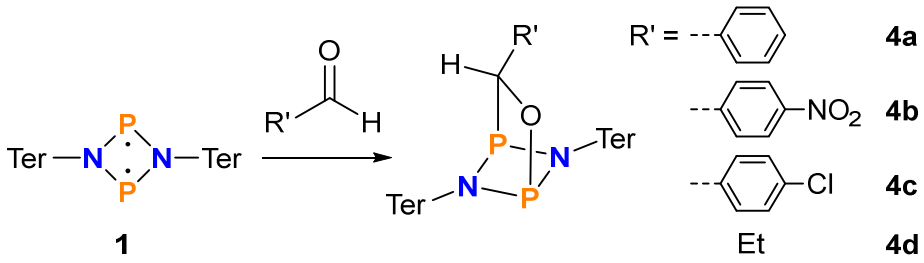

Scheme 9. Addition of different aldehydes to **1**.

The reactions afforded solely the *syn*-addition products and proceeded very quickly (almost instantaneous color change). Structurally, in all reactions a hetero-bicyclo[2.1.1]hexane with a CO bridge between the two phosphorus atoms is formed when the aldehyde carbonyl group adds to the two phosphorus atoms. All addition products could be fully characterized by IR-, Raman- and NMR-spectroscopy, mass spectrometry and SCXRD. An overview over the molecular structures in the crystal and the key structural data is given in Figure 3.

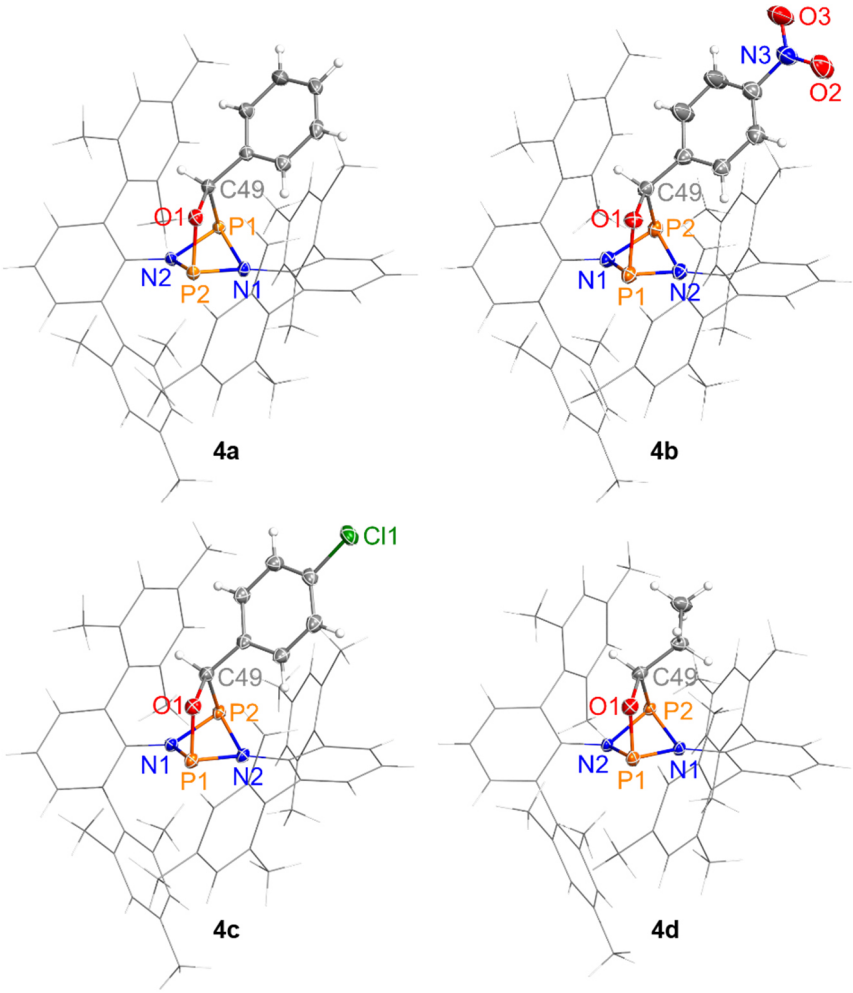

Figure 3. Molecular structures of the addition products **4a** to **4d** in the crystal. Thermal ellipsoids at 50% probability (123 K). Ter substituents depicted as wireframe for clarity. Selected bond lengths (Å): **4a**: N1–P1 1.776(1), N1–P2 1.743(1), N2–P1 1.740(1), N2–P2 1.734(2), P1–C49 1.911(2), P2–O1 1.672(1), O1–C49 1.450(2); **4b**: N1–P1 1.727(4), N1–P2 1.734(4)(4), N2–P1 1.745(4), N2–P2 1.774(4), P2–C49 1.927(4), P1–O1 1.680(2), O1–C49 1.455(5); **4c**: N1–P1 1.739(2), N1–P2 1.740(1), N2–P1 1.745(1), N2–P2 1.776(2), P2–C49 1.916(1), P1–O1 1.673(1), O1–C49 1.455(2); **4d**: N1–P1 1.736(1), N1–P2 1.770(1), N2–P1 1.753(1), N2–P2 1.746(1), P2–C49 1.900(2), P1–O1 1.656(1), O1–C49 1.451(2).[50]

To obtain further insights into the mechanism of the aldehyde addition, quantum chemistry calculations were performed. First a model system (**1H**, H-substituted **1**) reacting with

formaldehyde was examined. As depicted in Figure 4, a symmetry-allowed, concerted reaction can be assumed.

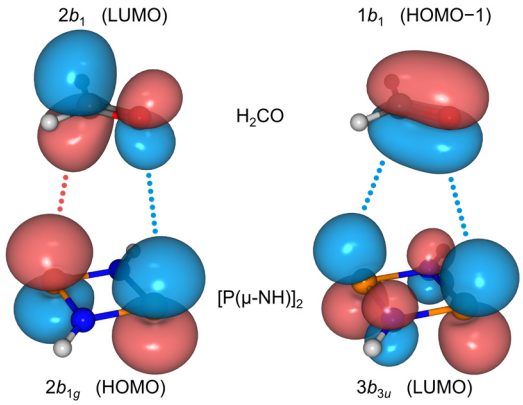

Figure 4. Schematic representation of the interaction of the frontier MOs of the model system **1H** (D_{2h} symmetry) and H_2CO (C_{2v}).[50]

However, finding a transition state proved to be very difficult. Various typical DFT methods (e.g. PBE-D3, B3LYP-D3) indicated a barrierless reaction and no transition state could be located. Using ab-initio MO methods, it was finally possible to find the expected concerted transition state for the model system. To ensure reliable structures and energies, we opted for calculations at the CCSD(T)/def2-TZVP level of theory and DPLNO-CCSD(T)/def2-QZVPP for the final electronic energies.

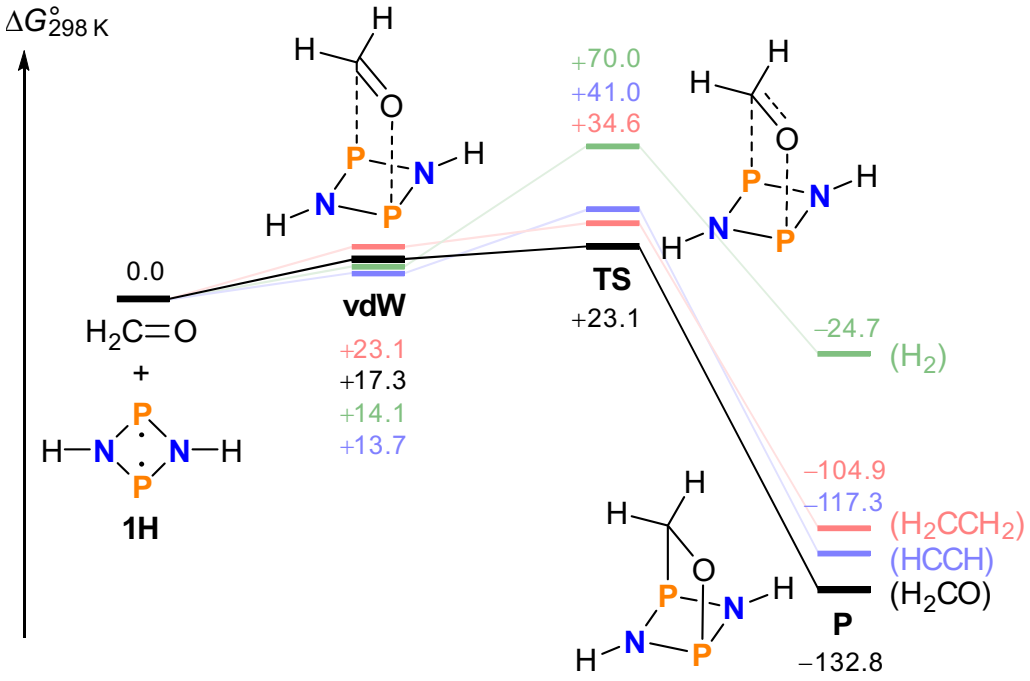

Figure 5. Schematic representation of the Gibbs free energy surface (298.15 K, c° = 1 mol/L) of the addition of formaldehyde to biradical **1H** (black line). The analogous reactions profiles of the additions of acetylene (blue), ethylene (red), and dihydrogen (green) are shown for comparison. Computed at the DLPNO-CCSD(T)/def2-QZVPP//CCSD(T)/def2-TZVP level of theory.[50]

Computations utilizing the coupled-cluster method confirm that the potential energy surface for adduct formation is very flat, the TS being only 1.6 kJ/mol (U_0) above the van-der-Waals complex. As this van-der-Waals complex is 13.1 kJ/mol more stable than the separate starting materials, the overall cycloaddition reaction is essentially barrierless on the PES including the zero-point energy. When considering changes in entropy (two molecules finally form one addition product) and looking at the Gibbs free energy surface (Figure 5), the TS for the model reaction is 23.1 kJ/mol higher in energy than the starting materials. This very low activation barrier is in good agreement with the observed almost instantaneous reactions of **1** with various aldehydes at ambient temperature.

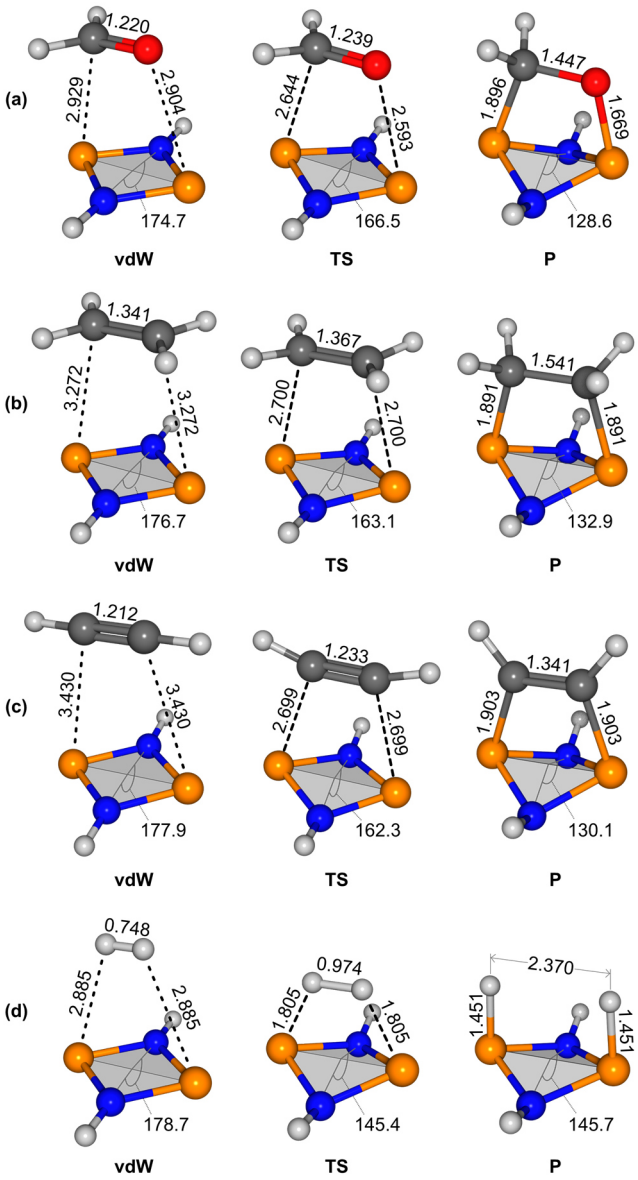

Figure 6. Calculated structures (CCSD(T)/def2-TZVP) of the van-der-Waals (**vdW**) complexes, transition states (**TS**), and products (**P**) of the addition of (a) formaldehyde, (b) ethylene, (c) acetylene, and (d) dihydrogen to the model biradical **1H**. Selected distances (Å) and dihedral angles (°) are given.[50]

For comparison, the reaction pathways of typical other concerted addition reactions to **1** (ethylene, acetylene, H_2) were also examined at the same level of theory (DLPNO-CCSD(T)//def2-QZVPP/CCSD(T)/def2-TZVP). The activation barrier is lowest in the reaction with aldehyde, followed by ethylene and acetylene. The addition of H_2 has a considerably higher activation barrier and the adduct is much less stable than the other reaction products, in agreement with previous calculations and the experimentally observed reversibility of the reaction at higher temperatures.[51]

Finally, the activation barrier of the "real" reaction of **1** with PhCHO was also estimated based on the vdW structure (attempts to optimize the TS structure remained unsuccessful) which seems reasonable given the flatness of the PES and resemblance of the vdW complex and TS (Figure 6). The calculated barrier (DLPNO-CCSD(T)/def2-TZVP//B3LYP-D3/def2-TZVP) ($\Delta U_0 = -7.8$ kJ/mol and $\Delta G°_{298\,K} = +46.1$ kJ/mol) for the formation of the vdW complex is once more only of entropic nature and indicates a very fast reaction which agrees with the experimental observation.

While the other computationally investigated concerted additions to **1** already had low activation barriers, the addition of aldehydes to **1** showed the lowest barrier examined so far. This could allow for reactions with other, less reactive biradicals or the usage of aldehydes as trapping reagents for transient biradical species. In conclusion, reaction of **1** with aldehydes is a typical example of a pericyclic reaction with a very low activation barrier.

3.2 Addition of bromoalkanes to [•P(μ-NTer)$_2$P•] and isolation of a persistent phosphorus-centered monoradical [•P(μ-NTer)$_2$P-Et]

(J. Rosenboom, L. Chojetzki, T. Suhrbier, J. Rabeah, A. Villinger, R. Wustrack, J. Bresien, A. Schulz, *Chem. Eur. J.* **2022**, *28*, e202200624)

When we started to investigate the addition reaction of bromoalkanes to **1** (Scheme 10) we first assumed this reaction would follow a similar concerted pathway like almost all the reactions with small molecules we studied before (e.g. addition of aldehydes[50], section 3.1). However, upon taking a closer look, several experimental hints quickly pointed towards a stepwise, radical reaction.

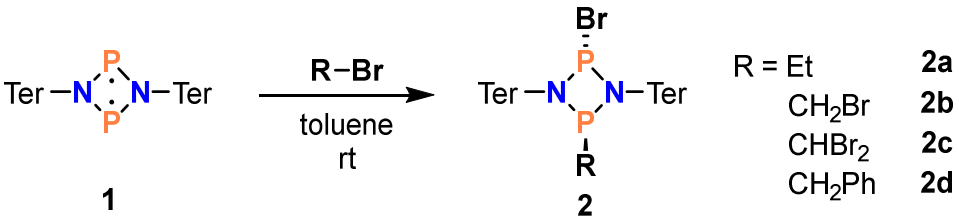

Scheme 10. Addition of bromoalkanes to **1** yielding the *trans*-addition products.

First, as determined by NMR spectroscopy and single crystal X-Ray diffraction, all reactions uniformly yielded only the *trans*-addition products (see Scheme 9 and Figure 7) compared to the *cis*- products in most other addition reactions of **1** with small molecules.[49] Moreover, we also observed the formation of small traces of dibrominated *trans*- product **2e** as side-product in *in-situ* ^{31}P NMR experiments.

To establish its identity, **2e** was also synthesized on purpose by reacting **1** with dry bromine, yielding 1,3-dibromo-*cyclo*-diphosphadiazane **2e** in a 1:3.5 mixture of the *cis*- and *trans*- isomer (δ[^{31}P] = 243.9 ppm (*cis*) and 277.9 ppm (*trans*)). After crystallization, almost pure *trans*-**2e** (97%) could be obtained and identified by SC-XRD.

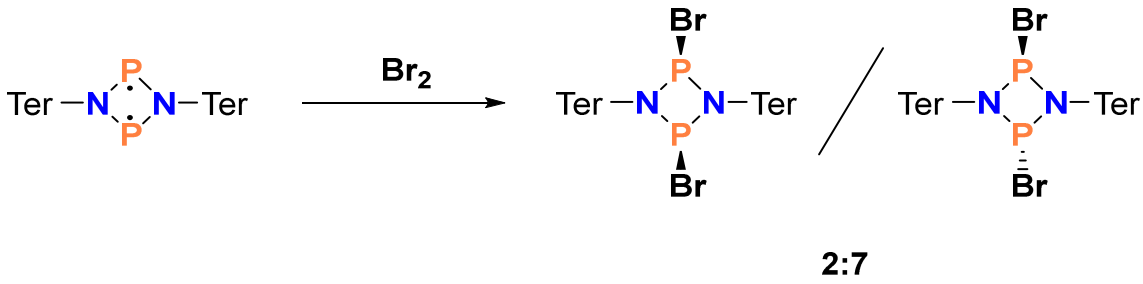

Scheme 11. Reaction of **1** with dry bromine resulting in the formation of *cis*-*trans*-**2e** in a ratio of 2:7.

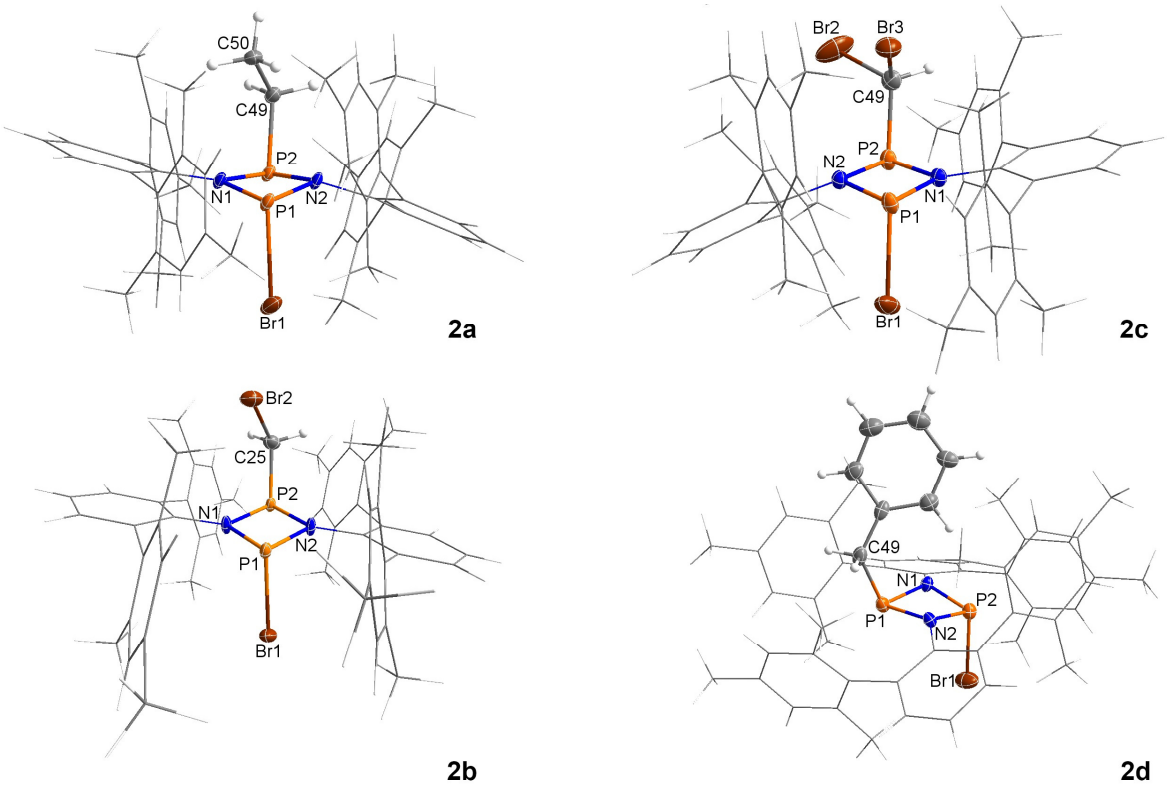

Figure 7. Molecular structure of *trans*-bromoalkane addition products **2a-2d** in the crystal. Ellipsoids set at 50% probability (123 K).[52]

While the presence of the *trans*-products could still be explained by an (unlikely) inversion at the phosphorus atom, the total absence of the *cis*- products and the presence of the 1,3-dibromo-*cyclo*-diphosphadiazane **2e**, even in small amounts, only left the explanation of another reaction mechanism, a radical one.

In the literature, while a few addition reactions of haloalkanes to biradicals had been observed prior to this work (e.g. CCl_4 activation by a Si_2N_2 biradical,[53] activation of CCl_3Br with a P_2B_2

biradical[54] and addition of alkyl iodides to a C_2P_2 biradical[55]), no detailed investigation of the mechanism of the addition of haloalkanes to biradicals had been carried out so far.

The assumption of a radical mechanism in the reaction of **1** with EtBr prompted us to perform a detailed study on the reaction mechanism of this formal addition reaction.

As a first step, the reaction was repeated in the presence of the radical starter AIBN. We prepared two batches of **2a**, one with the addition of AIBN and one without, but otherwise under the same conditions (60°C to activate the AIBN). After 2 h, ^{31}P NMR spectra were recorded. The ratio of biradical **1** (starting material) to addition product **2a** was 2:7 with AIBN and 2:3 without AIBN, indicating a significant acceleration (x2.5) of the addition reaction upon addition of AIBN. This acceleration can only be explained by a radical reaction mechanism and the presence of radical intermediates that are generated in larger amounts when a radical starter is used.

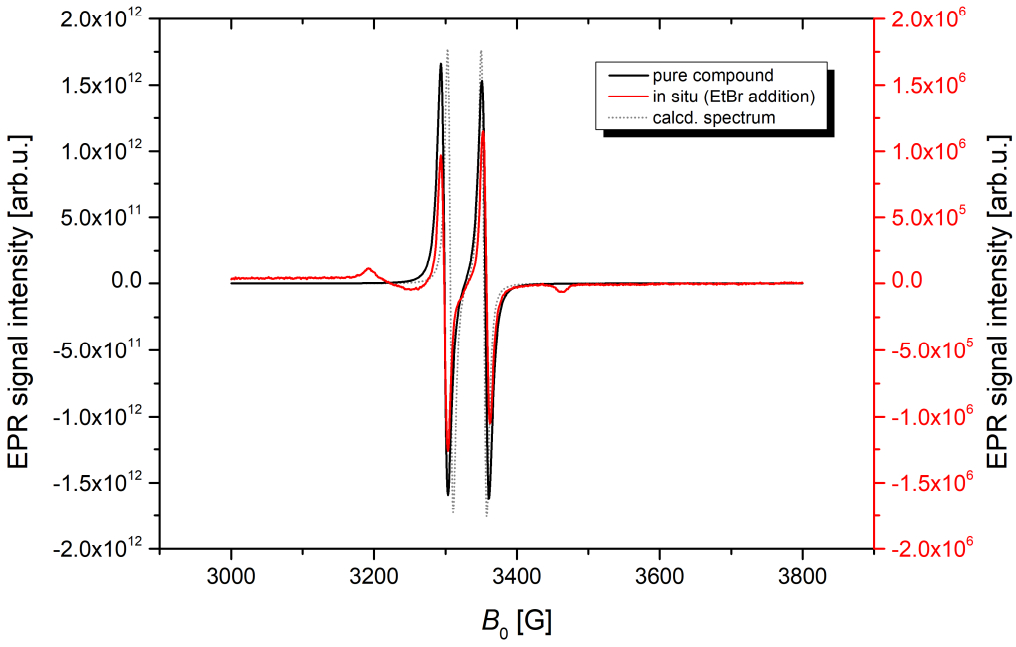

Figure 8. EPR spectra of **3Et•**, pure compound (black), in situ during EtBr addition (red), in silico (gray)[56–62] at ambient temperature. The small "side bands" in the red spectrum can be attributed to impurities (note the different scale of the red and black spectrum) as they did not change in intensity over time and were present even after the completion of the reaction.[52]

For a direct experimental proof of a radical intermediate during the addition of EtBr to **1** we measured an *in-situ* EPR spectrum during the reaction (Figure 8). The spectrum shows a two-

line signal at a *g*-value of 2.003 and a hyperfine coupling constant A = 59 G, caused by the coupling of an unpaired electron with a S = 1/2 nucleus. The observed signal disappeared after the completion of the reaction and thus strongly points towards a phosphorus-centered radical as an intermediate.

3.2.1 Synthesis of the persistent monoradical **3Et•**

With pure **2a** in hand, we wondered whether it would be possible to reduce this species. For this reason, we added an excess of magnesium in the solid. When THF was added to the mixture an instantaneous color change to dark red occurred, indicating a successful reduction.

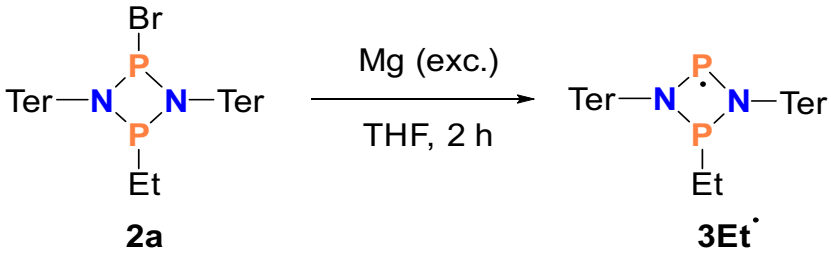

2a **3Et•**

Scheme 12. Reduction of **2a** with magnesium forming the persistent monoradical **3Et•**.

In the following, crystals suitable for single crystal X-Ray diffraction could be obtained. The newly formed species could thus be identified as the ethyl substituted phosphorus-centered monoradical [•P(μ-NTer)$_2$PEt] (**3Et•**).

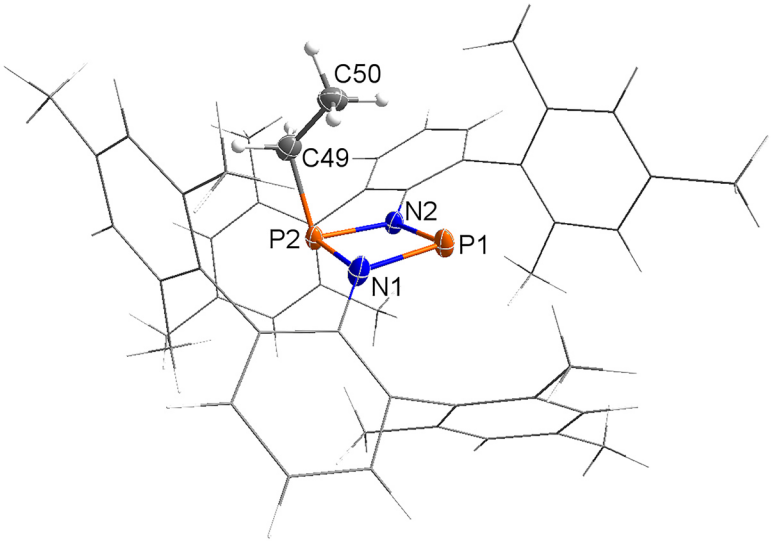

Figure 9. Molecular structure of **3Et•** in the crystal. Ellipsoids set at 50% probability (123 K). Selected bond lengths [Å] and dihedral angles [°]: N1–P1 1.743(3), N1–P2 1.741(3), N2–P2 1.761(4), N2–P1 1.730(4), P2–C49 1.846(2), N1-P2-P1-N2 174.7(3).[52]

Figure 9 illustrates the molecular structure of **3Et•** in the crystal, demonstrating that the radical center at the phosphorus atom is effectively shielded by the Ter substituents, preventing dimerization of the molecule.

An EPR spectrum of dissolved single crystals of **3Et•** was recorded and the observed two-line signal was identical with the signal observed during the addition of EtBr to **1** (see above, *cf.* Figure 8). Therefore, we concluded that **3Et•** is indeed a radical intermediate during the reaction of **1** with EtBr. The EPR parameters for **3Et•** were also calculated *in silico* and are in good agreement with the experimental data. Similar calculations were also performed for **3Br•** suggesting that it would have a much more complicated coupling pattern that does not match the experimental spectrum at all.

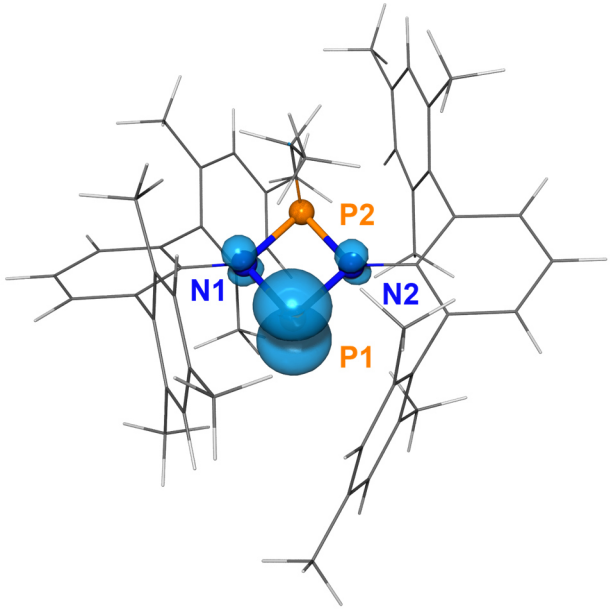

Figure 10. Calculated spin density distribution of **3Et•** (PBE-D3/def2-TZVP, iso value = 0.008).[52,63–67]

Spin density calculations confirm that the MULLIKEN spin density is mainly localized at P1 (~0.7) with only small contributions of N1 and N2 (~0.04 each, Figure 10).

3.2.2 Examination of the radical reaction mechanism

Following the experimental confirmation of the radical mechanism of the addition of bromoalkanes to **1** and the isolation of the radical intermediate **3Et•** several questions remained: How does the radical reaction proceed? Why is it preferred over a concerted mechanism?

To shed some light onto the exact mechanism, DFT and coupled cluster calculations were conducted on the kinetics and thermodynamics of the addition reaction.

First, the reaction mechanism was investigated using the model system MeBr instead of EtBr in the addition reaction with **1H**. It was impossible to locate a transition state for a concerted addition (e.g. the addition of aldehydes, section 3.1). All results pointed towards a stepwise radical mechanism, in agreement with the experimental data.

Since the calculations with the model system indicated that the abstraction of a **Br•** radical is the decisive initiation step of radical addition, we investigated this reaction theoretically in more detail.

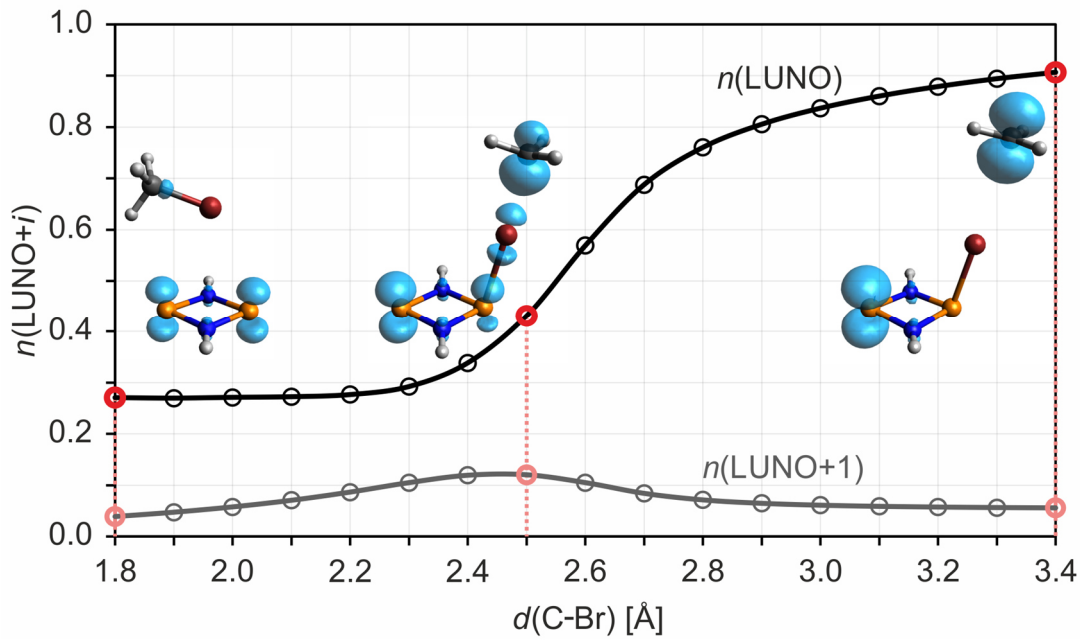

Figure 11. Change of the biradical character (LUNO occupancy; LUNO = lowest unoccupied natural orbital) and tetraradical character (LUNO+1 occupancy) along the MEP of the initiation reaction (using a model system). The insets show the local nondynamic correlation function[68–70] (iso = 0.0025) at the points indicated in red.[52]

A suitable parameter to look at is the biradical character along the initial reaction pathway. During the radical initiation step the biradical character gradually increases from the 25% attributed solely to the radical electrons at the two P-atoms of **1** to almost 100% when the two separate radicals are present at the end of the reaction (Figure 11).

In a concerted reaction on the other hand the biradical character approaches 0 over the course of the reaction, forming a closed-shell product molecule as the reaction proceeds.

The individual reaction steps were calculated using the real system (**1** + EtBr) including Ter substituents at the DLPNO-CCSD(T)/def2-TZVP//PBE-D3/def2-TZVP level of theory. The proposed radical mechanism of the addition of EtBr to **1** following the most favorable reaction steps is depicted in Scheme 2.

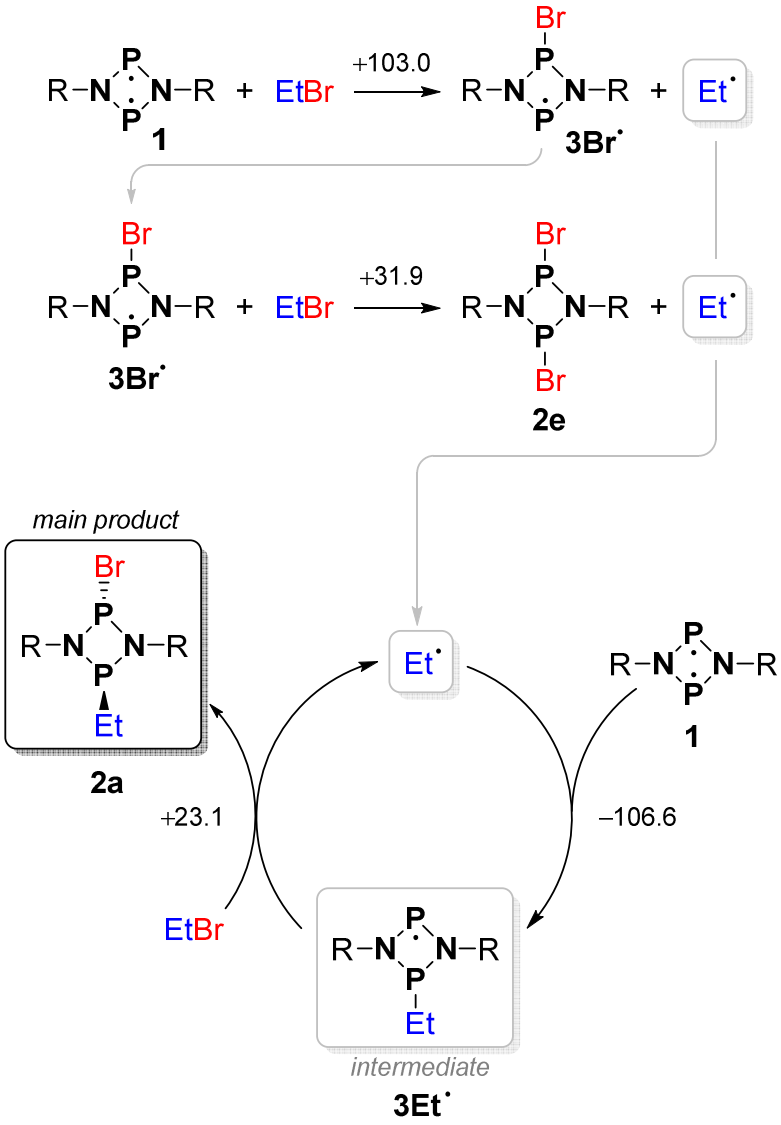

Scheme 13. Proposed radical reaction mechanism for the addition of EtBr to **1**. Free reaction energies ($\Delta_R G°$, $p°$ = 1 atm) in kJ mol^{-1} (DLPNO-CCSD(T)/def2-TZVP//PBE-D3/def2-TZVP).[52]

The radical reaction is initiated by a reaction of **1** with EtBr forming **3Br•** and **Et•** in an endergonic process ($\Delta_R G°$ = 103 kJ mol^{-1}). Compared to the reaction forming **3Et•** ($\Delta_R G°$ = 149 kJ mol^{-1}) as a first step, this reaction is significantly favored and can formally be regarded as activation barrier for the overall process.

The radical **3Br•** can now follow different reaction pathways. The first possibility is a highly exergonic termination reaction where **3Br•** reacts with free **Et•** forming *trans*-**2a** as a reaction product ($\Delta_R G° = -186.5$ kJ mol^{-1}). However, this reaction is unlikely due to the very low concentration of free **Et•** compared to EtBr. **3Br•** can further react with EtBr affording the experimentally observed by-product **2e** and another equivalent of Et• ($\Delta_R G° = +31.9$ kJ mol^{-1}). The actual reaction turnover proceeds via a catalytic cycle where the previously generated free **Et•** reacts with **1** forming the experimentally observed radical intermediate **3Et•** in an exergonic reaction ($\Delta_R G° = -106.6$ kJ mol^{-1}). **3Et•** then reacts with EtBr forming *trans*-**2a** and a new **Et•** radical completing the catalytic cycle. All termination reactions are highly exergonic as two radicals recombine, leading to the formation of closed-shell molecules.

The fact that the **3Et•** and not **3Br•** is the crucial intermediate in the addition reaction that can be detected spectroscopically can be explained by the possible reactions both species can undergo with EtBr. The reaction of **3Br•** with EtBr leads to the formation of brominated side product **2e** (+31.9 kJ mol^{-1}). The formation of **2a** and **Br•** is thermodynamically unfavored (+69.9 kJ mol^{-1}). On the other hand, **3Et•** and EtBr react to form **2a** (+23.1 kJ mol^{-1}) whereas the formation of the hypothetical side product **2f** is strongly unfavored (+98.6 kJ mol^{-1}) and was not observed experimentally. Thus, the formation of the reaction product **2a** via **3Et•** corresponds to the minimum energy path on the potential energy surface.

For the overall reaction, the formation of the *trans*- addition product is thermodynamically favored by 24.3 kJ mol^{-1} over the *cis*-product. Following our calculations, we also investigated the reactivity of **3Et•** with EtBr and Br_2 to gain further experimental insights into the reactivity of **3Et•** and its role as an intermediate during the reaction towards **2a**.

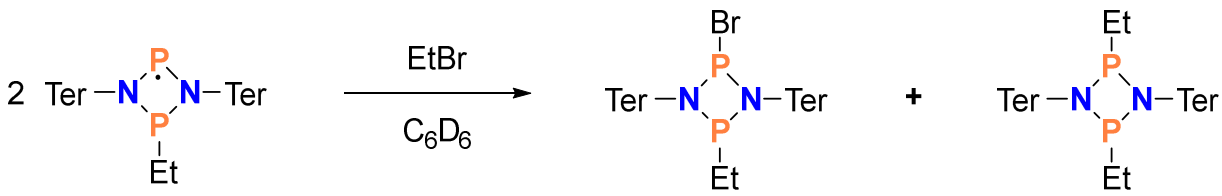

Scheme 14. Reaction of **3Et•** with EtBr.

The reaction of **3Et•** with EtBr (Scheme 14) yielded a 1:1 mixture of *trans*-**2a** ($\delta[^{31}P]$ = 229.1 ppm and 255.2 ppm) and two other species (225.2 ppm and 266.7 ppm). These were assigned to *cis*- and *trans*- [EtP(μ-NTer)$_2$PEt] (**2f**) as a coupling/broadening is visible in the ^{31}P–^{1}H-coupled NMR spectra which disappears in the decoupled $^{31}P\{^{1}H\}$ spectrum. The formation of a 1:1 mixture of **2a** and **2f** when a stoichiometric amount of EtBr is used is in line with our computational results. For every equivalent of **2a** that is formed when **3Et•** reacts with EtBr, one equivalent of Et• is formed that can react with another equivalent of **3Et•** forming one equivalent of **5a**.

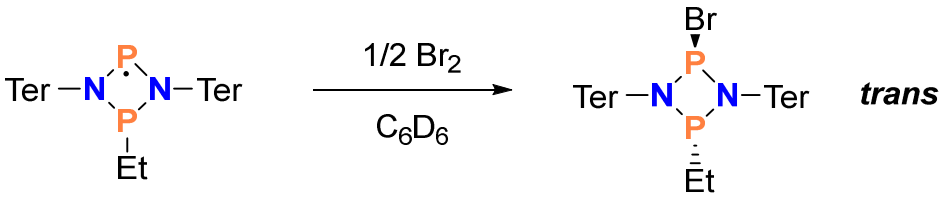

Scheme 15. Reaction of **3Et•** with Br_2.

In the reaction of **3Et•** with Br_2 **2a** is formed which is also consistent with the proposed radical addition reaction of EtBr to **1**.

3.3 Design and synthesis of a phosphorus-centered disbiradical

(J. Rosenboom, F. Taube, L. Teichmeier, A. Villinger, M. Reinhard, S. Demeshko, M. Bennati, J. Bresien, B. Corzilius, A. Schulz, *Angew. Chem. Int. Ed.* **2024**, 63, e202318210.)

After the successful reaction of **1** with various bromoalkanes and subsequent reduction of **2a** with magnesium resulting in the synthesis of **3Et•** on a gram scale, a new question arose: Could the same method for creating asymmetrically substituted diphosphadiazanes also allow for the combination of two N_2P_2 units if a sufficiently large dibromoalkane was used?

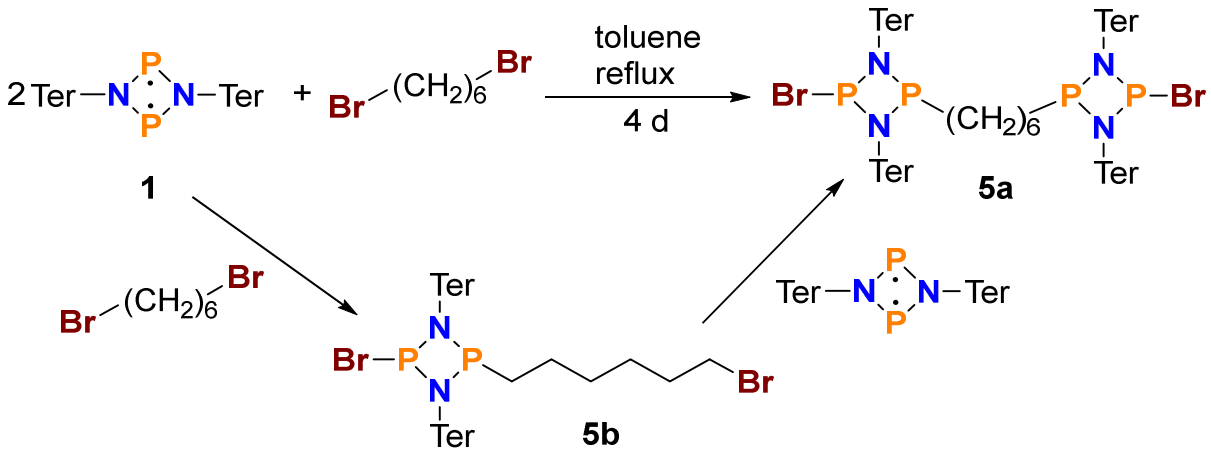

Scheme 16. Reaction of **1** with dibromohexane forming **5a** and **5b**.

In a first step it was indeed possible to add 1,6-dibromohexane to **1** in a 1:1 stoichiometry forming the bromoalkane adduct **5b** analogous to the formation **2a** with EtBr in 52% yield of isolated crystalline substance. When **5b** was reacted with another equivalent of **1** in toluene the linked species **5a** was obtained. This compound was also accessible via a direct reaction of **1** with dibromohexane in a 2:1 stoichiometry. Due to the high steric demand of the four Ter-substituents this reaction required significantly higher reaction temperatures and longer reaction times (111°C over 4 d) compared to the reactions of **1** with the other (mono-) bromoalkanes (minutes to days at RT).

In a next step it was attempted to reduce **5a** with different reducing agents. Interestingly, a reduction with magnesium under the same conditions as with the structurally very similar monoradical **3Et•** was unsuccessful despite repeated attempts with different means of activation (heating, sonification in an ultrasonic bath and addition of iodine).

When the stronger reducing agent KC_8 was used instead, an instantaneous color change occurred, indicating a successful reduction. However, only after repeated attempts it was possible to isolate the disbiradical **6a** in its pure form.

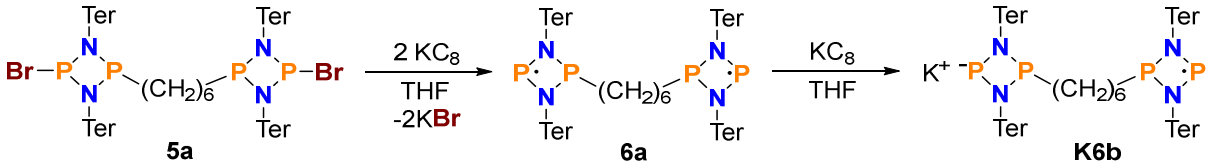

Scheme 17. Synthesis of the disbiradical **6a** and distonic radical anion **6b**$^-$ from **5a**.

When **5a** and two equivalents of KC_8 were mixed in the solid and THF was added, overreduction took place. Due to the low solubility of **5a** in THF in solution an excess of KC_8 was present resulting in the partial formation of the potassium salt **K6b** bearing the radical anion **6b**$^-$. In the end we could suppress the formation of this species by a portion-wise addition of the reducing agent over a period of 15 min. Also, the reaction mixture was filtered over *celite*® in order to remove any charged species from the solution. Using this protocol, we could obtain pure crystalline **6a** in a yield of 59%.

Single crystals from this sample were suitable for SCXRD and it was possible to determine the molecular structure in the crystal as depicted in Figure 12. Each half of the molecule is structurally very similar to the monoradical **3Et**$^\bullet$. The most notable parameter obtained from SCXRD data is the large P···P distance of the two P atoms bearing the unpaired electrons of 10.913(6) Å. Other selected bond lengths and angles can be found in the caption of Figure 12.

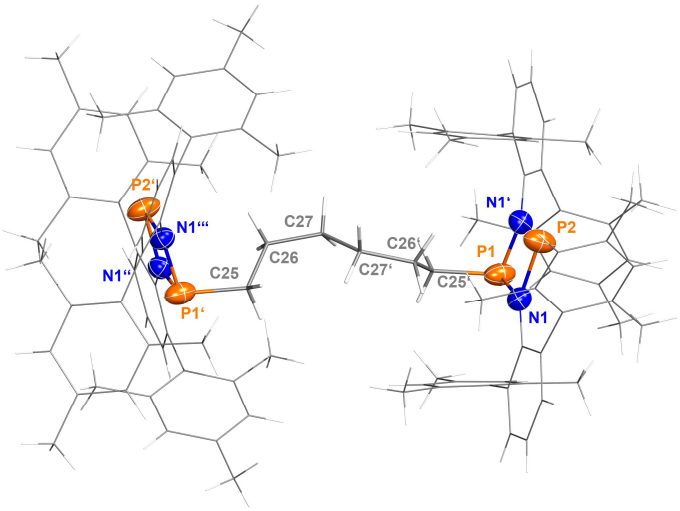

Figure 12. Molecular structure of the disbiradical **6a** in the crystal. Thermal ellipsoids at 50% probability (123 K). Ter substituents and alkyl bridge depicted as wireframe for clarity. Selected bond lengths (Å) and torsion angles [°]: N1–P1 1.749(4), N1'–P1 1.673(4), N1–P2 1.805(4), N1'–P2 1.683(4), P1–C25' 1.85(1), P2···P2' 10.913(6); P1–N1–N1'–P2 178.0 (2), N1–P1–N1'–C25 101.2 (4), N1'–P1–N1–C25 102.4 (4).[27]

3.3.1 EPR-spectroscopy of the disbiradical **6a**

Following the successful synthesis of the disbiradical **6a**, due to its paramagnetism, EPR spectroscopy (besides single-crystal XRD) became the key analytical method during this project. Based on the EPR data of the structurally very similar monoradical **3Et•** (two-line signal due to coupling with one ^{31}P nucleus) we were very surprised by the signal observed in the first EPR spectra of the disbiradical **6a** which featured a 3-line signal with a 1:2:1 intensity ratio.

Due to the very large distance (10.9 Å) in between the two phosphorus atoms bearing the unpaired electron determined in the solid via single-crystal X-Ray diffraction one would have expected the signal of a (nearly) perfect disbiradical with no significant exchange coupling between the two unpaired electrons (also see section 2.6). As **6a** and **3Et•** are also structurally very similar, in case of two isolated radical sites their EPR signals should also be virtually identical (*cf.* Figure 2, two-line case).

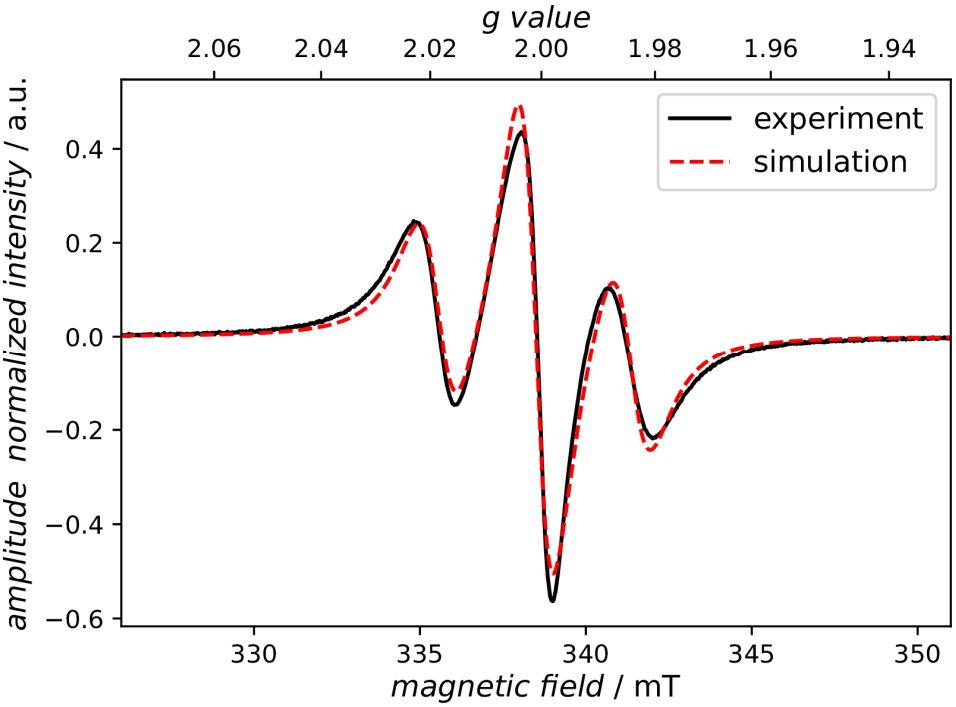

Figure 13. X-band (9.48 GHz) EPR spectrum of **6a** in THF, T = 293 K (S = 1, g_{iso} = 2.001, $A_1(^{31}P)/2$ = $A_2(^{31}P)/2$ = -40 MHz, $A_3(^{31}P)/2$ = 324 MHz, lw = 1.713 mT (100% LORENTZIAN, FWHM), τ_R = 0.035 ns; for details on simulation see below).[27]

Therefore, it was very surprising at first to observe a three-line signal with a spectroscopically significant *J*-coupling clearly visible from the line-shape. After some considerations the only plausible explanation was that the structure of **6a** had to be subject to dynamics in solution, allowing for a significantly shorter P···P distance than in the solid.

Thus, a conformer search using CREST[71,72] and CENSO[73] together with GFN-FF force field[74] and GFN2-xTB[75] //GFN-FF composite methods was performed. The screening of more than 500 conformers showed that the most favorable structures in solution are those with a much shorter P···P distance.

The most energetically favorable and therefore dominant conformer in solution (T1, x = 47%, Figure 14, right) has a P···P distance of only 7.31 Å and is energetically stabilized with respect to the conformer observed in the solid state (T5, d(P···P) = 10.39 Å, x < 0.1%, Figure 14, left) by 17 kJ/mol. Hence, the unusual EPR signal of **6a** in solution can be explained by exchange coupling of the two electrons not through the unconjugated CH_2-chain but "through space" in accord with computed EPR data. A comparison of the optimized molecular structures of the conformer found in the solid state and the most favorable conformer in solution are displayed in Figure 14.

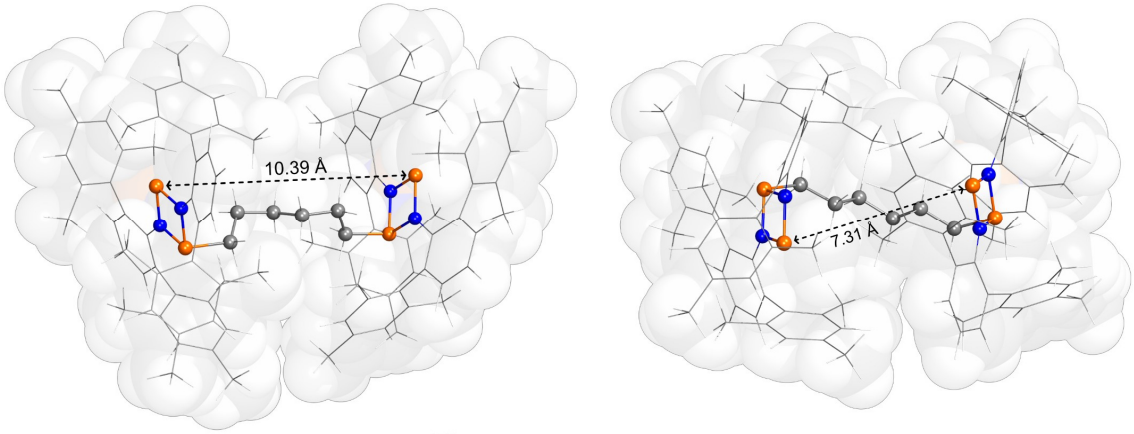

Figure 14. Comparison of the optimized molecular structures originating from the solid state data (T5, left) and most favorable conformer in toluene solution (T1, right; conformer search using CREST/CENSO, GFN2-xTB[75] //GFN-FF, optimization @B97-3c, solvent correction for toluene).[27]

To confirm **6a** is indeed a phosphorus-centered disbiradical the spin density distribution of the molecule was calculated (level of theory: B97-3c). Similar to the monoradical **3Et•** the MULLIKEN spin density is mainly centered around the divalent P2 (~0.75 for **6a** vs 0.70 for **3Et•**). Only minor values are computed for N1 and N1' (both 0.03). The spin density distribution for both T1 and T5 is plotted in Figure 15.

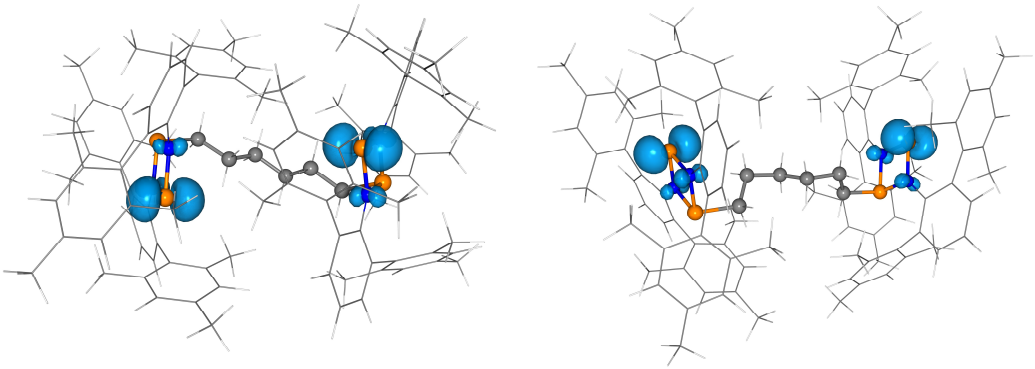

Figure 15. Calculated spin density distribution of **6a** (left: conformer T1 and right: T5, level of theory: B97-3c, iso value = 0.008).[27]

To confirm that our model of the EPR signal of **6a** in solution is consistent, we studied the change of the EPR signal at different temperatures and with different microwave frequencies (X-band and Q-band).

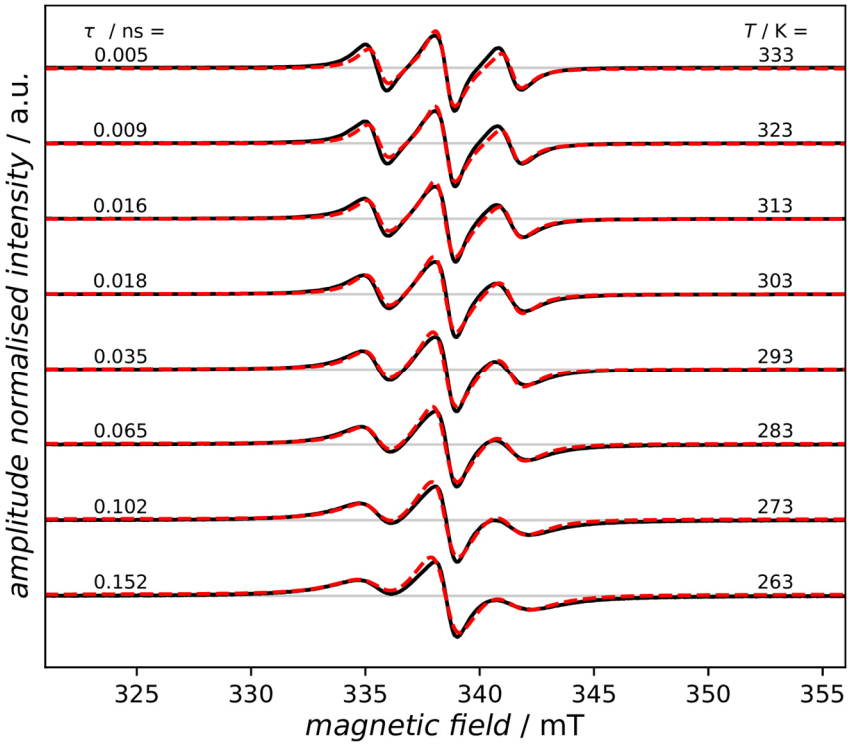

Figure 16. X-band (9.48 GHz) EPR spectra of **6a** dissolved in THF at different temperatures. The hyperfine interaction tensor ***A*** determined from simulation of the experimental EPR spectrum of **3** at 100 K was kept constant for the different temperatures, varying only the rotational correlation time τ_R.[27]

At higher temperatures, an increase in the amplitude of the outer transitions occurred which allows an investigation of dynamic effects within the system caused by partial averaging of the ***g*** – and ***A*** – anisotropies by rotational diffusion of the molecule.[76,77] A deviation of the spin system from the isotropic limit seems conceivable considering the high molar mass of $M = 1517$ g/mol. To get access to the ***g*** – and ***A*** – tensors, a spectrum of the Et-substituted monoradical **3Et•** was recorded in frozen and evaluated. With this data, simulations were performed, taking into account the isotropic rotation-correlation time τ_R which varies between 0.005 ns and 0.152 ns depending on the measurement temperature. These correlation times are at least an order of magnitude shorter than what is expected from the STOKES-EINSTEIN-DEBYE equation for a rigid spherical particle. Therefore, we conclude that internal conformational dynamics are allowing the radical moieties to reorient on a much faster timescale than the molecule as whole. The fact that all spectra can easily be reproduced considering a $S = 1$ system coupling to two equivalent phosphorous atoms with $A(^{31}P)/2$ demonstrates that the resulting dynamically averaged J must still be much larger than the isotropic $A(^{31}P)$ and that isotropic (exchange) J is dominating over dipolar e-e interaction.[27]

Considering the definition for a disbiradical given above ($J \approx 0$, *cf.* section 2.3) one might wonder whether the term “disbiradical” is still suitable for a molecule like **6a**.

Firstly, the transition from a disbiradical to a biradical(oid) is continuous in terms of the magnitude of the *J*-coupling. Furthermore, the understanding of a significant interaction between the electrons in such a species may differ between spectroscopists and molecular chemists. The coupling constant of $J > 500$ MHz for **6a** as determined by the solution EPR spectrum equals a singlet-triplet gap of $\Delta E_{S\text{-}T} > 4.0 \cdot 10^{-4}$ kJ/mol.[27] While being *spectroscopically* significant, from a *chemical reactivity point of view* this indicates virtually degenerate singlet and triplet states. Therefore, **6a** is still referred to as a disbiradical despite the observed three-line EPR signal which arises due to *J* coupling.

The singlet-triplet energy gap of **6a** in the solid was additionally estimated using SQUID magnetometry. The coupling constant *J* was determined at -0.19 cm^{-1} equaling to a $\Delta E_{S\text{-}T}$ of -0.38 cm^{-1} or about $-4.5 \cdot 10^{-3}$ kJ/mol indicating a singlet ground state with a biradical character of virtually 100%. As intermolecular interactions also play a role in the solid compared to a low-concentrated sample in solution, this is to be considered as a maximum value and is thus in good agreement with the data obtained by EPR spectroscopy and computations ($-3.2 \cdot 10^{-3}$ kJ/mol).

3.3.2 Synthesis of the phosphorus-centered distonic radical anion **6b**$^-$

Apart from the synthesis of **6a** it was also possible to prove the existence of the above-mentioned phosphorus-centered distonic radical anion **6b**$^-$ by SCXRD and EPR spectroscopy.

It was attempted repeatedly via different routes to isolate it in its pure form. However, this proved to be very difficult. EPR and NMR data suggest an overreduction towards a Ter-phosphide while there were still significant amounts of **6a** detectable.

Therefore, it was only possible to use mixed crystals of **6a** and **K6b** to obtain analytical data on **6b**$^-$. As determined by SCXRD, **6b**$^-$ crystallized very similarly to **6a** in the space group *Fddd*. The molecular structure of **6b**$^-$ is displayed in Figure 17.

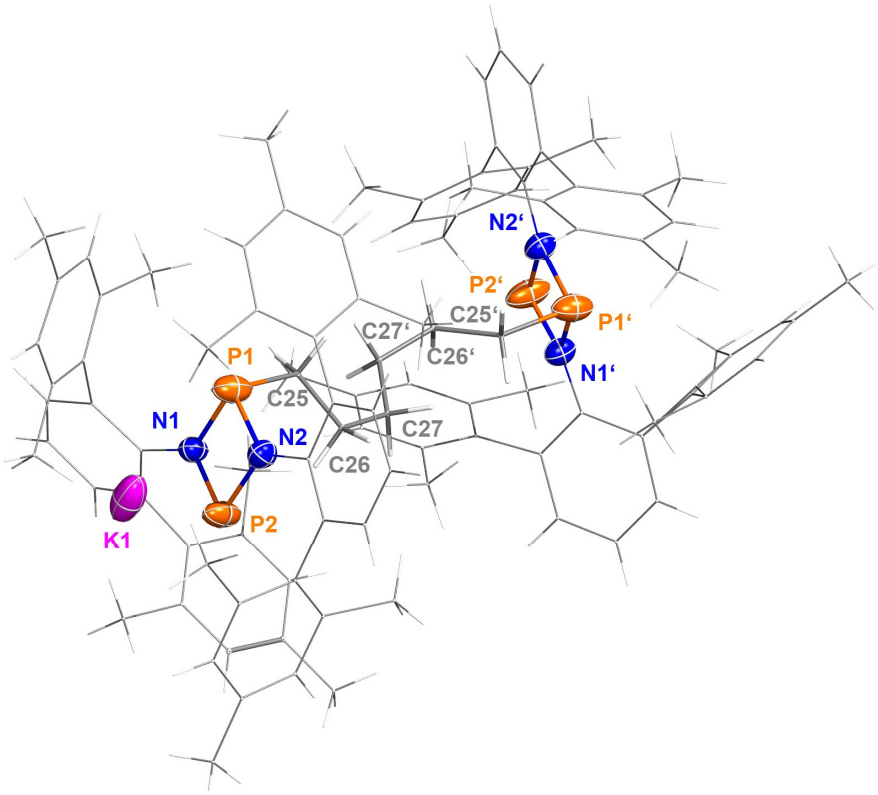

Figure 17. Molecular structures of the salt **K6b** bearing the distonic radical anion **6b**$^-$ in the crystal. Thermal ellipsoids at 50% probability (123 K). Ter substituents depicted as wireframe for clarity. Selected bond lengths (Å) and torsion angles [°]: N1–P1 1.70 (1), N2–P1 1.771 (9), N2–P2 1.74 (1), N1–P2 1.71 (1), P1–C25 1.879 (7), K1–P2 2.810 (7), P1–N1–N2–P2 179.1 (7), N1–P1–N2–C25 97.6(5).[27]

Mixed crystals of **6a** and **6b**$^-$ with a ratio of 83% to 17% as determined by SCXRD were dissolved and an X-Band EPR spectrum of that solution recorded.

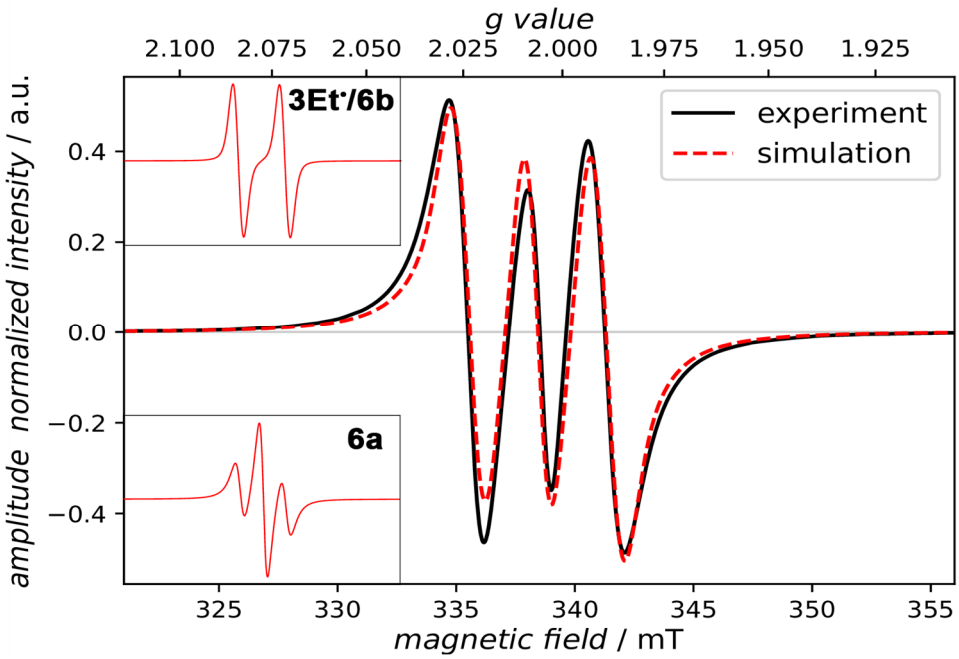

Figure 18. X-band (9.48 GHz) EPR spectrum and simulation of a mixture (83:17) of **6a** and **K6b** in toluene; simulated spectra of pure components are shown in inserts (magnetic field axis at same scale). EPR parameters for pure components in toluene: Monoradical: S = 1/2 , g_{iso} = 2.0011, $A_{iso}(^{31}P)$ = 164 MHz, *lw* = 1.1 mT : 1 mT (GAUSSIAN : LORENTZIAN, FWHM); Biradical: S = 1, g_{iso} = 2.001, $A_1(^{31}P)/2$ = $A_2(^{31}P)/2$ = -40 MHz, $A_3(^{31}P)/2$ = 324 MHz, *lw* = 1.713 mT (100% LORENTZIAN, FWHM), τ_R = 0.044 ns Simulation was done by using ratios obtained from single crystal XRD and EPR parameters of pure **6a** and pure ethyl substituted monoradical **3Et•**.[27]

Due to the structural similarity also the EPR-parameters *g* and *A* of the two compounds are virtually identical. The only difference is that in **6a** there is the *J*-coupling to the second unpaired electron causing a three-line signal, which is of course absent in **6b**$^-$. Therefore, for **6a** a three-line signal as discussed above is observed and a two-line signal for **6b**$^-$.

These two signals are superimposed due to their nearly identical EPR parameters causing a three-line signal with seemingly an intensity ratio of almost 1:1:1. Using the composition of the crystals as obtained from SCXRD (83%:17%) and the simulations of the individual compounds, it was possible to simulate a spectrum matching the experimental data very well (Figure 18). As no EPR data on pure **6b**$^-$ was available we used the simulation parameters for a spectrum of the monoradical **3Et•**. The parameters of these two compounds should be virtually identical as they are structurally very similar and only differ very far away from the radical center where no hyperfine coupling of a nucleus with the unpaired electron is to be expected.

4 Summary and Outlook

In the course of this work, it was possible to further elucidate the reactivity of the biradical [•P(μ-NTer)$_2$P•] and to show how its reactive behavior depends strongly on the substrate with which it is reacted. While the reaction with aldehydes proceeds in a classic closed-shell-like, concerted mechanism with a very low activation barrier, it has been demonstrated that [•P(μ-NTer)$_2$P•] exhibits radical reactivity during the reaction with bromoalkanes. The persistent phosphorus-centered monoradical [•P(μ-NTer)$_2$PEt] could be confirmed as a radical intermediate during the addition reaction of EtBr to [•P(μ-NTer)$_2$P•]. It was subsequently isolated in the solid by reduction of the bromoalkane adduct and fully characterized including single crystal X-Ray diffraction and EPR spectroscopy.

This synthetic route paved the way for the synthesis of novel biradicals by using dibromoalkanes to combine two diphosphadiazane rings. The addition product of two equivalents [•P(μ-NTer)$_2$P•] with dibromohexane was synthesized and successfully reduced with KC_8. The resulting molecule is a phosphorus-centered disbiradical and was characterized via extensive EPR experiments and single crystal X-Ray crystallography. Quantum chemical calculations revealed a highly dynamical conformational space explaining the coupling of the two unpaired electrons in solution despite a large distance in between the radical centers in the solid. Further reduction of the previously synthesized disbiradical led to the formation of a phosphorus-centered distonic radical anion, which could unfortunately not be isolated in its pure form. However, the presence of this species was confirmed by single crystal crystallography combined with EPR spectroscopy.

While several new fields related to phosphorus radical and biradical chemistry based on **1** could be opened during this work, there remain various areas where this work could be continued. A first focus for future experiments could be the activation chemistry of both **3Et•** and **6a**.

In addition to the reactivity described above, a number of small molecules have been pre-examined as possible substrates for further activation chemistry with **3Et•**. Preliminary unpublished results are shown in Table 1. $B(C_6F_5)_3$ was added when no reaction was observed to form a frustrated Lewis acid radical pair, which may allow activation of substrates that do not react with a radical alone.

Table 1. Attempted activation chemistry of **3Et•** with small molecules (red: no reactivity observed, yellow: reactivity observed, but no defined product, green: reactivity observed, defined product).

	substrate only	with addition of $B(C_6F_5)_3$
S_8	Reaction observed (NMR), many species, possible scrambling products	-
tolane	Reaction observed (NMR), fitting signals for triple-bond activation, no crystals obtained	-
isonitriles	no reaction observed (NMR)	no reaction observed (NMR)
P_4	no reaction observed, P_4 signal still present in NMR	no reaction observed, P_4 signal still present in NMR
CS_2	no reaction observed (NMR)	in solution Raman spectrum indicates possible additional bands, otherwise no reactivity observed (NMR)
H_2	no reaction observed (NMR)	no reaction observed (NMR)
TEMPO	oxidation	-
$W(CO)_6$	no reaction observed (NMR)	-
Se	many additional NMR signals, no crystals	-
H_2O	Reaction observed, O-activation product	slow reaction over months by diffusion into flask, SCXRD indicates OH^- activation with $B(C_6F_5)_3$
TMS-N_3	no reaction observed (NMR + no gas evolution,	-
cyclohexadiene	no reaction observed (NMR)	-
propionaldehyde	no reaction observed (NMR)	-

By finding substrates of just the right size, it may be possible to activate molecules with **6a** via a different, cooperative pathway involving both radical centers. The concept of such a cooperative activation is shown in Scheme 18.

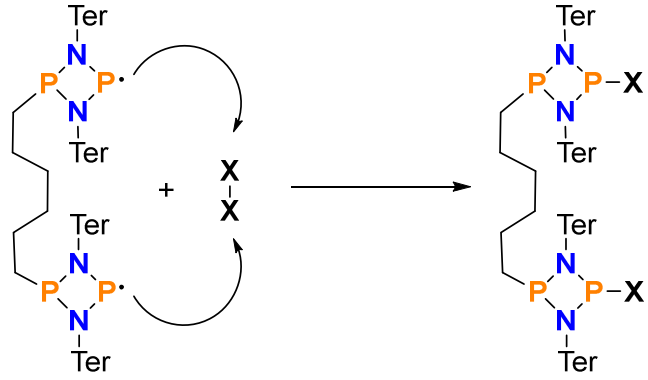

Scheme 18. Possible cooperative activation of substrates with the by disbiradical **6a**.

To prove that conformational change causes the coupling in solution seen in the recorded EPR spectra of **6a**, similar systems with less flexible linkers such as naphthyl- or xylyl- ((a) and (b) in Scheme 19) could be synthesized in the future. Another target motive might be the synthesis of triradicals ((c) and (d) in Scheme 19).

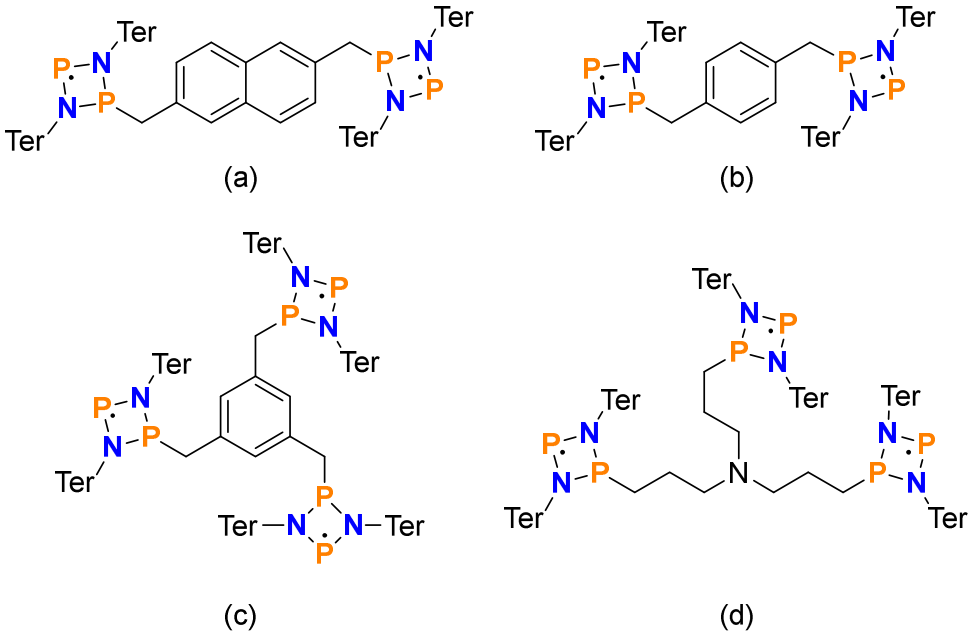

Scheme 19. Possible disbiradicals with less flexible naphtyl- and xylyl-linkers, (a) and (b), hindering conformational change. Possible triradicals that could be synthesized with suitable bromoalkanes, (c) and (d).

In addition to activating small molecules, the synthesized disbiradical may also find application as a polarizing agent in DNP-NMR spectroscopy, similar to many (dis-) biradicals such as

bisnitroxides.[78] **6a** could expand the toolbox of existing agents due to its relatively large *J*-coupling, a factor that has been suggested to contribute to a large DNP signal enhancements of nitroxide polarizing agents.[42]

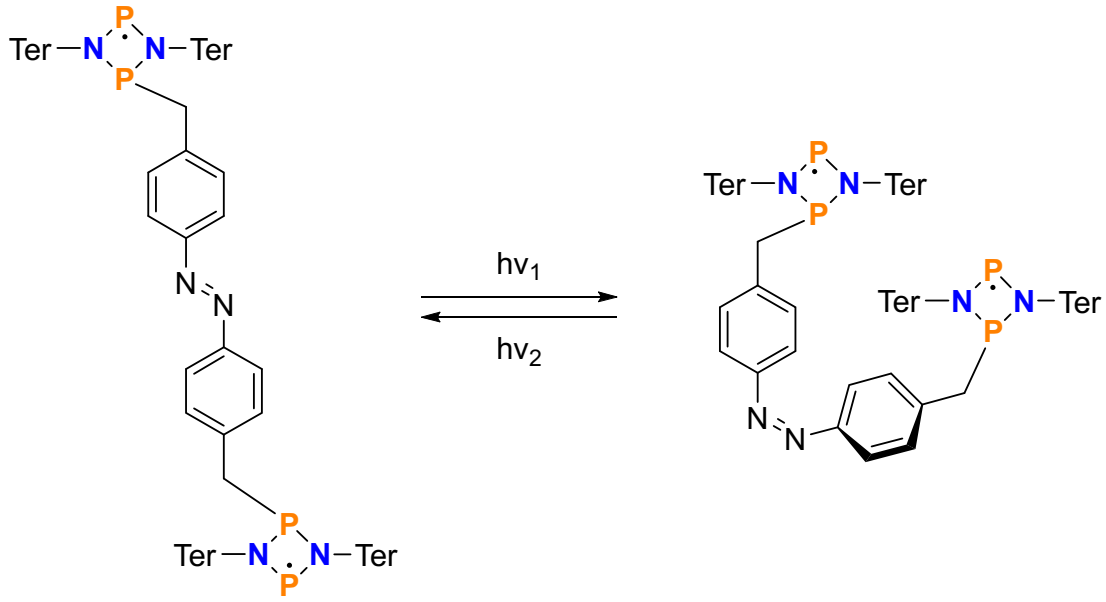

Scheme 20. Possible light switchable (dis-)biradical with a diazo- linker.

Using the bromoalkane route presented here it may also be possible to introduce a diazo linker connecting two biradical units as shown in Scheme 20. Such a system might allow the coupling between the unpaired electrons to be switched "on" and "off" by light, due to conformational changes upon irradiation at different frequencies. Nitroxide-based systems with similar capabilities have previously been investigated by FERINGA *et al.*[79]

Despite many repeated attempts the isolation of the pure radical anion **6b**$^-$ has been unsuccessful so far and remains of great interest, as this species may also offer a unique behavior in the activation of small molecules due to the fact that one phosphorus atom carries an unpaired electron and the other carries a negative charge, possibly allowing unique activation reactions.

Starting from the dibrominated compounds **2a** and **5a**, preliminary results also indicate the possibility of synthesizing phosphenium cations and dications using LEWIS acids such as $GaCl_3$, which should be further investigated.

Finally, the existing arsenic-centered biradical [$^{\bullet}As(\mu\text{-NTer})_2As^{\bullet}$][80] could be used to obtain arsenic-centered persistent radicals and an arsenic-centered disbiradical, similar to what was done with the phosphorus-centered derivatives in this work.

5 References

[1] M. Gomberg, *Ber. Dtsch. Chem. Ges.* **1900**, *33*, 3150–3163.

[2] G. N. Lewis, *J. Am. Chem. Soc.* **1916**, *38*, 762–785.

[3] W. Heisenberg, *Zeitschrift für Phys.* **1925**, *33*, 879–893.

[4] A. Hinz, J. Bresien, F. Breher, A. Schulz, *Chem. Rev.* **2023**, *123*, 10468–10526.

[5] M. Nič, J. Jirát, B. Košata, A. Jenkins, A. McNaught, Eds. , in *IUPAC Compendium of Chemical Terminology, 2nd Ed. ("The Gold Book")*, IUPAC, Research Triagle Park, NC, **2009**, pp. 168 TS-CrossRef.

[6] J. Thiele, H. Balhorn, *Ber. Dtsch. Chem. Ges.* **1904**, *37*, 1463–1470.

[7] A. E. Tschitschibabin, *Ber. Dtsch. Chem. Ges.* **1907**, *40*, 1810–1819.

[8] W. Schlenk, M. Brauns, *Ber. Dtsch. Chem. Ges.* **1915**, *48*, 661–669.

[9] E. G. Rozantsev, V. A. Golubev, M. B. Neiman, *Bull. Acad. Sci. USSR Div. Chem. Sci.* **1965**, *14*, 382–383.

[10] É. G. Rozantsev, V. A. Golubev, M. B. Neiman, Y. V Kokhanov, *Bull. Acad. Sci. USSR, Div. Chem. Sci.* **1965**, *14*, 559–560.

[11] R. M. Dupeyre, H. Lemaire, A. Rassat, *J. Am. Chem. Soc.* **1965**, *87*, 3771–3772.

[12] R. Briére, R. M. Dupeyre, H. Lemair, C. Morat, A. Rassat, *Bull. Soc. Chim. Fr.* **1965**, *11*, 3290.

[13] E. K. Zavoisky, *PhD Thesis, Kazan University,* **1944**.

[14] I D Morozova, M E Dyatkina, *Russ. Chem. Rev.* **1968**, *37*, 376.

[15] E. Niecke, A. Fuchs, F. Baumeister, M. Nieger, W. W. Schoeller, *Angew. Chem.* **1995**, *107*, 640–642.

[16] D. Scheschkewitz, H. Amii, H. Gornitzka, W. W. Schoeller, D. Bourissou, G. Bertrand, *Science* **2002**, *295*, 1880 LP – 1881.

[17] T. Vogler, A. Studer, *Synthesis (Stuttg).* **2008**, *2008*, 1979–1993.

[18] S. L. Hinchley, C. A. Morrison, D. W. H. Rankin, C. L. B. Macdonald, R. J. Wiacek, A. H. Cowley, M. F. Lappert, G. Gundersen, J. A. C. Clyburne, P. P. Power, *Chem.*

Commun. **2000**, 2045–2046.

[19] P. Agarwal, N. A. Piro, K. Meyer, P. Müller, C. C. Cummins, *Angew. Chem. Int. Ed.* **2007**, *46*, 2956.

[20] S. Ishida, F. Hirakawa, T. Iwamoto, *J. Am. Chem. Soc.* **2011**, *133*, 12968–12971.

[21] S. Ito, M. Kikuchi, M. Yoshifuji, A. J. Arduengo III, T. A. Konovalova, L. D. Kispert, *Angew. Chem. Int. Ed.* **2006**, *45*, 4341–4345.

[22] J.-P. Bezombes, P. B. Hitchcock, M. F. Lappert, J. E. Nycz, *Dalton Trans.* **2004**, 499–501.

[23] N. A. Giffin, A. D. Hendsbee, T. L. Roemmele, M. D. Lumsden, C. C. Pye, J. D. Masuda, *Inorg. Chem.* **2012**, *51*, 11837–11850.

[24] N. J. Hill, G. Reeske, A. H. Cowley, *Main Group Chem.* **2010**, *9*, 5–10.

[25] N. A. Giffin, A. D. Hendsbee, J. D. Masuda, *Dalton Trans.* **2016**, *45*, 12636–12638.

[26] A. Schulz, *Dalton Trans.* **2018**, *47*, 12827–12837.

[27] J. Rosenboom, F. Taube, L. Teichmeier, A. Villinger, M. Reinhard, S. Demeshko, M. Bennati, J. Bresien, B. Corzilius, A. Schulz, *Angew. Chem. Int. Ed.* **2024**, *63*, e202318210.

[28] M. Abe, *Chem. Rev.* **2013**, *113*, 7011–7088.

[29] J. Bresien, L. Eickhoff, A. Schulz, E. Zander, in *Comprehensive Inorganic Chemistry III* (Eds.: J. Reedijk, K.R.B.T.-C.I.C.I.I.I. (Third E. Poeppelmeier), Elsevier, Oxford, **2023**, pp. 165–233.

[30] T. Beweries, R. Kuzora, U. Rosenthal, A. Schulz, A. Villinger, *Angew. Chem. Int. Ed.* **2011**, *50*, 8974–8978.

[31] L. Chojetzki, A. Schulz, A. Villinger, R. Wustrack, *Zeitschrift für Anorg. und Allg. Chemie* **2020**, *646*, 614–624.

[32] A. Hinz, A. Schulz, A. Villinger, *Angew. Chem. Int. Ed.* **2016**, *55*, 12214–12218.

[33] J. Bresien, T. Kröger-Badge, S. Lochbrunner, D. Michalik, H. Müller, A. Schulz, E. Zander, *Chem. Sci.* **2019**, *10*, 3486–3493.

[34] A. Brückner, A. Hinz, J. B. Priebe, A. Schulz, A. Villinger, *Angew. Chem. Int. Ed.* **2015**, *54*, 7426–7430.

[35] G. Wittig, M. Leo, *Ber. Dtsch. Chem. Ges.* **1928**, *61*, 854–862.

[36] H. S. Jarrett, G. J. Sloan, W. R. Vaughan, *J. Chem. Phys.* **1956**, *25*, 697–701.

[37] E. Müller, R. Mayer, K. Scheffler, *Z. Naturforsch., B: J. Chem. Sci.* **1958**, *13*, 825.

[38] S. Macholl, H. Jóhannesson, J. H. Ardenkjaer-Larsen, *Phys. Chem. Chem. Phys.* **2010**, *12*, 5804–5817.

[39] B. D. Koivisto, R. G. Hicks, *Coord. Chem. Rev.* **2005**, *249*, 2612–2630.

[40] J. Soetbeer, P. Gast, J. J. Walish, Y. Zhao, C. George, C. Yang, T. M. Swager, R. G. Griffin, G. Mathies, *Phys. Chem. Chem. Phys.* **2018**, *20*, 25506–25517.

[41] R. Harrabi, T. Halbritter, F. Aussenac, O. Dakhlaoui, J. van Tol, K. K. Damodaran, D. Lee, S. Paul, S. Hediger, F. Mentink-Vigier, et al., *Angew. Chem. Int. Ed.* **2022**, *61*, e202114103.

[42] G. Menzildjian, J. Schlagnitweit, G. Casano, O. Ouari, D. Gajan, A. Lesage, *Chem. Sci.* **2023**, *14*, 6120–6148.

[43] B. Bleaney, K. D. Bowers, *Proc. R. Soc. London. Ser. A. Math. Phys. Sci.* **1952**, *214*, 451–465.

[44] P. Ravat, M. Baumgarten, *Phys. Chem. Chem. Phys.* **2015**, *17*, 983–991.

[45] T. Stuyver, B. Chen, T. Zeng, P. Geerlings, F. De Proft, R. Hoffmann, *Chem. Rev.* **2019**, *119*, 11291–11351.

[46] J. Bresien, L. Eickhoff, A. Schulz, E. Zander, in *Comprehensive Inorganic Chemistry III* (Eds.: J. Reedijk, K.R. Poeppelmeier), Elsevier, **2023**, pp. 165–233.

[47] A. Hinz, PhD thesis, University of Rostock, **2015**.

[48] A. Hinz, A. Schulz, A. Villinger, *Chem. Commun.* **2016**, *52*, 6328–6331.

[49] A. Hinz, R. Kuzora, U. Rosenthal, A. Schulz, A. Villinger, *Chem. – A Eur. J.* **2014**, *20*, 14659–14673.

[50] J. Rosenboom, A. Villinger, A. Schulz, J. Bresien, *Dalton Trans.* **2022**, *51*, 13479–13487.

[51] V. V. Zhivonitko, J. Bresien, A. Schulz, I. V. Koptyug, *Phys. Chem. Chem. Phys.* **2019**, *21*, 5890–5893.

[52] J. Rosenboom, L. Chojetzki, T. Suhrbier, J. Rabeah, A. Villinger, R. Wustrack, J.

Bresien, A. Schulz, *Chem. Eur. J.* **2022**, *28*, e202200624.

[53] K. Takeuchi, M. Ichinohe, A. Sekiguchi, *J. Am. Chem. Soc.* **2011**, *133*, 12478–12481.

[54] H. Amii, L. Vranicar, H. Gornitzka, D. Bourissou, G. Bertrand, *J. Am. Chem. Soc.* **2004**, *126*, 1344–1345.

[55] X. Chen, C. Hu, X. Zhang, S. Liu, Y. Mei, G. Hu, L. L. Liu, Z. Li, C.-Y. Su, *Inorg. Chem.* **2021**, *60*, 5771–5778.

[56] F. Neese, F. Wennmohs, U. Becker, C. Riplinger, *J. Chem. Phys.* **2020**, *152*, 224108.

[57] F. Neese, *Wiley Interdiscip. Rev.-Comput. Mol. Sci.* **2012**, *2*, 73–78.

[58] F. Neese, *J. Chem. Phys.* **2003**, *118*, 3939–3948.

[59] F. Neese, *J. Chem. Phys.* **2005**, *122*, 34107.

[60] F. Neese, *eMagRes* **2017**, 1–22.

[61] F. Neese, *J. Chem. Phys.* **2001**, *115*, 11080–11096.

[62] F. Neese, *Wiley Interdiscip. Rev.-Comput. Mol. Sci.* **2018**, *8*, e1327.

[63] *Gaussian 09, Revision E.01*, M. J. Frisch, G. W. Trucks, H. B. Schlegel, G. E. Scuseria, M. A. Robb, J. R. Cheeseman, G. Scalmani, V. Barone, B. Mennucci, G. A. Petersson, H. Nakatsuji, M. Caricato, X. Li, H. P. Hratchian, A. F. Izmaylov, J. Bloino, G. Zheng, J. L. Sonnenberg, M. Hada, M. Ehara, K. Toyota, R. Fukuda, J. Hasegawa, M. Ishida, T. Nakajima, Y. Honda, O. Kitao, H. Nakai, T. Vreven, J. A. Montgomery Jr., J. E. Peralta, F. Ogliaro, M. Bearpark, J. J. Heyd, E. Brothers, K. N. Kudin, V. N. Staroverov, T. Keith, R. Kobayashi, J. Normand, K. Raghavachari, A. Rendell, J. C. Burant, S. S. Iyengar, J. Tomasi, M. Cossi, N. Rega, J. M. Millam, M. Klene, J. E. Knox, J. B. Cross, V. Bakken, C. Adamo, J. Jaramillo, R. Gomperts, R. E. Stratmann, O. Yazyev, A. J. Austin, R. Cammi, C. Pomelli, J. W. Ochterski, R. L. Martin, K. Morokuma, V. G. Zakrzewski, G. A. Voth, P. Salvador, J. J. Dannenberg, S. Dapprich, A. D. Daniels, O. Farkas, J. B. Foresman, J. V. Ortiz, J. Cioslowski, D. J. Fox, Gaussian, Inc., Wallingford CT, **2013**.

[64] J. P. Perdew, K. Burke, M. Ernzerhof, *Phys. Rev. Lett.* **1996**, *77*, 3865–3868.

[65] J. P. Perdew, K. Burke, M. Ernzerhof, *Phys. Rev. Lett.* **1997**, *78*, 1396–1396.

[66] S. Grimme, S. Ehrlich, L. Goerigk, *J. Comput. Chem.* **2011**, *32*, 1456–1465.

[67] S. Grimme, J. Antony, S. Ehrlich, H. Krieg, *J. Chem. Phys.* **2010**, *132*, 154104.

[68] E. Ramos-Cordoba, P. Salvador, E. Matito, *Phys. Chem. Chem. Phys.* **2016**, *18*, 24015–24023.

[69] E. Ramos-Cordoba, E. Matito, *J. Chem. Theory Comput.* **2017**, *13*, 2705–2711.

[70] T. Lu, F. Chen, *J. Comput. Chem.* **2012**, *33*, 580–592.

[71] S. Grimme, *J. Chem. Theory Comput.* **2019**, *15*, 2847–2862.

[72] P. Pracht, F. Bohle, S. Grimme, *Phys. Chem. Chem. Phys.* **2020**, *22*, 7169–7192.

[73] S. Grimme, F. Bohle, A. Hansen, P. Pracht, S. Spicher, M. Stahn, *J. Phys. Chem. A* **2021**, *125*, 4039–4054.

[74] S. Spicher, S. Grimme, *Angew. Chem. Int. Ed.* **2020**, *59*, 15665–15673.

[75] C. Bannwarth, S. Ehlert, S. Grimme, *J. Chem. Theory Comput.* **2019**, *15*, 1652–1671.

[76] E. G. Bagryanskaya, D. N. Polovyanenko, M. V Fedin, L. Kulik, A. Schnegg, A. Savitsky, K. Möbius, A. W. Coleman, G. S. Ananchenko, J. A. Ripmeester, *Phys. Chem. Chem. Phys.* **2009**, *11*, 6700–6707.

[77] S. Stoll, D. Goldfarb, John Wiley & Sons, **2018**.

[78] A. G. M. Rankin, J. Trébosc, F. Pourpoint, J.-P. Amoureux, O. Lafon, *Solid State Nucl. Magn. Reson.* **2019**, *101*, 116–143.

[79] J. Wang, L. Hou, W. R. Browne, B. L. Feringa, *J. Am. Chem. Soc.* **2011**, *133*, 8162–8164.

[80] S. Demeshko, C. Godemann, R. Kuzora, A. Schulz, A. Villinger, *Angew. Chem. Int. Ed.* **2013**, *52*, 2105–2108.

6 Publications

This chapter contains the three publications on phosphorus-centered radicals and biradicals originating from my PhD phase.

During the whole project, Axel Schulz, my PhD supervisor, provided the infrastructure and coordinated the research. We regularly discussed results and further research steps and he revised all three manuscripts.

Generally, all authors discussed results and revised a finalized version of the manuscript before submission.

The contributions to the papers are outlined below.

1. **Concerted addition of aldehydes to the singlet biradical [P(μ-NTer)]$_2$**

(J. Rosenboom, A. Villinger, A. Schulz, J. Bresien, *Dalton Trans.*, **2022**, 51, 13479-13487.)

I carried all the experimental work and first structural optimizations for this publication. Jonas Bresien carried out the mechanistic calculations. Alexander Villinger determined and refined the solid-state structures from SCXRD experiments. I wrote the supporting information and co-wrote the manuscript. My overall contribution amounts to approx. 50%.

2**. Radical reactivity of the biradical [˙P(μ-NTer)$_2$P˙] and isolation of a persistent phosphorus-centered monoradical [˙P(μ-NTer)$_2$P-Et]**

(J. Rosenboom, L. Chojetzki, T. Suhrbier, J. Rabeah, A. Villinger, R. Wustrack, J. Bresien, A. Schulz, *Chem. Eur. J.* **2022**, *28*, e202200624.)

I carried out all synthetic experimental work for this paper. Preliminary investigations on the addition of bromoalkanes to **1** were carried out by Lukas Chojetzki during his PhD project and by me during my master's thesis. The DFT calculations on the thermodynamics of the radical reactions were performed by me and the CCSD(T) by Jonas Bresien. Jabor Rabeah performed the EPR experiments. The EPR calculations were performed by Jonas Bresien. Alexander

Villinger determined and refined the solid-state structures from SCXRD experiments. I wrote the supporting information and co-wrote the manuscript.

Overall, my own contribution amounts to approx. 50%.

3**. Rational Design of a Phosphorus-centered Disbiradical**

(J. Rosenboom, F. Taube, L. Teichmeier, A. Villinger, M. Reinhard, S. Demeshko, M. Bennati, J. Bresien, B. Corzilius, A. Schulz, *Angew. Chem. Int. Ed.* **2024**, 63, e202318210.)

I carried out the synthetic experimental work for this paper. The optimization of the synthesis of **6a** and recording of the remaining analytical data were performed by Leon Teichmeier during his bachelor's thesis under my supervision. Florian Taube performed the EPR measurements. The simulations of the EPR-spectra were done by Florian Taube and me for the room temperature spectra, in case of the temperature dependent spectra and single-crystal data solely by Florian Taube. Björn Corzilius greatly contributed to the design, discussion and simulation of the EPR experiments. The computations were carried out by Jonas Bresien. Alexander Villinger determined and refined the solid-state structures from SCXRD experiments. Maik Reinhard performed the Q-Band EPR measurements of **6a**. Serhiy Demeshko performed the SQUID-measurements of **6a**. I wrote the supporting information and co-wrote the manuscript the paper.

My own contribution amounts to approx. 40%.

6.1 Concerted addition of aldehydes to the singlet biradical [P(μ-NTer)]$_2$

J. Rosenboom, A. Villinger, A. Schulz,* J. Bresien*

Dalton Trans., **2022**, 51, 13479-13487.

DOI: 10.1039/D2DT02229J

Dalton Transactions

ROYAL SOCIETY OF CHEMISTRY

PAPER

View Article Online
View Journal | View Issue

Cite this: *Dalton Trans.*, 2022, **51**, 13479

Concerted addition of aldehydes to the singlet biradical [P(μ-NTer)]$_2$†

Jan Rosenboom, [a] Alexander Villinger, [a] Axel Schulz *[a,b] and Jonas Bresien *[a]

Received 11th July 2022,
Accepted 17th August 2022

DOI: 10.1039/d2dt02229j

rsc.li/dalton

The reaction of the singlet biradical [P(μ-NTer)]$_2$ with various aldehydes selectively yielded the corresponding [2.1.1]-bicyclic addition products in a very fast reaction. All products were fully characterized, including by NMR and vibrational spectroscopy as well as single-crystal X-ray diffraction. The mechanism of the addition was investigated theoretically using high-level *ab initio* methods (CCSD(T) with triple- and quadruple-zeta basis sets) and corresponds to a concerted cycloaddition reaction with a very low activation barrier. For comparison, the mechanisms of the literature-known cycloadditions of H_2, alkenes, and alkynes were also studied, indicating a similar reaction profile for all unsaturated reactants.

Introduction

Singlet biradicals (biradicaloids) are highly reactive species with two antiferromagnetically coupled radical centres,[1–9] which are often formed as intermediates in bond-breaking and bond-formation processes.[5,7,10] During the last 20–25 years, however, a lot of progress has been made to also synthesize stable singlet biradicals that can be isolated in substance. The stability of these compounds mostly depends on two key factors: (i) the localization of the radical centres at (heavier) main group elements and (ii) kinetic stabilization by sterically demanding substituents.[9] In particular, research in the field of cyclic biradicals that can formally be derived from cyclobutanediyl[11,12] (Chart 1) has produced a variety of derivatives that are stable for long periods of time under inert conditions[13–30] or even when exposed to air.[31]

These formal hetero-cyclobutanediyls are known to readily activate small molecules in formal 1,1- or 1,3-addition reactions. As singlet biradicals, they can undergo either stepwise radical reactions[29,32,33] or concerted ("closed-shell") reactions,[17,19,34–40] depending on the strength of the antiferromagnetic coupling between the radical electrons and the reaction conditions.[8] It is worthy to note, though, that the classification as either radical or concerted reaction is frequently based on phenomenological observations alone, while the actual mechanisms of the addition reactions to hetero-cyclobutanediyls have often not been investigated in detail yet.

Our group is particularly interested in ring systems based on group 15 elements, such as the singlet biradical [P(μ-NTer)]$_2$ (**1**, structure type **F** in Chart 1; Ter = 2,6-dimesitylphenyl), which was first synthesized in 2011.[28] With a moderate biradical character of approx. 25%,[28,41] its electrons are rather strongly antiferromagnetically coupled. Combined with its small HOMO–LUMO gap (which is characteristic of all singlet biradicals),[8,9] it is therefore expected to readily undergo typical (closed-shell) cycloaddition reactions. Consequently, biradical **1** was used in a large variety of activation reactions, including a number of unsaturated (*e.g.* alkynes, alkenes, ketones)[17,34,40,42–46] and saturated compounds (*e.g.* H_2, chalcogens, haloalkanes)[17,33–35] as substrates (Scheme 1). Indeed, most of these addition reactions led selectively to *syn*-1,3-addition products, indicating a concerted (closed-shell) mechanism. One notable exemption was the addition of alkyl

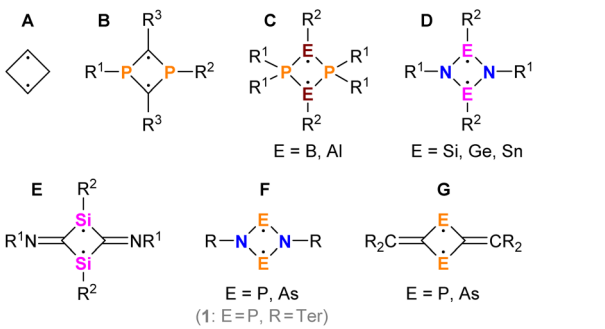

Chart 1 Transient cyclobutanediyl (**A**) and examples of symmetrical singlet hetero-cyclobutanediyls (**B–G**, R = sterically demanding substituents).[13–31]

[a]*Institute of Chemistry, University of Rostock, Albert-Einstein-Str. 3a, 18059 Rostock, Germany. E-mail: jonas.bresien@uni-rostock.de, axel.schulz@uni-rostock.de*
[b]*Leibniz Institute for Catalysis, Albert-Einstein-Str. 29a, 18059 Rostock, Germany*

†Electronic supplementary information (ESI) available: Experimental details, synthetic protocols, full set of analytical data, computational details. CCDC 2125924–2125928. For ESI and crystallographic data in CIF or other electronic format see DOI: https://doi.org/10.1039/d2dt02229j

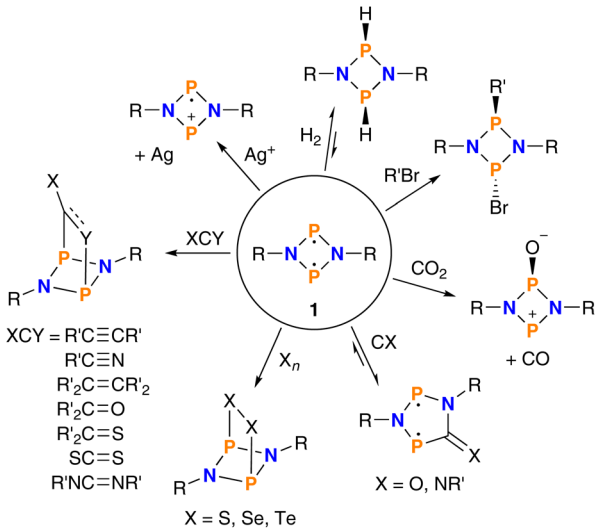

Scheme 1 Reactivity of the singlet biradical [P(μ-NTer)]$_2$ (**1**, R = Ter; R′ = alkyl/aryl).[17,33–35,40,42–46] For further examples of addition reactions, also including different hetero-cyclobutanediyls, see ref. 9.

bromides (R′Br, Scheme 1), which almost exclusively yielded *anti*-addition products and was recently shown to follow a radical mechanism.[33]

While the addition of a ketone to biradical **1** had previously been described,[34] aldehydes were still missing in the library of suitable addition reagents. We therefore set out to synthesize a few addition products of **1** with aldehydes as well as theoretically investigate the mechanism of this addition reaction. As the related additions of alkenes and alkynes had not been investigated mechanistically either, we included these in our computations for comparison.

Results and discussion

Synthesis

We chose two commercially available aldehydes (PhCHO, EtCHO) as well as two aldehydes that were in stock in our lab (*p*-NO_2–C_6H_4–CHO, *p*-Cl–C_6H_4–CHO) as test reagents, so as to cover different electronic situations, *i.e.* with different electron-donating and electron-withdrawing groups. All aldehydes were thoroughly dried and purified prior to use either by distillation or sublimation (for details, please see ESI†) to prevent (partial) hydrolysis or oxidation of the biradical **1**. After mixing the aldehydes with **1** in benzene or toluene solution at ambient temperature, immediate reactions were observed, as indicated by the disappearance of the intense orange colour of the biradical **1**. In the ^{31}P NMR spectra, the product formation could be verified by the appearance of an AX spin system (δ_A = 176–180, δ_X = 212–216 ppm; $^2J(^{31}P,^{31}P)$ = 14–17 Hz; toluene-d_8) that could be assigned to the expected reaction products **2**–**5** (Scheme 2). All reactions selectively yielded the *syn*-addition products, which could be isolated in yields of 57–84%.

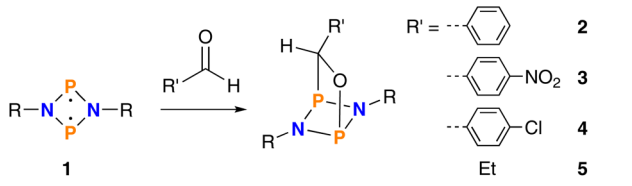

Scheme 2 Reaction of [P(μ-NTer)]$_2$ (**1**, R = Ter) with aldehydes.

Structural characterization

Crystallization of all products resulted in single crystals suitable for X-ray diffraction. All compounds crystallized in centrosymmetric space groups (**2**: $P2_1/c$, **3**: $P\bar{1}$, **4**: $P2_1/n$, **5**: $P2_1/c$) with four molecules per unit cell. In the case of compound **3**, there are two independent molecules in the asymmetric unit. Due to their similarity, the structure of only one of them will be discussed here.

The central motif of all four addition products is a heterobicyclo[2.1.1]hexane, with two phosphorus bridgehead atoms and a CO bridge that is created by the former carbonyl group of the aldehydes (Fig. 1). All N–P distances (1.727(4)–1.776(2) Å) are in the typical range of polarized N–P single bonds (*cf.* $\sum r_{cov}$(N–P) = 1.82 Å (ref. 47) or *d*(N–P) = 1.74 Å when consider-

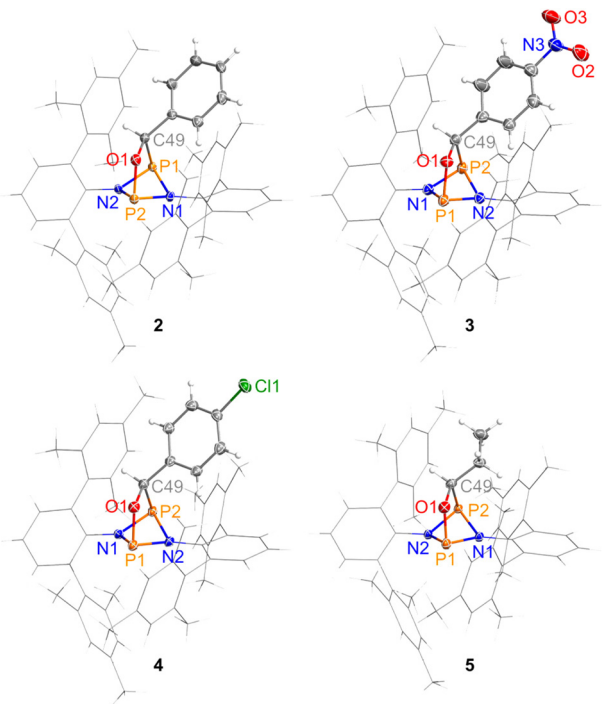

Fig. 1 Molecular structures of the addition products **2**–**5** in the crystal. Thermal ellipsoids at 50% probability (123 K). Ter substituents depicted as wireframe for clarity. Selected bond lengths (Å): **2**: N1–P1 1.776(1), N1–P2 1.743(1), N2–P1 1.740(1), N2–P2 1.734(2), P1–C49 1.911(2), P2–O1 1.672(1), O1–C49 1.450(2); **3**: N1–P1 1.727(4), N1–P2 1.734(4)(4), N2–P1 1.745(4), N2–P2 1.774(4), P2–C49 1.927(4), P1–O1 1.680(2), O1–C49 1.455(5); **4**: N1–P1 1.739(2), N1–P2 1.740(1), N2–P1 1.745(1), N2–P2 1.776(2), P2–C49 1.916(1), P1–O1 1.673(1), O1–C49 1.455(2); **5**: N1–P1 1.736(1), N1–P2 1.770(1), N2–P1 1.753(1), N2–P2 1.746(1), P2–C49 1.900 (2), P1–O1 1.656(1), O1–C49 1.451(2). For further data, see Table S4.†

ing the difference in electronegativity according to Schomaker and Stevenson).[48] The same holds true for the P–O distances (1.656(1)–1.680(2) Å; *cf.* $\sum r_{cov}$(P–O) = 1.74 Å, *d*(P–O) = 1.63 Å). In contrast, the P–C distances (1.900(2)–1.927(4) Å) are elongated compared to typical single bond lengths (*cf.* $\sum r_{cov}$(P–C) = 1.86 Å, *d*(P–C) = 1.83 Å), an effect that was also observed, for example, in adducts of **1** with acetone (1.92(1) Å)[34] or (thio)xanthione (1.975(2), 1.968(3) Å).[46] This is likely due to Pauli repulsion between the substituents at the aldehyde moiety and the bulky Ter groups, as well as the general strained nature of the bicyclic compounds. The C–O distances of the former carbonyl groups (1.450(2)–1.455(5) Å) are, as expected, in the range of typical C–O single bonds (*cf.* 1.43 Å in ethers).[49] The bicyclic structures are highly strained, as indicated by small P–N–P (90.8(1)–92.40(6)°; *cf.* **1**: 99.44(6)°)[28] as well as N–P–N angles (78.79(5)–80.1(2)°, *cf.* **1**: 80.56(8)°). In contrast to the planar biradical **1**, the N_2P_2 ring system in the products **2–5** is highly puckered (N–P–P–N dihedral angle: 131.73(8)–133.5(2)°). While the structures of all adducts are quite similar, it can be noted that the P–C and P–O distances are shortest in **5** (1.900(2), 1.656(1) Å), *i.e.* the derivative with both the smallest and most electron-donating substituent (Et), and longest in **3** (1.927(4), 1.680(2) Å) with the most electron-withdrawing substituent (*p*-NO_2–C_6H_5). The other two derivatives **2** and **4** have intermediate P–C and P–O distances (av. 1.915, 1.672 Å) that are identical within their uncertainty of measurement (Table S4†).

Mechanism

To gain further insight into the addition reactions, we calculated their Gibbs free energies of reaction at the DLPNO-CCSD(T)/def2-TZVP//PBE-D3/def2-TZVP[50–58] level of theory (for computational details, see the ESI, p. S30†). All addition reactions are highly exergonic (ΔG°_{298K} = −80 to −90 kJ mol^{-1}, cf. Fig. 5, top left, Table S9†). This is in line with the fact that we did not observe a reverse reaction even at elevated temperatures, contrary to the addition of, *e.g.*, thioketones or dimethylbutadiene.[40,46]

The symmetry of the frontier orbitals (see Fig. 2 for a model system) indicated a concerted mechanism for the addition of aldehydes to **1**. The search for a transition state (TS), however, proved to be rather difficult. Our initial attempts to locate a TS on the potential energy surface (PES) of the reaction **1** + PhCHO indicated that the reaction is barrierless (with respect to the electronic energy) at the PBE-D3/def2-TZVP level of theory. We therefore opted to investigate a model reaction, $[P(\mu\text{-NH})]_2$ (**1H**) + H_2CO, in more detail. Using typical DFT methods such as PBE-D3, PBE0-D3,[59] B3LYP-D3,[60] or M06-2X,[61] we could not locate a transition state for the model system either. However, using *ab initio* MO methods, the expected concerted TS was found (Fig. 3a). For reliable structures and energies, the model reaction was therefore investigated at the CCSD(T)/def2-TZVP level of theory, while final electronic energies were computed at the DLPNO-CCSD(T)/

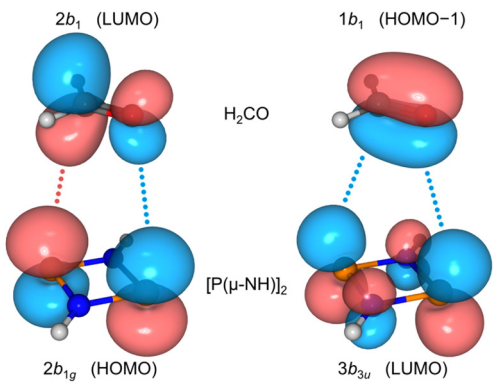

Fig. 2 Schematic representation of the interaction of the frontier MOs of the model system **1H** (D_{2h} symmetry) and H_2CO (C_{2v}).

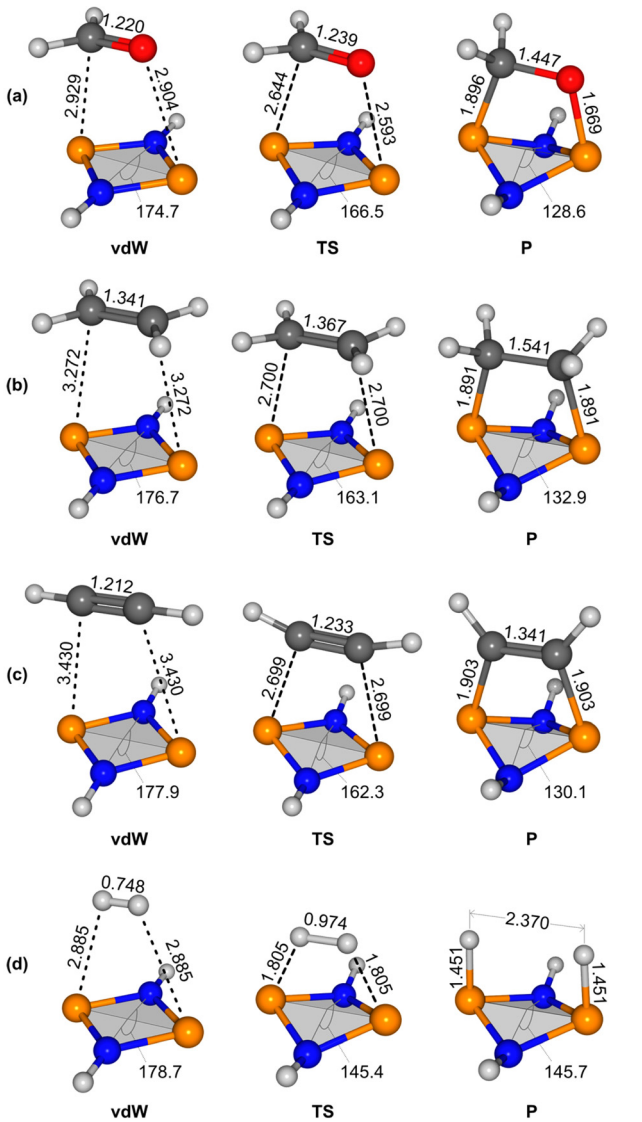

Fig. 3 Calculated structures (CCSD(T)/def2-TZVP) of the van der Waals (**vdW**) complexes, transition states (**TS**), and products (**P**) of the addition of (a) formaldehyde, (b) ethylene, (c) acetylene, and (d) dihydrogen to the model biradical **1H**. Selected distances (Å) and dihedral angles (°) are given.

def2-QZVPP level (Fig. 4; see also Table S9†). Here, the coupled-cluster treatment of the wavefunction ensures that the moderate biradical character of **1H** is adequately represented (*cf.* ESI†). The coupled-cluster results verify that the potential energy surface for adduct formation is indeed very flat, with a TS only 1.6 kJ mol^{-1} ($U_0 = E_{tot}$ + ZPE) above the van der Waals (vdW) complex **1H**···OCH_2, which in turn is 13.1 kJ mol^{-1} more stable than the separated starting materials. Thus, the TS is actually lower in energy than the isolated reactant molecules, rendering the overall cycloaddition reaction essentially barrierless on the electronic PES including the zero-point energy (ZPE). The flatness of the PES is also reflected in the similar structural parameters of the vdW complex and TS, especially with respect to the P–C and P–O distances, which only change by about 0.3 Å between the two stationary points (Fig. 3a).

When looking at the Gibbs free energy surface (Fig. 5), the TS for the formaldehyde addition to **1H** is 23.1 kJ mol^{-1} higher in energy than the starting materials due to the change in entropy. That is, the activation barrier of the reaction is effectively an entropic barrier, arising from the fact that two molecules must interact to form the final addition product. This low activation barrier for the model system agrees well with the observed, virtually instantaneous reactions between **1** and the different aldehydes.

To put the reaction path of the concerted cycloaddition of formaldehyde into perspective, we also calculated the concerted cycloadditions of ethylene, acetylene, and H_2 to **1H** at the same level of theory (Fig. 3–5). As indicated above, the addition mechanisms of the two unsaturated hydrocarbons had previously been proposed but not been investigated in detail.[17,34] Considering that ethylene can formally be derived from formaldehyde by isolobal replacement of the O atom by a CH_2 group, it is not surprising that their reaction profiles are

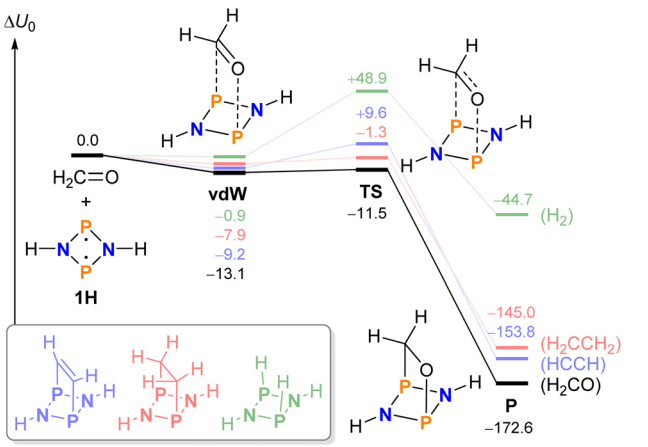

Fig. 4 Schematic representation of the potential energy surface (PES, incl. ZPE) of the addition of formaldehyde to biradical **1H** (black line). The analogous reactions profiles of the additions of acetylene (blue), ethylene (red), and dihydrogen (green) are shown for comparison (the resulting addition products **P** are shown in the inset). Computed at the DLPNO-CCSD(T)/def2-QZVPP//CCSD(T)/def2-TZVP level of theory.

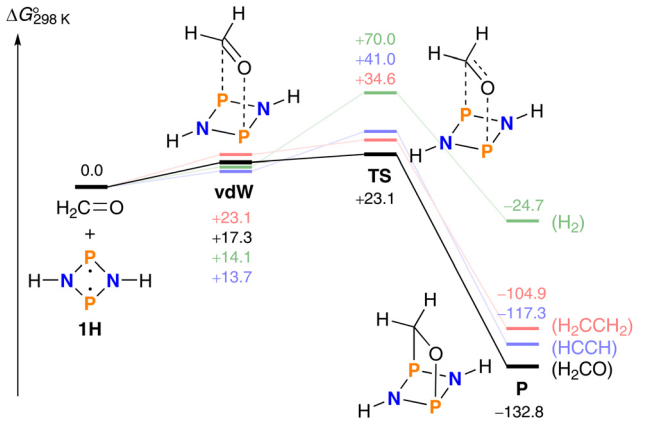

Fig. 5 Schematic representation of the Gibbs free energy surface (298.15 K, $c°$ = 1 mol L^{-1}) of the addition of formaldehyde to biradical **1H** (black line). The analogous reactions profiles of the additions of acetylene (blue), ethylene (red), and dihydrogen (green) are shown for comparison. Computed at the DLPNO-CCSD(T)/def2-QZVPP//CCSD(T)/def2-TZVP level of theory.

quite similar (red and black lines in Fig. 4 and 5), including an essentially entropic activation barrier (C_2H_4: $\Delta U_0^{\ddagger}$ = −1.3 kJ mol^{-1}, $\Delta G_{298K}^{\ddagger}$ = +34.6 kJ mol^{-1}). In the case of acetylene (blue line), there is a somewhat more pronounced activation barrier with a significant electronic contribution ($\Delta U_0^{\ddagger}$ = +9.6 kJ mol^{-1}, $\Delta G_{298K}^{\ddagger}$ = +41.0 kJ mol^{-1}). In contrast, the activation barrier for the addition of H_2 to **1H** is significantly higher (green line; $\Delta U_0^{\ddagger}$ = + 48.9 kJ mol^{-1}, $\Delta G_{298K}^{\ddagger}$ = +70.0 kJ mol^{-1}), which is in agreement with previous calculations.[62] Additionally, the H_2 adduct is significantly less stable than the other addition products ($\Delta G_{298\,K}^{\circ}$ = −24.7 kJ mol^{-1}), in accord with the reversibility of the reaction observed in the experiment. It is worthy to note that the barrier for the reverse reaction (*i.e.*, H_2 dissociation, $\Delta G_{298K}^{\ddagger}$ = 94.7 kJ mol^{-1}) is in excellent agreement with experimental results ($\Delta G_{298K}^{\ddagger} \approx 96$ kJ mol^{-1}),[62] showing that the choice of the model system is reasonable. All computed reaction barriers are low enough to allow for fast addition reactions at room temperature, in agreement with the experimentally observed quick addition reactions that were completed within minutes.[34,35,62] The addition of formaldehyde proceeds with the lowest barrier, followed by ethylene and acetylene, while the activation barrier for H_2 addition is the highest.

From a qualitative point of view, the structures of the computed vdW, TS and product structures of the different cycloadditions are quite similar (Fig. 3), especially when comparing the three unsaturated reactants formaldehyde, ethylene, and acetylene. The changes between the vdW and TS structures are generally small; most of the structural changes occur after the TS when forming the addition products. A more detailed look at the vdW complexes reveals that the intermolecular distances increase with an increasing activation barrier: while the P···C and P···O distances (2.929, 2.904 Å) in the vdW complex **1H**···OCH_2 are rather short, the P···C distances in the vdW complex **1H**···C_2H_2 (3.430 Å) are close to the sum of van der

Waals radii (*cf.* $\sum r_{vdW}$(P···C) = 3.50 Å).[63] The same holds true for the vdW complex **1H**···H_2 with P···H distances of 2.885 Å (*cf.* $\sum r_{vdW}$(P···H) = 2.90 Å).

The cycloaddition of unsaturated hydrocarbons to other singlet biradicals such as ozone has previously been investigated.[64] It was shown that the usage of high-level *ab initio* methods is crucial to obtain reliable results. In particular, for the cycloaddition of ozone to ethylene and acetylene, low activation barriers were found (C_2H_4: $\Delta U_0^{\ddagger}$ = +22.2 kJ mol^{-1}, $\Delta G_{298K}^{\ddagger}$ = +57.3 kJ mol^{-1}; C_2H_2: $\Delta U_0^{\ddagger}$ = +39.3 kJ mol^{-1}, $\Delta G_{298K}^{\ddagger}$ = +78.7 kJ mol^{-1}),[64] which display, despite being higher than those of the cycloadditions to **1H**, the same energetic trends. That is, the addition of ethylene was predicted to be significantly faster than the addition of acetylene.

Finally, to estimate the activation barrier for the "true" reaction, we searched for the TS and vdW complex of **1** + PhCHO using the B3LYP-D3 functional (which outperformed PBE(0)-D3 in case of the model system). Indeed, a vdW complex could be located, with structural parameters of the N_2P_2CO core (P–C 2.810, P–O 2.761, C–O 1.233 Å) in between the vdW and TS structures of the model system (*cf.* Fig. 3a). While our attempts to optimize the TS structure remained unsuccessful, the vdW structure should give a reasonable estimate at the barrier height, given the overall flatness of the PES in the vicinity of the vdW complex and TS. With ΔU_0 = −7.8 kJ mol^{-1} and $\Delta G^{\circ}_{298\,K}$ = +46.1 kJ mol^{-1} for the formation of the vdW complex (DLPNO-CCSD(T)/def2-TZVP//B3LYP-D3/def2-TZVP), the barrier is expected to be purely of entropic nature, indicating a very fast reaction like in the case of the model system and in agreement with experimental observation.

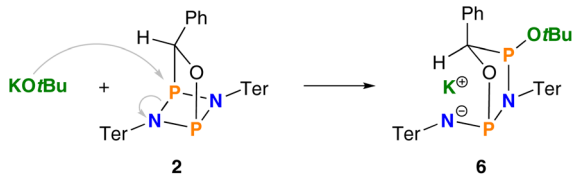

Scheme 3 Reaction of **2** and KO*t*Bu, leading to the formal addition product **6**.

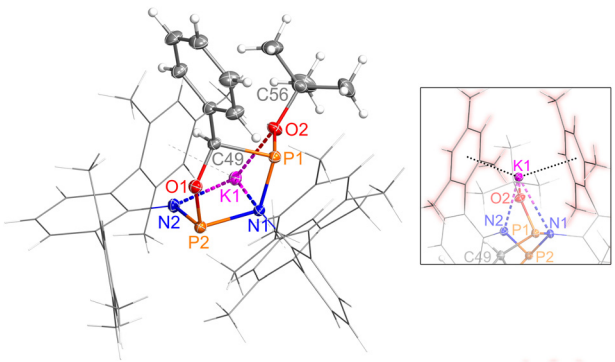

Fig. 6 Molecular structure of **6** in the crystal. Thermal ellipsoids at 50% probability (123 K). Ter substituents depicted as wireframe for clarity. Inset: η^6 coordination of the K1 atom by two Mes rings (highlighted in red). Selected bond lengths (Å): N1–P1 1.715(1), N1–P2 1.826(1), N2–P2 1.650(1), P1–O2 1.670(1), P2–O1 1.676(1), P1–C49 1.885(1), O1–C49 1.439(2), N1–K1 2.982(1), N2–K1 2.672(1), O2–K1 2.617(1), K1–C(Mes) average 3.11(3). See also Table S4.†

Attempted deprotonation

The aromatic aldehyde adducts **2–4** displayed slightly acidic methine protons in the ^{1}H NMR spectra (4.74–4.86 ppm, $^2J(^1H,^{31}P) \approx 11$ Hz, toluene-d_8, Table S5†). Thus, we were interested whether it would be feasible to deprotonate the addition products to functionalize the aldehyde moieties. As derivative **2** was characterized by the highest downfield shift, it was chosen for deprotonation attempts, using a variety of bases such as KH (in THF), DBU (toluene/benzene), DMAP (benzene), LiN(SiMe$_3$)$_2$ (THF), or NEt$_3$ (toluene). However, according to *in situ* NMR spectra, no reaction was observed in any of these cases. Only when treating **2** with KO*t*Bu in toluene solution (with a few drops of THF for solubility), a slow colour change was observed. A look at the ^{1}H NMR spectrum revealed that the starting materials had been consumed and the signal of the O*t*Bu group showed a small doublet splitting of 0.6 Hz, indicating that it was now attached to a P atom. Moreover, the acidic proton was still present in the reaction product as indicated by a doublet at 6.15 ppm ($^2J(^1H,^{31}P)$ = 4.3 Hz).

Indeed, crystallization after workup afforded single crystals suitable for X-ray diffraction, which unequivocally identified the newly formed substance as a formal addition product of **2** and KO*t*Bu (**6**, Scheme 3 and Fig. 6). Hence, the deprotonation did not work as expected, but the formal *t*BuO$^-$ moiety performed a nucleophilic attack at one of the P atoms, resulting in breaking of one of the N–P bonds.

Compound **6** crystallized in the monoclinic space group $P2_1/c$ with four formula units per cell. The most notable feature is the central NP_2CO five-membered ring system (that is, a 1,3,2,4-oxazadiphospholidine), with an O*t*Bu group attached to P1 and an NTer group attached to P2. The interatomic distances between neighbouring atoms in the ring lie in the range of typical (polarized) single bonds and are similar to the values found for the starting material **2** (*cf.* Fig. 6 and Table S4†), apart from the elongated N1–P2 distance (1.826(1) Å; *cf.* N1–P1 = 1.715(1) Å, $\sum r_{cov}$(N–P) = 1.82 Å (ref. 47)). The exocyclic N2–P2 distance, on the other hand, is significantly shortened (1.650(1) Å; *cf.* $\sum r_{cov}$(N=P) = 1.62 Å). According to NBO analysis, this can be explained by negative hyperconjugation of the lone pair (LP) at N2 into the σ*(P2–N1) orbital ($\Delta E^{(2)}$ = 22.8 kJ mol^{-1}), which results in partial double bond character of the N2–P2 bond while simultaneously weakening the N1–P2 bond. The exocyclic P1–O2 distance (1.670(1) Å) is again very similar to the P2–O1 distance in the ring system (1.676(1) Å) and in the range of a typical polarized single bond.

The formal K1 counterion is coordinated by the exocyclic N2 and O2 atoms (K1–N2 2.672(1), K1–O2 2.617(1) Å) as well as the N1 atom of the five-membered ring (K1–N1 2.982(1) Å) in a pincer-like coordination (*cf.* $\sum r_{ion}$(K–N) = 2.84 Å, $\sum r_{ion}$(K–O) =

2.78 Å).[65] Additionally, K1 is stabilized by η^6 coordination from two flanking Mes groups of the two Ter substituents (Fig. 6, inset), with average K–C distances of 3.11(3) Å (*cf.* $\sum r_{cov}$(K–C) = 2.71 Å, $\sum r_{vdW}$(K···C) = 4.45 Å).[63] According to NBO analysis, K1 has a natural charge of +0.89, that is, the charge transfer from the anion (0.11*e*) is rather low. There is no single large stabilizing donor–acceptor interaction from the anion to the empty 4s orbital of K1, but small contributions from all heteroatoms in the central five-membered ring as well as from the π-bonding system of the flanking Mes groups. Compound **6** is therefore best understood as an ion pair.

Conclusions

The addition of aldehydes to the singlet biradical [P(μ-NTer)]$_2$ (**1**) was shown to proceed very quickly at ambient temperature and afforded the *syn*-addition products **2–5** in moderate to high yields. The addition products can be understood as hetero-bicyclo[2.1.1]hexane derivatives. To the best of our knowledge, this is the first demonstration of the addition of aldehydes to formal hetero-cyclobutanediyls in general.

The addition of aldehydes to **1** was shown to follow a classical concerted cycloaddition mechanism[66] with a very low activation barrier ($\Delta G^{\ddagger}_{298K}$ = +23.1 kJ mol^{-1} for the model reaction **1H** + H_2CO), which is essentially of entropic nature. Moreover, we investigated the mechanism of the additions of related unsaturated hydrocarbons (ethylene, acetylene), which also add to **1** in a concerted cycloaddition with low activation barriers. Nonetheless, the addition of aldehydes is predicted to be the fastest addition reaction of the investigated set. We therefore propose that aldehydes may also be a suitable addition reagent for other, less reactive singlet biradicals. Moreover, they could be used as trapping reagents for short-lived singlet biradicals due to their fast reaction time.

The computational results are a reminder that seemingly simple reactions may sometimes be hard to describe using DFT techniques when biradicals are involved. This can be attributed to the non-dynamical electron correlation present in these species, which is insufficiently described using standard DFT functionals.

Lastly, the functionalization of the addition product **2** by deprotonation was attempted, which, however, led to nucleophilic substitution at one of the phosphorus atoms. The resulting potassium salt contains an unprecedented 1,3,2,4-oxazadiphospholidine scaffold in the anion and can be understood as an N–P bond activation product. Due to its various donor atoms, its use as ligand might be studied in the future.

Experimental

All manipulations were carried out under oxygen- and moisture-free conditions under an inert atmosphere of argon using standard Schlenk or Drybox techniques. Starting materials were either purchased or synthesized according to literature procedures. For detailed information, including a full set of analytical data for the synthesized compounds, please refer to the ESI, p S2ff.†

Synthesis of 2

PhCHO (30 mg, 0.28 mmol) is added to a solution of [P(μ-NTer)]$_2$ (200 mg, 0.28 mmol) in benzene (10 mL) at RT with a microliter syringe, resulting in an immediate colour change from orange to light yellow. The reaction mixture is stirred for further three hours. After the reaction time, all volatile components are removed *in vacuo* (1×10^{-3} mbar) at 50 °C (water bath). The residue is dissolved in fresh benzene and insoluble solids are removed by filtration over Celite. The clear solution is concentrated *in vacuo* (1×10^{-3} mbar) to incipient crystallization and stored overnight. After removal of the supernatant colourless crystals remain. Yield: 193 mg (0.234 mmol, 84%).

Mp. 138–143 °C. CHN calcd (found) in %: C 80.27 (79.70), H 6.86 (6.56), N 3.40 (3.22). $^{31}P\{^1H\}$ NMR (toluene-d_8, 121.5 MHz) δ = 178.5 (d, $^2J(^{31}P, ^{31}P)$ = 15 Hz, 1 P, *P*–CH), 214.9 (d, $^2J(^{31}P, ^{31}P)$ = 15 Hz, 1 P, *P*–O). MS (CI, pos., isobutane) *m*/*z*: 823 [MH]$^+$, 716 [(TerNP)$_2$]$^+$, 418 [TerNCHPhH]$^+$, 330 [TerNH$_3$]$^+$, 107 [PhCHOH]$^+$.

Synthesis of 3

p-Nitrobenzaldehyde (42.1 mg, 0.28 mmol) and [P(μ-NTer)]$_2$ (200 mg, 0.28 mmol) are dissolved in toluene (10 mL) at RT, resulting in a brown solution that is stirred for three hours. After the reaction time, all volatile components are removed *in vacuo* (1×10^{-3} mbar) at 50 °C (water bath). The residue is dissolved in fresh toluene and insoluble solids are removed by filtration over Celite. The clear solution is concentrated *in vacuo* (1×10^{-3} mbar) to incipient crystallization and stored overnight. Brown crystals can be obtained. Yield: 140 mg (0.16 mmol, 57%).

Mp. 150–155 °C CHN calcd (found) in %: C 76.11 (75.83), H 6.39 (6.56), N 4.84 (4.72). $^{31}P\{^1H\}$ NMR (toluene-d_8, 121.5 MHz): δ = 180.1 (d, $^2J(^{31}P, ^{31}P)$ = 17 Hz, 1 P, *P*–CH), 216.6 (d, $^2J(^{31}P, ^{31}P)$ = 17 Hz, 1 P, *P*–O). MS (CI, pos., isobutane) *m*/*z*: 659, 463 [TerNCHPhNO$_2$H]$^+$, 386 [TerNH$_2$C$_4$H$_9$]$^+$, 372, 368, 330 [TerNH$_3$]$^+$, 326, 152 [PhNO$_2$CHOH]$^+$.

Synthesis of 4

p-Chlorobenzaldehyde (39 mg, 0.28 mmol) and [P(μ-NTer)]$_2$ (200 mg, 0.28 mmol) are dissolved in toluene (10 mL) at RT, resulting in a light green solution that is stirred for three hours. After the reaction time, all volatile components are removed *in vacuo* (1×10^{-3} mbar) at 50 °C (water bath). The residue is dissolved in fresh toluene and insoluble solids are removed by filtration over Celite. The clear solution is concentrated *in vacuo* (1×10^{-3} mbar) to incipient crystallization and stored overnight. After removal of the supernatant colourless crystals are obtained. Yield: 199 mg (0.23 mmol, 83%).

Mp. 157–162 °C CHN calcd (found) in %: C 77.04 (76.57), H 6.47 (6.00), N 3.27 (3.07). $^{31}P\{^1H\}$ NMR (C_6D_6, 202.5 MHz): δ = 178.3 (s (br), 1 P, *P*–CH), 215.4 (s (br), 1 P, *P*–O). $^{31}P\{^1H\}$ NMR (toluene-d_8, 121.5 MHz): δ = 178.4 (d, $^2J(^{31}P, ^{31}P)$ = 16 Hz, 1 P,

P–CH), 215.5 (d, $^2J(^{31}P, ^{31}P)$ = 16 Hz, 1 P, *P*–O). MS (CI, pos., isobutane) *m*/*z*: 893 $[M]^+$, 716 $[(TerNP)_2]^+$, 452 $[TerNCHPhClH]^+$, 358 $[TerNP]^+$, 141 $[PhClCHOH]^+$.

Synthesis of 5

EtCHO (16 mg, 0.28 mmol) is added to a solution of $[P(\mu\text{-NTer})]_2$ (200 mg, 0.28 mmol) in toluene (10 mL) at RT with a microliter syringe, resulting in an immediate colour change from orange to light yellow. The reaction mixture is stirred for further three hours. After the reaction time, all volatile components are removed *in vacuo* (1×10^{-3} mbar) at 50 °C (water bath). The residue is dissolved in fresh toluene and insoluble solids are removed by filtration over Celite. The clear solution is concentrated *in vacuo* (1×10^{-3} mbar) to incipient crystallization and stored overnight. After removal of the supernatant colourless crystals remain. Yield: 172 mg (0.22 mmol, 79%).

Mp. 140–145 °C CHN calcd (found) in %: C 78.92 (78.52), H 7.15 (6.74), N 3.68 (3.27). $^{31}P\{^1H\}$ NMR (C_6D_6, 121.5 MHz): δ = 176.6 (d, $^2J(^{31}P, ^{31}P)$ = 13 Hz, 1 P, *P*–CH), 212.1 (d, $^2J(^{31}P, ^{31}P)$ = 13 Hz, 1 P, *P*–O). $^{31}P\{^1H\}$ NMR (toluene-d_8, 121.5 MHz): δ = 176.4 (d, $^2J(^{31}P, ^{31}P)$ = 14 Hz, 1 P, *P*–CH), 211.9 (d, $^2J(^{31}P, ^{31}P)$ = 14 Hz, 1 P, *P*–O). MS (CI, pos., isobutane) *m*/*z*: 831 $[MC_4H_9]^+$, 775 $[MH]^+$, 716 $[(TerNP)_2]^+$, 330 $[TerNH_3]^+$.

Synthesis of 6

KO*t*Bu (27 mg, 0.24 mmol) is added to a solution of $[P(\mu\text{-NTer})]_2 \cdot PhCHO$ (200 mg, 0.24 mmol) in toluene (10 mL) at RT. For solubility a few drops of THF are added. The reaction mixture is stirred overnight, its colour starting to change from orange to light orange after about 30 minutes. After the reaction, all volatile components are removed *in vacuo* (1×10^{-3} mbar) at 50 °C (water bath). The residue is dissolved in fresh toluene and insoluble solids are removed by filtration over Celite. The clear solution is concentrated *in vacuo* (1×10^{-3} mbar) to incipient crystallization and stored until crystallization. After removal of the supernatant brownish crystals remain. Yield: 176 mg (0.188 mmol, 78%).

Mp. 137–145 °C CHN calcd (found) in %: C 75.85 (75.39), H 6.91 (7.11), N 3.00 (2.74). $^{31}P\{^1H\}$ NMR (toluene-d_8, 202.5 MHz): δ = 148.6 (s, 1 P, *P*–CH), 183.9 (s, 1 P, *P*–O). MS (CI, pos., isobutane) *m*/*z*: 823 $[(TerNP)_2PhCHOH]^+$, 716 $[(TerNP)_2]^+$, 687, 540, 506, 484, 432 $[TerNPOtBuH]^+$, 418 $[TerNCHPhH]^+$, 330 $[TerNH_3]^+$, 107 $[PhCHOH]^+$.

Computational details

Computations were carried out using Gaussian09,[67] ORCA 5.0.3,[68–70] and NBO 6.0.[71–74] Structure optimizations and frequency calculations were performed using either DFT (PBE-D3/def2-TZVP or B3LYP-D3/def2-TZVP) or coupled-cluster methods (CCSD(T)/def2-TZVP). Accurate electronic energies were computed at the DLPNO-CCSD(T)/def2-TZVP or DLPNO-CCSD(T)/def2-QZVPP levels using the optimized structures. Reaction paths were investigated using a combination of relaxed potential energy surface scans, the nudged elastic band (NEB) method,[75–80] as well as transition state searches using the eigenvector-following method.[81–84] For more details, please refer to the ESI, p. S30ff.†

Conflicts of interest

There are no conflicts to declare.

Acknowledgements

We wish to thank the ITMZ at the University of Rostock for access to the cluster computer, and especially Malte Willert for his assistance with the queuing system and software installations. This project received funding from the Deutsche Forschungsgemeinschaft (DFG; SCHU 1170/12-2). J. R. thanks the Konrad-Adenauer-Stiftung for financial and non-material support. Lastly, we would like to thank the reviewers for their insightful comments.

References

1 L. Salem and C. Rowland, *Angew. Chem., Int. Ed. Engl.*, 1972, **11**, 92–111.
2 *Diradicals*, ed. W. T. Borden, Wiley-Interscience, New York, 1982.
3 V. Bonačić-Koutecký, J. Koutecký and J. Michl, *Angew. Chem., Int. Ed. Engl.*, 1987, **26**, 170–189.
4 H. Grützmacher and F. Breher, *Angew. Chem., Int. Ed.*, 2002, **41**, 4006–4011.
5 F. Breher, *Coord. Chem. Rev.*, 2007, **251**, 1007–1043.
6 S. González-Gallardo and F. Breher, in *Comprehensive Inorganic Chemistry II*, ed. J. Reedijk and K. Poeppelmeier, Elsevier, 2013, vol. 1, pp. 413–455.
7 M. Abe, *Chem. Rev.*, 2013, **113**, 7011–7088.
8 T. Stuyver, B. Chen, T. Zeng, P. Geerlings, F. De Proft and R. Hoffmann, *Chem. Rev.*, 2019, **119**, 11291–11351.
9 J. Bresien, L. Eickhoff, A. Schulz and E. Zander, in *Comprehensive Inorganic Chemistry III*, ed. J. Reedijk and K. Poeppelmeier, Elsevier, 2021, DOI: **10.1016/B978-0-12-823144-9.00029-7**.
10 M. Abe, J. Ye and M. Mishima, *Chem. Soc. Rev.*, 2012, **41**, 3808–3820.
11 S. Ito, *Tetrahedron Lett.*, 2018, **59**, 1–13.
12 W. W. Schoeller, *Eur. J. Inorg. Chem.*, 2019, **2019**, 1495–1506.
13 E. Niecke, A. Fuchs, F. Baumeister, M. Nieger and W. W. Schoeller, *Angew. Chem., Int. Ed. Engl.*, 1995, **34**, 555–557.
14 D. Scheschkewitz, H. Amii, H. Gornitzka, W. W. Schoeller, D. Bourissou and G. Bertrand, *Science*, 2002, **295**, 1880–1881.
15 S. Demeshko, C. Godemann, R. Kuzora, A. Schulz and A. Villinger, *Angew. Chem., Int. Ed.*, 2013, **52**, 2105–2108.
16 A. Hinz, A. Schulz and A. Villinger, *Angew. Chem., Int. Ed.*, 2015, **54**, 668–672.

17 A. Hinz, R. Kuzora, A.-K. Rölke, A. Schulz, A. Villinger and R. Wustrack, *Eur. J. Inorg. Chem.*, 2016, **2016**, 3611–3619.
18 D. Rottschäfer, B. Neumann, H.-G. Stammler and R. S. Ghadwal, *Chem. – Eur. J.*, 2017, **23**, 9044–9047.
19 Z. Li, X. Chen, D. M. Andrada, G. Frenking, Z. Benkő, Y. Li, J. R. Harmer, C.-Y. Su and H. Grützmacher, *Angew. Chem., Int. Ed.*, 2017, **56**, 5744–5749.
20 C. B. Yildiz, K. I. Leszczyńska, S. González-Gallardo, M. Zimmer, A. Azizoglu, T. Biskup, C. W. M. Kay, V. Huch, H. S. Rzepa and D. Scheschkewitz, *Angew. Chem., Int. Ed.*, 2020, **59**, 15087–15092.
21 T. Brückner, F. Fantuzzi, T. E. Stennett, I. Krummenacher, R. D. Dewhurst, B. Engels and H. Braunschweig, *Angew. Chem., Int. Ed.*, 2021, **60**, 13661–13665.
22 H. Steffenfauseweh, Y. V. Vishnevskiy, B. Neumann, H.-G. Stammler, D. M. Andrada and R. Ghadwal, *Angew. Chem., Int. Ed.*, 2022, **61**, e202207415.
23 H. Sugiyama, S. Ito and M. Yoshifuji, *Angew. Chem., Int. Ed.*, 2003, **42**, 3802–3804.
24 C. Cui, M. Brynda, M. M. Olmstead and P. P. Power, *J. Am. Chem. Soc.*, 2004, **126**, 6510–6511.
25 H. Cox, P. B. Hitchcock, M. F. Lappert and L. J. M. Pierssens, *Angew. Chem., Int. Ed.*, 2004, **43**, 4500–4504.
26 X. Wang, Y. Peng, M. M. Olmstead, J. C. Fettinger and P. P. Power, *J. Am. Chem. Soc.*, 2009, **131**, 14164–14165.
27 P. Henke, T. Pankewitz, W. Klopper, F. Breher and H. Schnöckel, *Angew. Chem., Int. Ed.*, 2009, **48**, 8141–8145.
28 T. Beweries, R. Kuzora, U. Rosenthal, A. Schulz and A. Villinger, *Angew. Chem., Int. Ed.*, 2011, **50**, 8974–8978.
29 K. Takeuchi, M. Ichinohe and A. Sekiguchi, *J. Am. Chem. Soc.*, 2011, **133**, 12478–12481.
30 S.-H. Zhang, H.-W. Xi, K. H. Lim, Q. Meng, M.-B. Huang and C.-W. So, *Chem. – Eur. J.*, 2012, **18**, 4258–4263.
31 Y. Ueta, K. Mikami and S. Ito, *Angew. Chem., Int. Ed.*, 2016, **55**, 7525–7529.
32 H. Amii, L. Vranicar, H. Gornitzka, D. Bourissou and G. Bertrand, *J. Am. Chem. Soc.*, 2004, **126**, 1344–1345.
33 J. Rosenboom, L. Chojetzki, T. Suhrbier, J. Rabeah, A. Villinger, R. Wustrack, J. Bresien and A. Schulz, *Chem. – Eur. J.*, 2022, e202200624.
34 A. Hinz, R. Kuzora, U. Rosenthal, A. Schulz and A. Villinger, *Chem. – Eur. J.*, 2014, **20**, 14659–14673.
35 A. Hinz, A. Schulz and A. Villinger, *Angew. Chem., Int. Ed.*, 2016, **55**, 12214–12218.
36 Z. Li, Y. Hou, Y. Li, A. Hinz and X. Chen, *Chem. – Eur. J.*, 2018, **24**, 4849–4855.
37 J. Bresien, A. Hinz, A. Schulz and A. Villinger, *Eur. J. Inorg. Chem.*, 2018, **2018**, 1679–1682.
38 X. Zhang, X. Chen, H. Zhai, S. Liu, C. Hu, L. L. Liu, S. Wang and Z. Li, *Dalton Trans.*, 2020, **49**, 6384–6390.
39 H. Beer, K. Bläsing, J. Bresien, L. Chojetzki, A. Schulz, P. Stoer and A. Villinger, *Dalton Trans.*, 2020, **49**, 13655–13662.
40 L. Chojetzki, A. Schulz, A. Villinger and R. Wustrack, *Z. Anorg. Allg. Chem.*, 2020, **646**, 614–624.
41 J. Bresien, A. Hinz, A. Schulz and A. Villinger, *Dalton Trans.*, 2018, **47**, 4433–4436.
42 A. Hinz, A. Schulz and A. Villinger, *Angew. Chem., Int. Ed.*, 2015, **54**, 2776–2779.
43 A. Hinz, A. Schulz and A. Villinger, *J. Am. Chem. Soc.*, 2015, **137**, 9953–9962.
44 J. Bresien, T. Kröger-Badge, S. Lochbrunner, D. Michalik, H. Müller, A. Schulz and E. Zander, *Chem. Sci.*, 2019, **10**, 3486–3493.
45 H. Beer, J. Bresien, D. Michalik, A.-K. Rölke, A. Schulz, A. Villinger and R. Wustrack, *J. Org. Chem.*, 2020, **85**, 14435–14445.
46 H. Beer, A. Linke, J. Bresien, G. Mlostoń, M. Celeda, A. Villinger and A. Schulz, *Inorg. Chem.*, 2022, **61**, 2031–2038.
47 P. Pyykkö and M. Atsumi, *Chem. – Eur. J.*, 2009, **15**, 12770–12779.
48 V. Schomaker and D. P. Stevenson, *J. Am. Chem. Soc.*, 1941, **63**, 37–40.
49 G. Gunbas, N. Hafezi, W. L. Sheppard, M. M. Olmstead, I. V. Stoyanova, F. S. Tham, M. P. Meyer and M. Mascal, *Nat. Chem.*, 2012, **4**, 1018–1023.
50 C. Riplinger and F. Neese, *J. Chem. Phys.*, 2013, **138**, 034106.
51 D. G. Liakos, M. Sparta, M. K. Kesharwani, J. M. L. Martin and F. Neese, *J. Chem. Theory Comput.*, 2015, **11**, 1525–1539.
52 C. Riplinger, P. Pinski, U. Becker, E. F. Valeev and F. Neese, *J. Chem. Phys.*, 2016, **144**, 024109.
53 D. G. Liakos, Y. Guo and F. Neese, *J. Phys. Chem. A*, 2020, **124**, 90–100.
54 F. Weigend and R. Ahlrichs, *Phys. Chem. Chem. Phys.*, 2005, **7**, 3297–3305.
55 J. P. Perdew, K. Burke and M. Ernzerhof, *Phys. Rev. Lett.*, 1996, **77**, 3865–3868.
56 J. P. Perdew, K. Burke and M. Ernzerhof, *Phys. Rev. Lett.*, 1997, **78**, 1396–1396.
57 S. Grimme, J. Antony, S. Ehrlich and H. Krieg, *J. Chem. Phys.*, 2010, **132**, 154104.
58 S. Grimme, S. Ehrlich and L. Goerigk, *J. Comput. Chem.*, 2011, **32**, 1456–1465.
59 C. Adamo and V. Barone, *J. Chem. Phys.*, 1999, **110**, 6158–6170.
60 P. J. Stephens, F. J. Devlin, C. F. Chabalowski and M. J. Frisch, *J. Phys. Chem.*, 1994, **98**, 11623–11627.
61 Y. Zhao and D. G. Truhlar, *Theor. Chem. Acc.*, 2007, **120**, 215–241.
62 V. V. Zhivonitko, J. Bresien, A. Schulz and I. V. Koptyug, *Phys. Chem. Chem. Phys.*, 2019, **21**, 5890–5893.
63 M. Mantina, A. C. Chamberlin, R. Valero, C. J. Cramer and D. G. Truhlar, *J. Phys. Chem. A*, 2009, **113**, 5806–5812.
64 S. E. Wheeler, D. H. Ess and K. N. Houk, *J. Phys. Chem. A*, 2008, **112**, 1798–1807.
65 A. F. Hollemann, E. Wiberg and N. Wiberg, *Lehrbuch der Anorganischen Chemie*, Walter de Gruyter, Berlin, Germany, 102nd edn, 2007.

66 D. H. Ess and K. N. Houk, *J. Phys. Chem. A*, 2005, **109**, 9542–9553.
67 M. J. Frisch, G. W. Trucks, H. B. Schlegel, G. E. Scuseria, M. A. Robb, J. R. Cheeseman, G. Scalmani, V. Barone, B. Mennucci, G. A. Peterson, H. Nakatsuji, M. Caricato, X. Li, H. P. Hratchian, A. F. Izmaylov, J. Bloino, G. Zheng, J. L. Sonnenberg, M. Hada, M. Ehara, K. Toyota, R. Fukuda, J. Hasegawa, M. Ishida, T. Nakajima, Y. Honda, O. Kitao, H. Nakai, T. Vreven, J. A. Montgomery, Jr., J. E. Peralta, F. Ogliaro, M. Bearpark, J. J. Heyd, E. Brothers, K. N. Kudin, V. N. Staroverov, T. Keith, R. Kobayashi, J. Normand, K. Raghavachari, A. Rendell, J. C. Burant, S. S. Iyengar, J. Tomasi, M. Cossi, N. Rega, J. M. Millam, M. Klene, J. E. Know, J. B. Cross, V. Bakken, C. Adamo, J. Jaramillo, R. Gomperts, R. E. Stratmann, O. Yazyev, A. J. Austin, R. Cammi, C. Pomelli, J. W. Ochterski, R. L. Martin, K. Morokuma, V. G. Zakrezewski, G. A. Voth, P. Salvador, J. J. Dannenberg, S. Dapprich, A. D. Daniels, O. Farkas, J. B. Foresman, J. V. Ortiz, J. Cioslowski and D. J. Fox, *Gaussian 09, Revision E.01*, Gaussian Inc., Wallingford CT, 2013.
68 F. Neese, *Wiley Interdiscip. Rev.: Comput. Mol. Sci.*, 2012, **2**, 73–78.
69 F. Neese, F. Wennmohs, U. Becker and C. Riplinger, *J. Chem. Phys.*, 2020, **152**, 224108.
70 F. Neese, *Wiley Interdiscip. Rev.: Comput. Mol. Sci.*, 2022, e1606.
71 F. Weinhold and J. E. Carpenter, in *The Structure of Small Molecules and Ions*, ed. R. Naaman and Z. Vager, Springer, Boston, MA, 1988, pp. 227–236.
72 F. Weinhold and C. R. Landis, *Valency and Bonding. A Natural Bond Orbital Donor-Acceptor Perspective*, Cambridge University Press, 2005.
73 E. D. Glendening, J. K. Badenhoop, A. E. Reed, J. E. Carpenter, J. A. Bohmann, C. M. Morales, C. R. Landis and F. Weinhold, *NBO 6.0*, Theoretical Chemistry Institute, University of Wisconsin, Madison, 2013.
74 F. Weinhold, C. R. Landis and E. D. Glendening, *Int. Rev. Phys. Chem.*, 2016, **35**, 399–440.
75 G. Mills, H. Jónsson and G. K. Schenter, *Surf. Sci.*, 1995, **324**, 305–337.
76 H. Jónsson, G. Mills and K. W. Jacobsen, in *Classical and Quantum Dynamics in Condensed Phase Simulations*, World Scientific, 1998, pp. 385–404.
77 G. Henkelman and H. Jónsson, *J. Chem. Phys.*, 2000, **113**, 9978–9985.
78 G. Henkelman, B. P. Uberuaga and H. Jónsson, *J. Chem. Phys.*, 2000, **113**, 9901–9904.
79 E. Maras, O. Trushin, A. Stukowski, T. Ala-Nissila and H. Jónsson, *Comput. Phys. Commun.*, 2016, **205**, 13–21.
80 V. Ásgeirsson, B. O. Birgisson, R. Bjornsson, U. Becker, F. Neese, C. Riplinger and H. Jónsson, *J. Chem. Theory Comput.*, 2021, **17**, 4929–4945.
81 J. Baker, *J. Comput. Chem.*, 1986, **7**, 385–395.
82 H. B. Schlegel, in *Advances in Chemical Physics: Ab Initio Methods in Quantum Chemistry Part I, Volume 67*, ed. K. P. Lawley, John Wiley & Sons, 1987, pp. 249–286.
83 H. B. Schlegel, in *Modern Electronic Structure Theory*, ed. D. R. Yarkony, World Scientific, 1995, pp. 459–500.
84 F. Eckert, P. Pulay and H.-J. Werner, *J. Comput. Chem.*, 1997, **18**, 1473–1483.

6.2 Radical reactivity of the biradical [•P(μ-NTer)$_2$P•] and isolation of a persistent phosphorus-centered monoradical [•P(μ-NTer)$_2$P-Et]

J. Rosenboom, L. Chojetzki, T. Suhrbier, J. Rabeah, A. Villinger, R. Wustrack, J. Bresien,* A. Schulz*

Chem. Eur. J. **2022**, *28*, e202200624.)

DOI: 10.1002/chem.202200624

Chemistry–A European Journal
Research Article
doi.org/10.1002/chem.202200624
Chemistry Europe
European Chemical Societies Publishing
www.chemeurj.org

Radical Reactivity of the Biradical [•P(μ-NTer)$_2$P•] and Isolation of a Persistent Phosphorus-Centered Monoradical [•P(μ-NTer)$_2$P-Et]

Jan Rosenboom,[a] Lukas Chojetzki,[a] Tim Suhrbier,[a] Jabor Rabeah,[b] Alexander Villinger,[a] Ronald Wustrack,[a] Jonas Bresien,*[a] and Axel Schulz*[a, b]

Abstract: The activation of C–Br bonds in various bromoalkanes by the biradical [•P(μ-NTer)$_2$P•] (**1**) (Ter = 2,6-bis-(2,4,6-trimethylphenyl)-phenyl) is reported, yielding *trans*-addition products of the type [Br–P(μ-NTer)$_2$P–R] (**2**), so-called 1,3-substituted *cyclo*-1,3-diphospha-2,4-diazanes. This addition reaction, which represents a new easy approach to asymmetrically substituted *cyclo*-1,3-diphospha-2,4-diazanes, was investigated mechanistically by different spectroscopic methods (NMR, EPR, IR, Raman); the results suggested a stepwise radical reaction mechanism, as evidenced by the in-situ detection of the phosphorus-centered monoradical [•P(μ-NTer)$_2$P-R]. < To provide further evidence for the radical mechanism, [•P(μ-NTer)$_2$P-Et] (**3Et•**) was synthesized directly by reduction of the bromoethane addition product [Br-P(μ-NTer)$_2$P-Et] (**2a**) with magnesium, resulting in the formation of the persistent phosphorus-centered monoradical [•P(μ-NTer)$_2$P-Et], which could be isolated and fully characterized, including single-crystal X-ray diffraction. Comparison of the EPR spectrum of the radical intermediate in the addition reaction with that of the synthesized new [•P(μ-NTer)$_2$P-Et] radical clearly proves the existence of radicals over the course of the reaction of biradical [•P(μ-NTer)$_2$P•] (**1**) with bromoethane. Extensive DFT and coupled cluster calculations corroborate the experimental data for a radical mechanism in the reaction of biradical [•P(μ-NTer)$_2$P•] with EtBr. In the field of hetero-cyclobutane-1,3-diyls, the demonstration of a step-wise radical reaction represents a new aspect and closes the gap between P-centered biradicals and P-centered monoradicals in terms of radical reactivity.

Introduction

Open-shell singlet biradical(oid)s, such as [•P(μ-NTer)$_2$P•] (**1**; Scheme 1) with a biradical character of 25 %,[1] are molecular species with a spin density of exactly zero at any point in space,[2] even though the two radical electrons tend to avoid each other.[3] There are many classifications and names for biradicals (diradical, biradicaloid, etc.);[4] however, throughout this paper we will only use the term biradical since the transitions between open-shell singlet biradical→biradicaloid→closed-shell singlet species are smooth in terms of electronic interaction.[5,6] Depending on the strength of the antiferromagnetic coupling between the electrons and therefore on the degree of biradical character, singlet biradicals usually feature a reactivity that lies between typical closed-shell and radical species.[3,7–12] That is, biradicals can undergo pericyclic, concerted reactions, or step-wise, radical-type reactions.

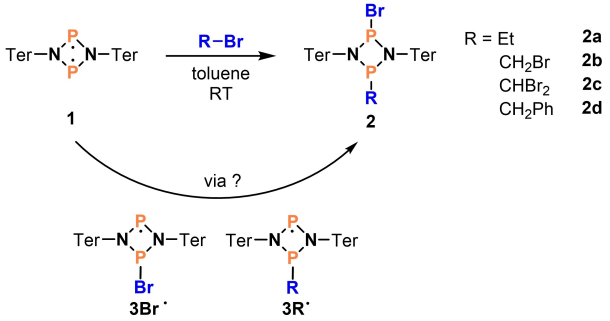

Scheme 1. Addition of different bromoalkanes to biradical **1**.

Herein, we report on the activation of C–Br bonds in the reaction of biradical **1** with bromoalkanes featuring a radical mechanism. Phosphorus-centered biradical **1** that was first synthesized in 2011 (Scheme 1)[13] belongs to the class of hetero-cyclobutane-1,3-diyls, which was made accessible by the Niecke group who published the first stable congener in 1995 ([ClC(μ-PMes*)]$_2$, Mes* = 2,4,6-tri-*tert*-butylphenyl).[14] Ever since, various congeneric hetero-cyclobutanediyls have been

[a] J. Rosenboom, Dr. L. Chojetzki, Dr. T. Suhrbier, Dr. A. Villinger, Dr. R. Wustrack, Dr. J. Bresien, Prof. Dr. A. Schulz
Institut für Chemie, Universität
Albert-Einstein-Straße 3a, 18059 Rostock (Germany)
E-mail: jonas.bresien@uni-rostock.de
axel.schulz@uni-rostock.de
Homepage: http: www.schulz.chemie.uni-rostock.de
[b] Dr. J. Rabeah, Prof. Dr. A. Schulz
Leibniz-Institut für Katalyse e.V.
Albert-Einstein-Straße 29a, 18059 Rostock (Germany)

Supporting information for this article is available on the WWW under https://doi.org/10.1002/chem.202200624

discovered,[15–24] and their activation chemistry has been extensively studied.[15,18,23–28] To our knowledge, there are only few examples of the activation of carbon-halogen bonds by biradicals in the literature. For example, Sekiguchi and co-workers were able to activate CCl_4 with a Si_2N_2 biradical resulting in the formation of the chlorinated four-membered ring.[19] Bertrand and co-workers achieved the activation of CCl_3Br with a P_2B_2 biradical.[29]

Very recently the groups of Zu and Li reported the activation of alkyl iodides by a NHC-stabilized C_2P_2 biradical forming an ion pair (Scheme 2), bottom, NHC=N-heterocyclic carbene).[30] However, to the best of our knowledge, the mechanism of the activation chemistry of these hetero-cyclobutanediyls with respect to radical behavior has not yet been investigated. This is because many biradical reactions follow a classical "closed-shell"-like concerted reaction path (Scheme 2). For example, we could show that **1** is capable of activating small molecules bearing single (H_2, chalkogenes) and multiple bonds (alkenes, alkynes, isonitriles).[13,31–33] Mechanistically, these reactions mostly represent concerted [2+2] additions or insertion reactions (i.e., typical "closed-shell" reactivity).[34] Radical reactivity of **1** (i.e., stepwise addition reactions), which would close the gap between P-centered biradicals and P-centered monoradicals, has not been described so far.

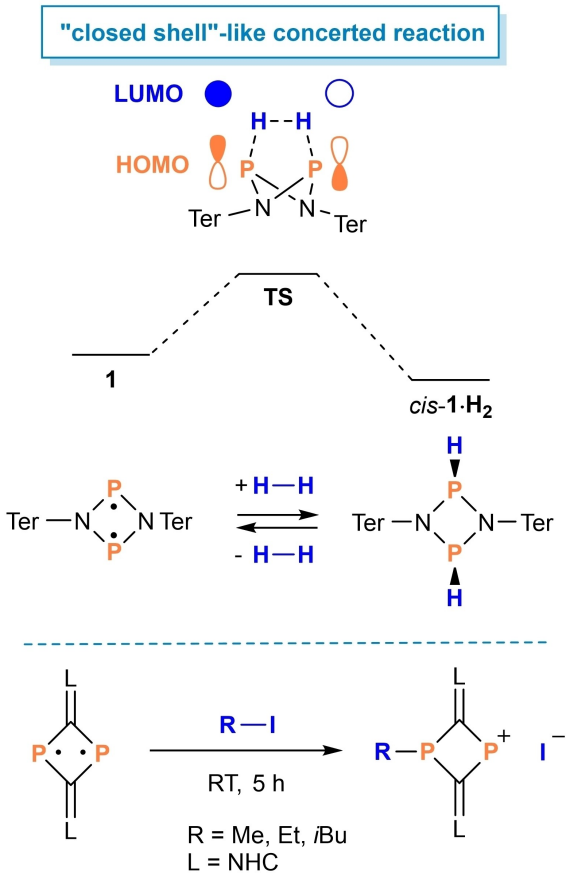

Scheme 2. Addition of different bromoalkanes to biradical **1**. Top: reversible addition of H_2 to **1**.[2,35] Bottom: activation of alkyl iodides with a C_2P_2 biradical.[30]

Results and Discussion

Bromoalkane addition: Synthesis of 1,3-substituted cyclo-1,3-diphospha-2,4-diazanes

We started this project with addition reactions between biradical **1** and a series of bromoalkanes (Scheme 1), affording addition products **2**, so-called 1,3-substituted cyclo-1,3-diphospha-2,4-diazanes. Over the course of the addition, the C–Br bond of the bromoalkane is cleaved and the bromine atom is attached to one phosphorus atom and the organic substituent to the other. The dominant product of the reaction was always the *trans*-addition product (Figure 1).

The reactions were carried out in toluene at ambient temperature and gave the products in good yields (between 65–90%). Using ^{31}P NMR spectroscopy, the addition reactions could be easily traced as the characteristic singlet of biradical **1** ($\delta[^{31}P] = 276$ ppm)[13] disappeared while two signals appeared in the 195–278 ppm region for the products **2** (**2a**: 229/255; **2b**: 195/251, **2c**: 210/278, and **2d**: 242/273 ppm). Interestingly, only the *trans*-isomers of **2** and always small traces of the dibrominated species *trans*-[Br-P(μ-NTer)$_2$P-Br] (**4**, 278 ppm) could be characterized (Figure 2), hinting at a radical mechanism of the reaction (see below).

1,3-Dibromo-*cyclo*-diphosphadiazane **4** could also be synthesized directly by reacting **1** with dry bromine in benzene at ambient temperature, however, yielding a mixture of the *cis*- and *trans*-isomer in a ratio of 2:7 ($\delta[^{31}P] = 243.9$ for *cis*- and 277.9 ppm for *trans*-**4**). After crystallization, almost pure *trans*-**4** (97% *trans* isomer) was obtained. **4** has not been reported before and completes the series of 1,3-dihalogen-*cyclo*-1,3-diphospha-2,4-diazanes (formal dihalogen addition products of **1**).[36–38] ^{31}P NMR shifts of all dihalogen addition products are compiled in Table 1. The ^{31}P NMR shift increases towards heavier halogens, so the data of **4** fits in with the data of the other adducts. The molecular structure of **4** as determined by single crystal X-ray diffraction is shown in Figure 2. It reveals a planar N_2P_2 ring system and typical P–Br single bond lengths (2.311(1) Å).

All addition products **2** (see above) could be crystallized and fully characterized (see the Supporting Information). After repeated recrystallization the bromoalkane adducts **2** still contained small impurities, mainly *trans*-**4**. Corresponding NMR spectra can be found in the Supporting Information. As depicted in Figure 1, the molecular structures were determined by single-crystal X-ray diffraction and reveal slightly puckered N_2P_2 ring systems (in contrast to **4**) with somewhat shortened N–P single bonds (1.70–1.78 Å, cf. Σr_{cov}(P–N) = 1.82 Å[39]).

Table 1. ^{31}P NMR shifts (in ppm) of halogen addition products *trans*- and *cis*-[XP(μ-NTer)$_2$PX] (X=F-I, all recorded in C_6D_6).

	cis	*trans*
[FP(μ-NTer)$_2$PF][36]	202.9	249.8
[ClP(μ-NTer)$_2$PCl][37]	227.4	264.1
[BrP(μ-NTer)$_2$PBr] (**4**)	243.9	277.9
[IP(μ-NTer)$_2$PI][38]	267.3	296.7

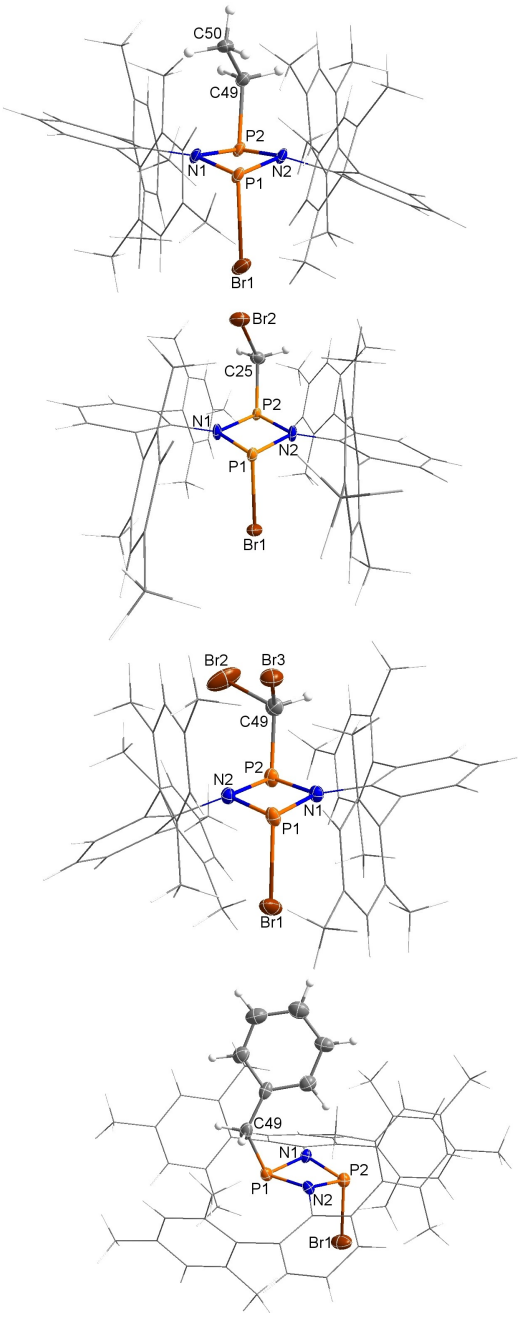

Figure 1. Molecular structure of bromoalkane products **2** in the crystal (from top to the bottom: **2a**, **2b**, **2c**, and **2d**). Ellipsoids set at 50% probability (123 K). Selected bond lengths [Å] and dihedral angles [°] are listed in Table S4 in the Supporting Information.

NBO[40–43] analysis revealed substantial bond polarization (N: 77% valence electron density, P: 23%; data for **2a**), indicating polar covalent N–P bonding. The newly formed P–C bonds (1.81–1.88 Å) are in the typical range of P–C single bonds (Σr_{cov}(P–C) = 1.86 Å),[39] while the P–Br bonds (2.33-2.43 Å) are somewhat elongated in comparison to the sum of the covalent radii Σr_{cov}(P–Br) = 2.25 Å).[39]

1,3-Substituted *cyclo*-1,3-diphospha-2,4-diazanes have been known for many decades,[44,45] however, almost all synthesis

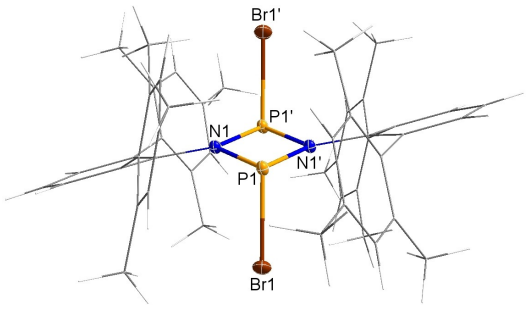

Figure 2. Molecular structure of 1,3-dibromo-cyclo-1,3-diphospha-2,4-diazane **4** in the crystal. Ellipsoids set at 50% probability (123 K). Selected bond lengths [Å] and dihedral angles [°]: N1–P1 1.730(2), N1–P1′ 1.726(2), P1–Br1 2.311 (1), N1–P1′–P1–N1′ −180.0(1).

routes lead to symmetrically substituted species.[46–60] Therefore, the biradical route described here is an elegant alternative, which can be used to generate asymmetrically substituted *cyclo*-1,3-diphospha-2,4-diazanes (such as **2a–d**).

Mechanistic studies for the reaction of biradical 1 with EtBr

Although only small amounts of 1,3-dibromo-*cyclo*-1,3-diphosphadiazane **4** were found in all reactions of **1** with bromoalkanes, this observation prompted us to further investigate the mechanism of the formation of 1,3-substituted *cyclo*-1,3-diphospha-2,4-diazanes (**2**), since only a radical mechanism (Scheme 3) should allow the formation of **4**. Moreover, concerted addition of R–Br to **1** should always give the *cis*-products of **2**, but we observed only the *trans*-products. To answer these questions, a series of kinetic studies were performed along with EPR studies for the addition reaction of EtBr giving **2a**.

First, the reaction of **1** with EtBr was traced by ^{31}P NMR spectroscopy. Spectra were recorded over several days in shorter intervals at the beginning and longer ones towards the end of the experiment. The reaction rate was determined by modeling second order kinetics to the experimental data as illustrated in Figure 3. In particular, the in situ NMR spectra (see the Supporting Information) display the appearance and

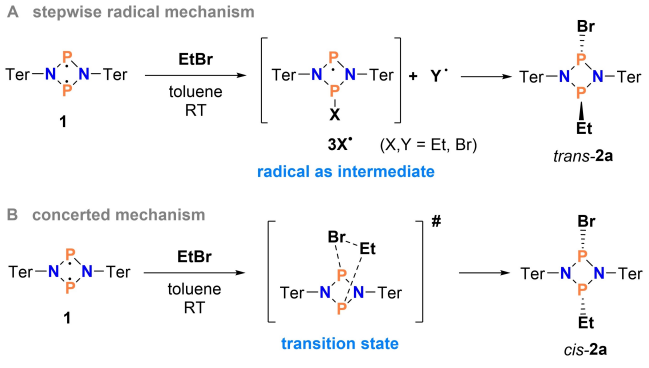

Scheme 3. Two conceivable reaction mechanisms for the reaction of biradical **1** with EtBr.

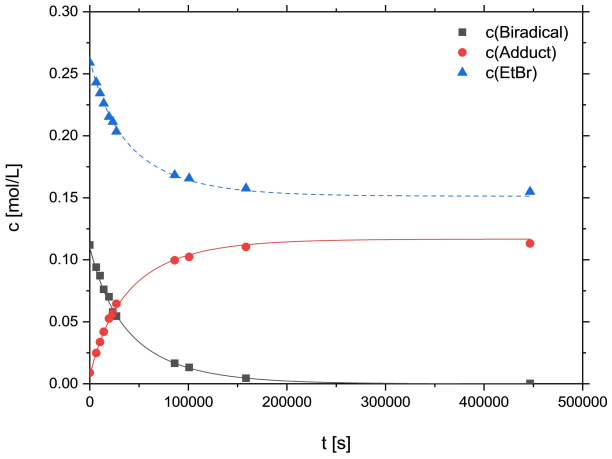

Figure 3. Kinetics of the reaction modeled to ^{31}P NMR spectroscopic data as second order kinetics with [Biradical, **1**]$_0$ = 0.110(1), [EtBr]$_0$ = 0.261(1), [Adduct, **2a**]$_0$ = 0.007(1) mol L^{-1}, and k = 1.11(3) × 10^{-4} L mol^{-1} s^{-1}).

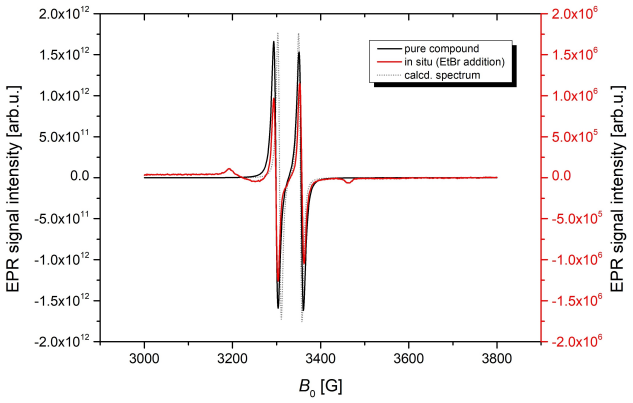

Figure 4. EPR spectra of **3Et•**, pure compound (black), in situ during EtBr addition (red), in silico (gray)[61–67] at ambient temperature. The small "side bands" in the red spectrum can be attributed to impurities (note the different scale of the red and black spectra) as they did not change in intensity over time and were present even after the completion of the reaction.

disappearance of several small signals, including the above-mentioned by-product [BrP(μ-NTer)$_2$PBr] (**4**). Thus, the by-products were attributed to typical chain-termination reactions (see also Computational Studies below).

Considering the evidence for a radical mechanism, the reaction of EtBr with **1** was repeated in the presence of azobis(isobutyronitrile) (AIBN; Figure S12). To compare the outcomes of the addition reaction with and without radical starter, two batches of **2a** were prepared, one with and one without the use of AIBN, but otherwise under exactly the same conditions. A reaction temperature of 60 °C was chosen to activate AIBN. After 2 h, ^{31}P NMR spectra were recorded. The ratio of biradical **1** (starting material) to addition product **2a** was 2:7 with AIBN and 2:3 without AIBN (Figure S12), indicating a significant acceleration (x2.5) of the addition reaction upon addition of AIBN. Only a radical reaction mechanism can explain this acceleration.

To finally prove that the addition of EtBr is indeed a radical reaction, in situ EPR spectra (red graph in Figure 4) were recorded during the reaction. The spectrum displays a doublet (g = 2.003) with a large hyperfine coupling constant (a(^{31}P) = 59 G) due to the coupling of an unpaired electron with a phosphorus nucleus. This and the disappearance of the signal once the reaction is completed suggests the presence of a phosphorus-centered radical intermediate during the reaction.

To elucidate the identity of this intermediate radical, we tried to generate both the bromine-substituted radical **3Br•** and the Et-substituted radical **3Et•** directly (Scheme 3). When the dibromine adduct **4** ([BrP(μ-NTer)$_2$PBr]) is treated with magnesium, always biradical **1** ([•P(μ-NTer)$_2$P•]) is formed, while the reduction of the EtBr adduct **2a** leads to the persistent radical **3Et•** that can be isolated in substance (see below). The recorded EPR spectrum of **3Et•** is virtually identical to the spectrum taken from the reaction solution of **1** + EtBr (Figure 4), so that we have a direct proof that **3Et•** forms in situ as intermediate.

Also, DFT computations (see the Supporting Information for further details) indicated that the phosphorus-centered radical intermediate is the ethyl substituted radical **3Et•** (Scheme 3). The EPR parameters calculated for **3Et•** in silico are in good agreement with the experimental data (gray graph in Figure 4). Additionally, calculations on the other possible, bromine-substituted radical intermediate **3Br•** hint at a different, more complicated EPR coupling pattern, not at all in alignment with the experimental data.

Spin density computations of **3Et•** also confirm it as a phosphorus-centered radical. The Mulliken spin density is mainly localized at P1 (0.70); while only small values are computed for N1 (0.043) and N2 (0.045), respectively (Figure 5).

Synthesis and characterization of 1-ethyl-1,3-diphospha-2,4-diaza-3-yl (3Et•)

As discussed above, the radical **3Et•** was synthesized purposely by reducing **2a** with an excess of magnesium in THF (Scheme 4), by analogy with the reduction of [ClP(μ-NTer)$_2$PCl] to form the biradical **1**.[73] Indeed, the reduction with magne-

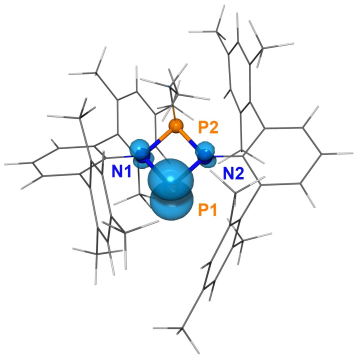

Figure 5. Calculated spin density distribution of **3Et•** (PBE-D3/def2-TZVP, iso value = 0.008).[68–72]

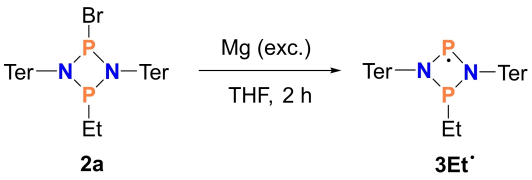

Scheme 4. Synthesis of **3Et•**.

sium worked nicely and the P–Br bond was reductively cleaved within 2 h, yielding after recrystallization the desired, dark red, persistent phosphorus-centered radical **3Et•** in good yields (83 %). The presence of the molecular radical **3Et•** in the solid state was unequivocally proven by single crystal X-ray diffraction (Figure 6). Surprisingly, the oxygen- and moisture-sensitive radical **3Et•** is stable for long periods as a solid when stored sealed in an ampoule under inert gas. Thermally, decomposition only begins above its melting point of 195 °C. These properties, together with its good solubility in many organic solvents, allowed a full characterization (see the Supporting Information) and suggest an interesting follow-up chemistry for radical **3Et•**.

Red crystals of **3Et•** crystallized in the monoclinic space group $P2_1/n$ with four formula units per cell. As depicted in Figure 6, the molecular radical sits well protected in a pocket formed by the terphenyl substituents attached to both N atoms. The ethyl substituent adopts an *endo* position, which is thermodynamically slightly favored over the *exo*-species by 9.2 kJ mol^{-1} (level of theory: DLPNO-CCSD(T)/def2-TZVP//PBE–D3/def2-TZVP, see the Supporting Information), and the four-membered N_2P_2 ring system is almost planar (∢(N1-P2-P1-N2) = 174.7(3)°). The P–N bond lengths range between 1.730(4) Å (P1–N2) and 1.761(4) Å (P2–N2) and are shortened compared to the sum of covalent radii for a P–N single bond (Σr_{cov}(P–N) = 1.82 Å),[39] thus suggesting polarized covalent N–P bonds. This is, however, less pronounced than in the starting material **2a** (see above).

EPR spectra of a solution of a crystalline sample of **3Et•** (black graph in Figure 4) are virtually identical with the in situ EPR signal during the formation of **2a** in the reaction of **1** with EtBr (small "side bands" in the in situ spectrum are attributed to impurities as they did not change over time, see above). Thus, we conclude that **3Et•** is in fact an intermediate in the addition of EtBr to **1**. The measured EPR parameters ($g = 2.003$, A = 59 G) are in alignment with other literature-known P-centered radicals.[74] Also note the different scales of the two measurements depicted in Figure 4 with an intensity difference of six orders of magnitude, showing the difference in concentration between a sample of the pure compound and the in situ measurement.

The UV-vis spectrum of **3Et•** shows a distinct absorption band at 399 nm (Figure S8), responsible for the dark red color of the compound. DFT calculations indicate that the red color is caused by a combination of excitations, in particular the excitation of the unpaired electron at P1 into a π* orbital of the Ter substituents (see the Supporting Information for TD-DFT data and NTO transformation, Figures S23 and S24).

Persistent radical[75] **3Et•** belongs to the class of P-centered radicals (Scheme 5). Since the discovery of the first persistent radical (triphenylmethyl) by Gomberg in 1900,[76] considerable advances have been made in persistent radical chemistry and radicals such as TEMPO (2,2,6,6-tetramethylpiperidin-1-yl)oxyl) have found widespread applications in organic chemistry.[77] However, only very few phosphorus-centered persistent radicals that can be isolated as a solid are known. An overview with examples of neutral phosphorus radicals that could be structurally characterized is presented in Scheme 5. Phosphorus-centered radicals are known to activate various small molecules, such as P_4,[78,79] chalcogens,[79,80] CS_2 and CO_2.[81] Thus, persistent P-centered radicals are a worthy synthetic target for the investigation of small-molecule activation.[74,75,82–90]

Finally, with the ethyl-substituted radical **3Et•** in hand, we studied the reaction of **3Et•** with EtBr as well as Br_2 (see Sections 4.3/4.4 in the Supporting Information). Whereas the reaction with bromine led to the formation of *trans*-**2a** and oxidation products, the stoichiometric reaction with EtBr resulted in the

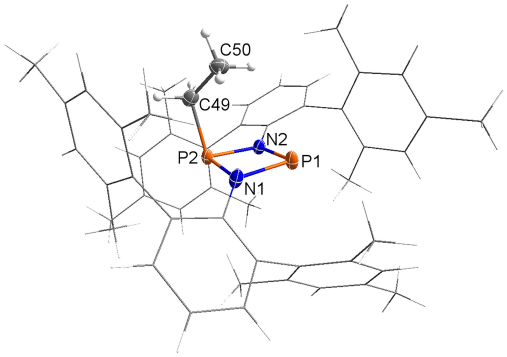

Figure 6. Molecular structure of **3Et•** in the crystal. Ellipsoids set at 50 % probability (123 K). Selected bond lengths [Å] and dihedral angles [°]: N1–P1 1.743(3), N1–P2 1.741(3), N2–P2 1.761(4), N2–P1 1.730(4), P2–C49 1.846(2), N1–P2–P1–N2 174.7(3).

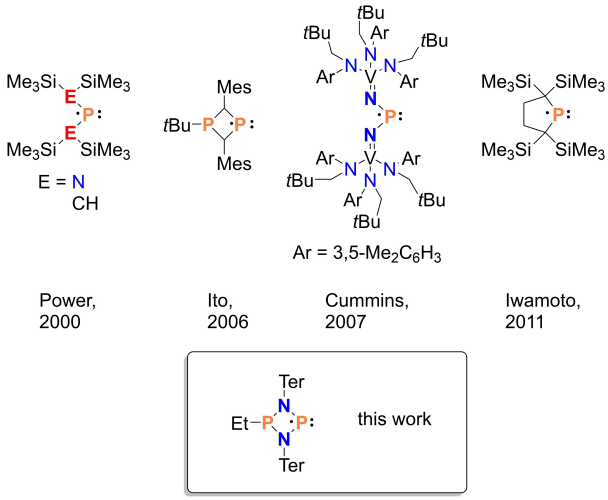

Scheme 5. Selected examples of neutral, persistent P-centered radicals.[74,83–85]

formation of a 1:1 mixture of *trans*-**2a** and [EtP(μ-NTer)$_2$PEt] (**5a**) as shown by ^{31}P NMR studies (*trans*-**2a**: 229.2/255.2 ppm; *cis/trans*-**5a**: 225.2/266.7 ppm). The formation of *trans*-**2a** is consistent with the result of the reaction of biradical **1** with EtBr, where only *trans*-**2a** was obtained, but not **5a**. Still, the formation of **5a** in the reaction of **3Et•** with EtBr is not surprising, since in this instance there is a very large concentration of the **3Et•** radical in solution at the beginning of the reaction, which can react directly with another Et• radical that is formed upon reaction of EtBr with **3Et•** (see reaction 4 in Scheme 7, below), finally yielding [EtP(μ-NTer)$_2$PEt] (**5a**). In contrast, the formation of **5a** is very unlikely in the reaction of biradical **1** with EtBr, as **3Et•** is only formed as a low-concentrated intermediate in this case. From these combined experimental (and theoretical) studies, we can summarize that in the reaction of biradical **1** with EtBr, persistent radical **3Et•** occurs as an intermediate, indicating a radical mechanism for the addition reaction.

Computational studies

From the experimental studies on the mechanism of the EtBr addition to biradical **1**, several questions arose, such as why is the radical mechanism preferred over a concerted mechanism (Scheme 3) or which radicals form preferentially? To answer these questions, DFT and coupled cluster calculations on kinetics and thermodynamics were performed (see the Supporting Information for details). Furthermore, to account for the open-shell biradical character of biradical **1** along the reaction pathway, Complete Active Space SCF (CASSCF) methods were applied. The orbitals of the active space and their contributions are listed in Table S5. To account for dynamic correlation, the CASSCF reference wavefunctions were subjected to multireference perturbation calculations, using the Fully Internally Contracted N-Electron Valence State Perturbation Theory (FIC-NEVPT2).[91–93]

Model system. To obtain an initial idea of possible reaction pathways, the model reaction of [•P(μ-NH)$_2$P•] (**1^H**) with MeBr was investigated. Therefore, a variety of nudged elastic band (NEB)[94–98] and relaxed potential energy surface (PES) scans were performed at the UPBE–D3/def2-SVP[99] level of theory using ORCA 4.2.1[61,67] or Gaussian 09,[68] respectively. Different orientations of the starting materials and configurations of the product were considered. We could not locate a transition state for a concerted mechanism (e.g., analogous to the addition of H_2 to the singlet biradical [•P(μ-NTer)$_2$P•], Scheme 2).[35,100,101] All results pointed towards a stepwise (i.e., radical) mechanism of the reaction, in agreement with experimental observations. In

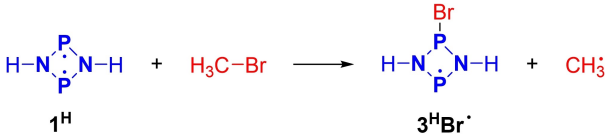

Scheme 6. Initial reaction step in the model reaction of **1^H** with MeBr.

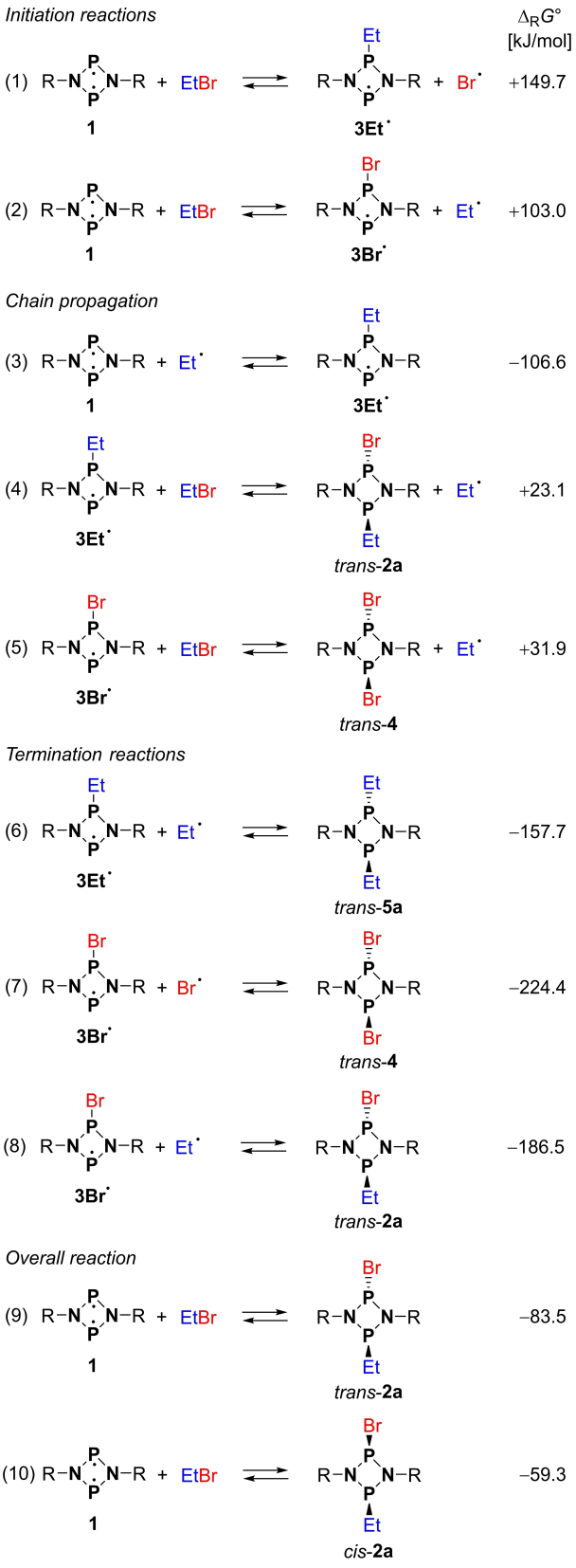

Scheme 7. Selected computed radical reaction steps, DLPNO-CCSD(T)/def2-TZVP//PBE–D3/def2-TZVP level of theory. Only the most likely reactions (based on $\Delta_R G°$ and concentrations) in each group are listed. See also Table S6.

particular, our model computations implied that the formal abstraction of a Br• radical from the bromoalkane by the singlet biradical initiated the radical chain reaction (see also section "Real system" below). It was therefore of special interest to investigate this first reaction step in more detail (Scheme 6).

Thus, the minimum-energy path (MEP) on the singlet PES of the reaction of $\mathbf{1}^{H}$ with MeBr was computed at the FIC-NEVPT2/def2-TZVP//UPBE-D3/def2-TZVP (Figure 7) as well as FIC-NEVPT2/def2-TZVP//CASSCF(4,4)/def2-TZVP levels of theory. The results of both approaches are similar (Figure S18). The biradical character increases smoothly as the reaction progresses, ultimately leading to two separate radical species (Figures 7 and 8).

Therefore, this initiation reaction (resulting in a radical chain reaction, see below and Scheme 6) is an intrinsically biradical process with a steadily decreasing singlet-triplet gap and an increasing biradical character (Figures 7 and 8). At the end of the reaction, when only the two separate radicals $\mathbf{3}^{H}\mathbf{Br}^{\bullet}$ and $CH_3^{\bullet}$ are present, the singlet and triplet states are degenerate, that is, two separate doublet species are present. Along the path on the singlet PES, no barrier is found but the formation of the two doublet species is endergonic. For the separated molecules $\mathbf{1}^{H}$ and MeBr, the biradical character (about 25%) is attributed exclusively to the radical electrons at the two P atoms in $\mathbf{1}^{H}$ (as represented by the blue isosurfaces of the local nondynamic correlation function[102–104] depicted in Figure 8). The biradical character increases dramatically over the course of the reaction, while one of the associated radical electrons shifts across the bromine atom to the methyl-C atom. Note that the tetraradical character (Figure 8), although low throughout the process, reaches a maximum at about d(C–Br) = 2.5 Å, where the C–Br and P–Br bond orders are roughly equal (Figure 9), indicating a small admixture of a Lewis-type structure of the type $^{\bullet}P(\mu\text{-}NH)_2P^{\bullet}\cdots Br^{\bullet}\cdots Me^{\bullet}$ (see also Table S5 for a depiction of the active orbitals).

Real system. Possible radical reaction steps were computed using the actual molecular structures (i.e., including the Ter and Et substituents). The relevant steps are listed in Scheme 7 (a full set of all possible reactions can be found in Table S6). In agreement with our computations on the model system (see above), we identified the abstraction of Br• from EtBr by the biradical [•P(μ-NTer)$_2$P•] (**1**) as the probable initiation reaction in an endergonic process ($\Delta_R G^\circ = 103$ kJ mol^{-1}) yielding **3Br•**. The formation of the ethyl-substituted radical **3Et•** in this first step is thermodynamically significantly less favored ($\Delta_R G^\circ = 149$ kJ mol^{-1}, cf. reactions 1 and 2 in Scheme 7). In this sense, the initiation reaction(s) may be understood as the "reaction barrier" for the radical process (cf. Scheme 8). Radical **3Br•** now has different reactions channels it can follow: i) **3Br•** can react with the free Et• radical to give the (experimentally observed) final *trans* product **2a** in a highly exergonic reaction ($\Delta_R G^\circ = -186.5$ kJ mol^{-1}, reaction 8 in Scheme 7). Therefore, the overall reaction **1** + EtBr → *trans*-**2a** becomes energetically favored with −83.5 kJ mol^{-1} (reaction 9 in Scheme 7). However, this termination reaction is rather unlikely because the concentration of free Et• radicals is very small compared to the concentration of EtBr. ii) **3Br•** can further react with EtBr affording the experimentally observed by-product **4** and Et• ($\Delta_R G^\circ = +31.9$ kJ mol^{-1}, reaction 5). The actual reaction turnover proceeds through addition of the free Et• radical (which is

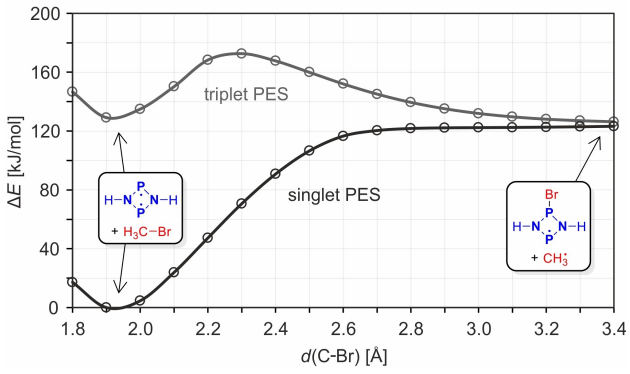

Figure 7. MEP of the reaction [•P(μ-NH)$_2$P•] + MeBr → [•P(μ-NH)$_2$PBr] + Me• on the singlet (S_0, blue) and triplet (T_1, red) PES at the FIC-NEVPT2/def2-TZVP//UPBE-D3/def2-TZVP level of theory. The near degeneracy of singlet and triplet at the end of the reaction indicates two separate radicals.

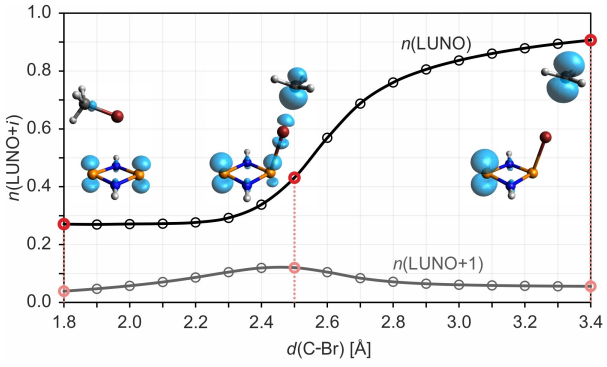

Figure 8. Change in the biradical character (LUNO occupancy; LUNO = lowest unoccupied natural orbital) and tetraradical character (LUNO + 1 occupancy) along the MEP of the initiation reaction (using a model system). The insets show the local nondynamic correlation function[102–104] (iso = 0.0025) at the points indicated in red.

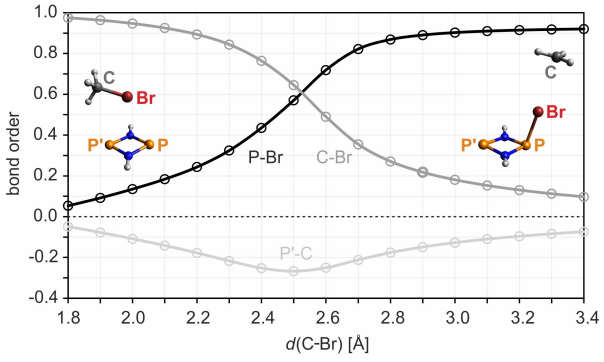

Figure 9. Change in the P–Br, C–Br, and P'–C bond orders along the MEP of the initiation reaction (using a model system). The C–Br bond order decreases (corresponding to the bond being broken), while the P–Br bond order increases smoothly. The interaction between the two radical centers (P', C) in the product is slightly antibonding throughout the reaction.

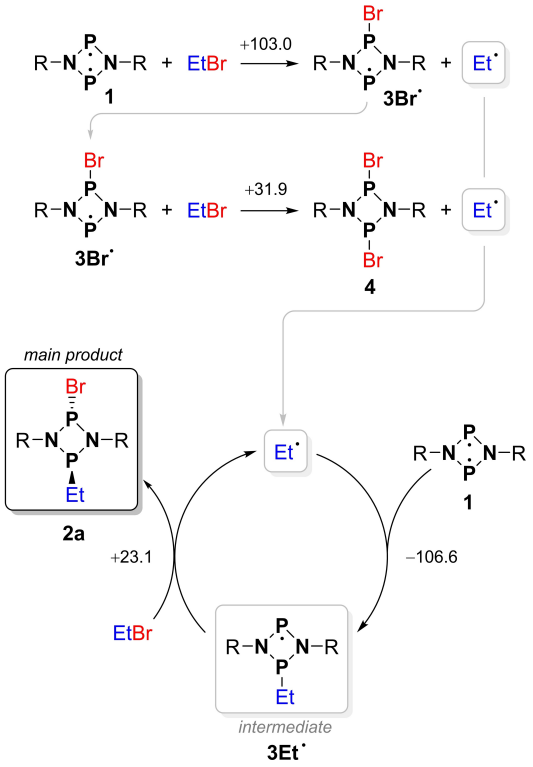

Scheme 8. Proposed radical reaction mechanism. Free reaction energies ($\Delta_R G^\circ$, $p^\circ = 1$ atm) in kJ mol^{-1} (DLPNO-CCSD(T)/def2-TZVP//PBE-D3/def2-TZVP).

initially generated by reactions 2 and 5 as discussed above) to the biradical [•P(μ-NTer)$_2$P•] (**1**), leading to the spectroscopically observed intermediate [•P(μ-NTer)$_2$P-Et] (**3Et•**) in an exergonic reaction ($\Delta_R G^\circ = -106.6$ kJ mol^{-1}, reaction 3). Radical **3Et•** then reacts with another equivalent of EtBr to the product [Br-P(μ-NTer)$_2$P-Et] (**2a**) and a new Et• radical ($\Delta_R G^\circ = +23.1$ kJ mol^{-1}, reaction 4). The free Et• radical can then repeat the reaction cascade outlined above (Scheme 8). All termination reactions are highly exergonic (Scheme 7 and Table S6).

Why is the radical **3Et•** the crucial intermediate (which we do observe experimentally), but not the bromine-substituted radical **3Br•**, which forms at the beginning of the reaction? This can be explained when considering the possible reactions of both radical species **3Et•** and **3Br•** with EtBr (e.g., reaction 4 in Scheme 7): The reaction of **3Br•** with EtBr leads preferentially to the side product **4** (+31.9 kJ mol^{-1}, reaction 5), while the reaction **3Br•** + EtBr → **2a** + Br• is thermodynamically unfavored (+69.9 kJ mol^{-1}, Table S6). In contrast, the formation of the product **2a** from **3Et•** and EtBr (+23.1 kJ mol^{-1}, reaction 4) is much more likely than the formation of the hypothetical by-product [Et-P(μ-NTer)$_2$P-Et] (**5a**, +98.6 kJ mol^{-1}), which was not observed experimentally (see above). Thus, formation of the final reaction product **2a** via the intermediate **3Et•** corresponds to the minimum energy path on the potential energy surface.

As outlined above, the by-product [Et-P(μ-NTer)$_2$P-Et] (**5a**) could in fact be generated when isolated **3Et•** was treated with EtBr. This is also in line with our computed radical reaction steps (Scheme 7 and Table S6). In this case, **5a** is likely formed by the termination reaction **3Et•** + Et• (−157.7 kJ mol^{-1}, reaction 6), owing to the very large concentration of **3Et•**, which is at least six orders of magnitude larger than the concentration of the intermediately formed **3Et•** in the reaction of **1** with EtBr. Thus, in the latter case, the same termination reaction is very unlikely to happen.

Finally, compared to *cis*-**2a**, the formation of *trans*-**2a** is energetically more favored by −24.3 kJ mol^{-1} (cf. reactions 9 and 10 in Scheme 7). This fact is best understood by looking at reaction 4 in Scheme 7. The formation of *trans*-**2a** is associated with a Gibbs energy of +23.1 kJ mol^{-1}, while the analogous reaction to the *cis*-**2a** product requires +47.7 kJ mol^{-1} (Table S6). Since these radical reaction steps are equilibrium reactions, it is understandable that the formation of *trans*-**2a** is thermodynamically significantly favored, which explains the exclusively observed formation of *trans*-**2a**. It is also worth noting that a solution of pure *trans*-**2a** does not isomerize to *cis*-**2a**.

Conclusion

We have demonstrated the radical reactivity of the biradical [•P(μ-NTer)$_2$P•] (**1**) for addition reactions of bromoalkanes. This approach represents a new synthesis route to asymmetrically substituted 1,3-substituted *cyclo*-1,3-diphospha-2,4-diazanes. Extensive experimental and theoretical studies revealed [•P(μ-NTer)$_2$PEt] (**3Et•**) as a radical intermediate for the addition process of ethyl bromide to **1**. With the direct synthesis of **3Et•**, it was possible to obtain a hitherto unknown persistent phosphorus-centered radical that can be generated on a large scale and stored for a long time under inert gas. It was possible to fully characterize **3Et•**, inter alia by EPR spectroscopy, single-crystal X-ray diffraction and UV-vis spectroscopy. Reactivity studies of **3Et•** with EtBr demonstrated its application in small-molecule activation processes, and we believe that it has the potential to open a new field of activation chemistry involving phosphorus, due to its relatively high thermal stability and good accessibility.

Experimental Section

All experiments were carried out under oxygen- and moisture-free conditions in an inert argon atmosphere using standard Schlenk or dry-box techniques. Experimental details including synthetic protocols, spectroscopic data and computational details can be found in the Supporting Information.

Deposition Numbers 2068187 (for **2a**), 2068188 (for **2b**), 2068189 (for **2c**), 2107762 (for **2d**), 2068190 (for **3Et•**), 2069052 (for **4**) contain the supplementary crystallographic data for this paper. These data are provided free of charge by the joint Cambridge Crystallographic Data Centre and Fachinformationszentrum Karlsruhe Access Structures service.

Acknowledgements

We wish to thank the ITMZ at the University of Rostock for access to the cluster computer, and especially Malte Willert for his assistance with the queuing system and software installations. This project received funding from the Deutsche Forschungsgemeinschaft (DFG, SCHU 1170/12-2). J.R. thanks the Konrad-Adenauer-Stiftung for financial and non-material support. Open Access funding enabled and organized by Projekt DEAL.

Conflict of Interest

The authors declare no conflict of interest.

Data Availability Statement

The data that support the findings of this study are available from the corresponding author upon reasonable request.

Keywords: biradicals · molecular chemistry · persistent radicals · phosphorus chemistry · radical chemistry

[1] A. Hinz, R. Kuzora, U. Rosenthal, A. Schulz, A. Villinger, *Chem. Eur. J.* **2014**, *20*, 14659–14673.
[2] A. Schulz, *Dalton Trans.* **2018**, *47*, 12827–12837.
[3] T. Stuyver, B. Chen, T. Zeng, P. Geerlings, F. De Proft, R. Hoffmann, *Chem. Rev.* **2019**, *119*, 11291–11351.
[4] *IUPAC. Compendium of Chemical Terminology* (*"The Gold Book"*), 2nd ed. (Eds.: A. D. McNaught, A. Wilkinson), Blackwell Scientific, Oxford, **1997**.
[5] F. Breher, *Coord. Chem. Rev.* **2007**, *251*, 1007–1043.
[6] J. Bresien, L. Eickhoff, A. Schulz, E. Zander, in *Comprehensive Inorganic Chemistry III* (Eds.: J. Reedijk, K. Poeppelmeier), Elsevier, **2021**, in press, DOI: 10.1016/B978-0-12-823144-9.000297.
[7] M. Abe, *Chem. Rev.* **2013**, *113*, 7011–7088.
[8] J. Michl, V. Bonačić-Koutecký, *Tetrahedron* **1988**, *44*, 7559–7585.
[9] H. Grützmacher, F. Breher, *Angew. Chem. Int. Ed.* **2002**, *41*, 4006–4011; *Angew. Chem.* **2002**, *114*, 4178–4184.
[10] F. Breher, *Coord. Chem. Rev.* **2007**, *251*, 1007–1043.
[11] W. C. Lineberger, W. T. Borden, *Phys. Chem. Chem. Phys.* **2011**, *13*, 11792–11813.
[12] S. González-Gallardo, F. Breher in *Comprehensive Inorganic Chemistry II*, Elsevier, **2013**, pp. 413–455.
[13] T. Beweries, R. Kuzora, U. Rosenthal, A. Schulz, A. Villinger, *Angew. Chem. Int. Ed.* **2011**, *50*, 8974–8978; *Angew. Chem.* **2011**, *123*, 9136–9140.
[14] E. Niecke, A. Fuchs, F. Baumeister, M. Nieger, W. W. Schoeller, *Angew. Chem. Int. Ed. Engl.* **1995**, *34*, 555–557; *Angew. Chem.* **1995**, *107*, 640–642.
[15] D. Scheschkewitz, H. Amii, H. Gornitzka, W. W. Schoeller, D. Bourissou, G. Bertrand, *Science* **2002**, *295*, 1880–1881.
[16] H. Sugiyama, S. Ito, M. Yoshifuji, *Angew. Chem. Int. Ed.* **2003**, *42*, 3802–3804; *Angew. Chem.* **2003**, *115*, 3932–3934.
[17] T. Brückner, F. Fantuzzi, T. E. Stennett, I. Krummenacher, R. D. Dewhurst, B. Engels, H. Braunschweig, *Angew. Chem. Int. Ed.* **2021**, *60*, 13661–13665; *Angew. Chem.* **2021**, *133*, 13774–13779.
[18] P. Henke, T. Pankewitz, W. Klopper, F. Breher, H. Schnöckel, *Angew. Chem. Int. Ed.* **2009**, *48*, 8141–8145; *Angew. Chem.* **2009**, *121*, 8285–8290.
[19] K. Takeuchi, M. Ichinohe, A. Sekiguchi, *J. Am. Chem. Soc.* **2011**, *133*, 12478–12481.
[20] S. Demeshko, C. Godemann, R. Kuzora, A. Schulz, A. Villinger, *Angew. Chem. Int. Ed.* **2013**, *125*, 2159–2162; *Angew. Chem.* **2013**, *125*, 2159–2162.
[21] A. Hinz, A. Schulz, A. Villinger, *Angew. Chem. Int. Ed.* **2015**, *54*, 2776–2779; *Angew. Chem.* **2015**, *127*, 2815–2819.
[22] C. B. Yildiz, K. I. Leszczyńska, S. González-Gallardo, M. Zimmer, A. Azizoglu, T. Biskup, C. W. M. Kay, V. Huch, H. S. Rzepa, D. Scheschkewitz, *Angew. Chem. Int. Ed.* **2020**, *59*, 15087–15092; *Angew. Chem.* **2020**, *132*, 15199–15204.
[23] Z. Li, X. Chen, D. M. Andrada, G. Frenking, Z. Benkö, Y. Li, J. R. Harmer, C.-Y. Su, H. Grützmacher, *Angew. Chem. Int. Ed.* **2017**, *56*, 5744–5749; *Angew. Chem.* **2017**, *129*, 5838–5843.
[24] D. Rottschäfer, B. Neumann, H.-G. Stammler, R. S. Ghadwal, *Chem. Eur. J.* **2017**, *23*, 9044–9047.
[25] M. K. Sharma, F. Ebeler, T. Glodde, B. Neumann, H.-G. Stammler, R. S. Ghadwal, *J. Am. Chem. Soc.* **2021**, *143*, 121–125.
[26] S. Ito, *Tetrahedron Lett.* **2018**, *59*, 1–13.
[27] M. Abe, J. Ye, M. Mishima, *Chem. Soc. Rev.* **2012**, *41*, 3808–3820.
[28] Z. Li, Y. Hou, Y. Li, A. Hinz, X. Chen, *Chem. Eur. J.* **2018**, *24*, 4738.
[29] H. Amii, L. Vranicar, H. Gornitzka, D. Bourissou, G. Bertrand, *J. Am. Chem. Soc.* **2004**, *126*, 1344–1345.
[30] X. Chen, C. Hu, X. Zhang, S. Liu, Y. Mei, G. Hu, L. L. Liu, Z. Li, C.-Y. Su, *Inorg. Chem.* **2021**, *60*, 5771–5778.
[31] A. Hinz, A. Schulz, *Phosphorus Sulfur Silicon Relat. Elem.* **2016**, *191*, 578–581.
[32] A. Hinz, A. Schulz, A. Villinger, *J. Am. Chem. Soc.* **2015**, *137*, 9953–9962.
[33] A. Hinz, R. Kuzora, U. Rosenthal, A. Schulz, A. Villinger, *Chem. Eur. J.* **2014**, *20*, 14659–14673.
[34] L. Chojetzki, A. Schulz, A. Villinger, R. Wustrack, *Z. Anorg. Allg. Chem.* **2020**, *646*, 614–624.
[35] A. Hinz, A. Schulz, A. Villinger, *Angew. Chem. Int. Ed.* **2016**, *55*, 12214–12218; *Angew. Chem.* **2016**, *128*, 12402–12406.
[36] A. Brückner, A. Hinz, J. B. Priebe, A. Schulz, A. Villinger, *Angew. Chem. Int. Ed.* **2015**, *54*, 7426–7430; *Angew. Chem.* **2015**, *127*, 7534–7538.
[37] F. Reiß, A. Schulz, A. Villinger, N. Weding, *Dalton Trans.* **2010**, *39*, 9962–9972.
[38] A. Hinz, A. Schulz, A. Villinger, J.-M. Wolter, *J. Am. Chem. Soc.* **2015**, *137*, 3975–3980.
[39] P. Pyykkö, M. Atsumi, *Chem. Eur. J.* **2009**, *15*, 186–197.
[40] E. D. Glendening, J. K. Badenhoop, A. E. Reed, J. E. Carpenter, J. A. Bohmann, C. M. Morales, C. R. Landis, F. Weinhold, *NBO 6.0*, Theoretical Chemistry Institute, University of Wisconsin, Madison, **2013**.
[41] J. E. Carpenter, F. Weinhold, *J. Mol. Struct.* **1988**, *169*, 41–62.
[42] F. Weinhold, J. E. Carpenter, in *The Structure of Small Molecules and Ions* (Eds.: R. Naaman, Z. Vager), Springer, Boston, MA, **1988**, pp. 227–236.
[43] F. Weinhold, C. R. Landis, *Valency and Bonding. A Natural Bond Orbital Donor–Acceptor Perspective*, Cambridge University Press, **2005**.
[44] G. He, O. Shynkaruk, M. W. Lui, E. Rivard, *Chem. Rev.* **2014**, *114*, 7815–7880.
[45] T. Chivers, I. Manners, *Inorganic Rings and Polymers of the P-Block Elements*, Royal Society of Chemistry, Cambridge, **2009**.
[46] H. Köhler, A. Michaelis, *Ber. Dtsch. Chem. Ges.* **1877**, *10*, 807–814.
[47] A. Michaelis, G. Schroeter, *Ber. Dtsch. Chem. Ges.* **1894**, *27*, 490–497.
[48] F. Reiss, A. Schulz, A. Villinger, N. Weding, *Dalton Trans.* **2010**, *39*, 9962–9972.
[49] L. Stahl, *Coord. Chem. Rev.* **2000**, *210*, 203–250.
[50] G. G. Briand, T. Chivers, M. L. Krahn, *Coord. Chem. Rev.* **2002**, *233–234*, 237–254.
[51] M. S. Balakrishna, D. J. Eisler, T. Chivers, *Chem. Soc. Rev.* **2007**, *36*, 650–664.
[52] M. S. Balakrishna, *Dalton Trans.* **2016**, *45*, 12252–12282.
[53] J. F. Nixon, B. Wilkins, *Z. Naturforsch.* **1970**, *25B*, 649.
[54] A. R. Davies, A. T. Dronsfield, R. N. Haszeldine, D. R. Taylor, *J. Chem. Soc. Perkin Trans. 1* **1973**, 379–385.
[55] K. W. Muir, *J. Chem. Soc. Dalton Trans.* **1975**, 259.
[56] G. Bulloch, R. Keat, D. G. Thompson, *J. Chem. Soc. Dalton Trans.* **1977**, 99–104.
[57] E. Fluck, D. Wachtler, *Liebigs Ann. Chem.* **1979**, *1979*, 1125–1129.
[58] H. J. Chen, R. C. Haltiwanger, T. G. Hill, M. L. Thompson, D. E. Coons, A. D. Norman, *Inorg. Chem.* **1985**, *24*, 4725–4730.
[59] R. Kuzora, A. Schulz, A. Villinger, R. Wustrack, *Dalton Trans.* **2009**, 9304–9311.
[60] A. Schulz, A. Villinger, A. Westenkirchner, *Inorg. Chem.* **2013**, *52*, 11457–11468.

[61] F. Neese, F. Wennmohs, U. Becker, C. Riplinger, *J. Chem. Phys.* **2020**, *152*, 224108.
[62] F. Neese, *Wiley Interdiscip. Rev.: Comput. Mol. Sci.* **2012**, *2*, 73–78.
[63] F. Neese, *J. Chem. Phys.* **2003**, *118*, 3939–3948.
[64] F. Neese, *J. Chem. Phys.* **2005**, *122*, 34107.
[65] F. Neese, *eMagRes* **2017**, 1–22.
[66] F. Neese, *J. Chem. Phys.* **2001**, *115*, 11080–11096.
[67] F. Neese, *Wiley Interdiscip. Rev.: Comput. Mol. Sci.* **2018**, *8*, e1327.
[68] *Gaussian 09, Revision E.01*, M. J. Frisch, G. W. Trucks, H. B. Schlegel, G. E. Scuseria, M. A. Robb, J. R. Cheeseman, G. Scalmani, V. Barone, B. Mennucci, G. A. Petersson, H. Nakatsuji, M. Caricato, X. Li, H. P. Hratchian, A. F. Izmaylov, J. Bloino, G. Zheng, J. L. Sonnenberg, M. Hada, M. Ehara, K. Toyota, R. Fukuda, J. Hasegawa, M. Ishida, T. Nakajima, Y. Honda, O. Kitao, H. Nakai, T. Vreven, J. A. Montgomery Jr., J. E. Peralta, F. Ogliaro, M. Bearpark, J. J. Heyd, E. Brothers, K. N. Kudin, V. N. Staroverov, T. Keith, R. Kobayashi, J. Normand, K. Raghavachari, A. Rendell, J. C. Burant, S. S. Iyengar, J. Tomasi, M. Cossi, N. Rega, J. M. Millam, M. Klene, J. E. Knox, J. B. Cross, V. Bakken, C. Adamo, J. Jaramillo, R. Gomperts, R. E. Stratmann, O. Yazyev, A. J. Austin, R. Cammi, C. Pomelli, J. W. Ochterski, R. L. Martin, K. Morokuma, V. G. Zakrzewski, G. A. Voth, P. Salvador, J. J. Dannenberg, S. Dapprich, A. D. Daniels, O. Farkas, J. B. Foresman, J. V. Ortiz, J. Cioslowski, D. J. Fox, Gaussian, Inc., Wallingford CT, **2013**.
[69] J. P. Perdew, K. Burke, M. Ernzerhof, *Phys. Rev. Lett.* **1996**, *77*, 3865–3868.
[70] J. P. Perdew, K. Burke, M. Ernzerhof, *Phys. Rev. Lett.* **1997**, *78*, 1396–1396.
[71] S. Grimme, S. Ehrlich, L. Goerigk, *J. Comput. Chem.* **2011**, *32*, 1456–1465.
[72] S. Grimme, J. Antony, S. Ehrlich, H. Krieg, *J. Chem. Phys.* **2010**, *132*, 154104.
[73] J. Bresien, T. Kröger-Badge, S. Lochbrunner, D. Michalik, H. Müller, A. Schulz, E. Zander, *Chem. Sci.* **2019**, *10*, 3486–3493.
[74] P. Agarwal, N. A. Piro, K. Meyer, P. Müller, C. C. Cummins, *Angew. Chem. Int. Ed.* **2007**, *46*, 2956; *Angew. Chem.* **2007**, *119*, 3014.
[75] D. Griller, K. U. Ingold, *Acc. Chem. Res.* **1976**, *9*, 13–19.
[76] M. Gomberg, *Ber. Dtsch. Chem. Ges.* **1900**, *33*, 3150–3163.
[77] T. Vogler, A. Studer, *Synthesis (Stuttg).* **2008**, *2008*, 1979–1993.
[78] J.-P. Bezombes, P. B. Hitchcock, M. F. Lappert, J. E. Nycz, *Dalton Trans.* **2004**, 499–501.
[79] N. A. Giffin, A. D. Hendsbee, T. L. Roemmele, M. D. Lumsden, C. C. Pye, J. D. Masuda, *Inorg. Chem.* **2012**, *51*, 11837–11850.
[80] N. J. Hill, G. Reeske, A. H. Cowley, *Main Group Chem.* **2010**, *9*, 5–10.
[81] N. A. Giffin, A. D. Hendsbee, J. D. Masuda, *Dalton Trans.* **2016**, *45*, 12636–12638.
[82] P. P. Power, *Chem. Rev.* **2003**, *103*, 789–809.
[83] S. L. Hinchley, C. A. Morrison, D. W. H. Rankin, C. L. B. Macdonald, R. J. Wiacek, A. H. Cowley, M. F. Lappert, G. Gundersen, J. A. C. Clyburne, P. P. Power, *Chem. Commun.* **2000**, 2045–2046.
[84] S. Ishida, F. Hirakawa, T. Iwamoto, *J. Am. Chem. Soc.* **2011**, *133*, 12968–12971.
[85] S. Ito, M. Kikuchi, M. Yoshifuji, A. J. Arduengo III, T. A. Konovalova, L. D. Kispert, *Angew. Chem. Int. Ed.* **2006**, *45*, 4341–4345; *Angew. Chem.* **2006**, *118*, 4447–4451.
[86] Y. Su, X. Zheng, X. Wang, X. Zhang, Y. Sui, X. Wang, *J. Am. Chem. Soc.* **2014**, *136*, 6251–4.
[87] P. P. Power, *Nature* **2010**, *463*, 171–177.
[88] *Biradicals, Radicals in Excited States, Carbenes and Related Species* (Ed.: H. Fischer), Springer, Berlin, Heidelberg, **1998**.
[89] F. Hartley, *The Chemistry of Organophosphorus Compounds*, Wiley, Hoboken, **1990**.
[90] B. Twamley, S. T. Haubrich, P. P. Power, *Advances in Organometallic Chemistry Vol. 44*, Elsevier, **1999**.
[91] C. Angeli, R. Cimiraglia, S. Evangelisti, T. Leininger, J.-P. Malrieu, *J. Chem. Phys.* **2001**, *114*, 10252–10264.
[92] C. Angeli, R. Cimiraglia, J.-P. Malrieu, *Chem. Phys. Lett.* **2001**, *350*, 297–305.
[93] C. Angeli, R. Cimiraglia, J.-P. Malrieu, *J. Chem. Phys.* **2002**, *117*, 9138–9153.
[94] G. Mills, H. Jónsson, G. K. Schenter, *Surf. Sci.* **1995**, *324*, 305–337.
[95] H. Jónsson, G. Mills, K. W. Jacobsen in *Classical and Quantum Dynamics in Condensed Phase Simulations*, World Scientific, **1998**, pp. 385–404.
[96] G. Henkelman, B. P. Uberuaga, H. Jónsson, *J. Chem. Phys.* **2000**, *113*, 9901–9904.
[97] G. Henkelman, H. Jónsson, *J. Chem. Phys.* **2000**, *113*, 9978–9985.
[98] E. Maras, O. Trushin, A. Stukowski, T. Ala-Nissila, H. Jónsson, *Comput. Phys. Commun.* **2016**, *205*, 13–21.
[99] F. Weigend, R. Ahlrichs, *Phys. Chem. Chem. Phys.* **2005**, *7*, 3297–305.
[100] V. V. Zhivonitko, J. Bresien, A. Schulz, I. V. Koptyug, *Phys. Chem. Chem. Phys.* **2019**, *21*, 5890–5893.
[101] V. V. Zhivonitko, H. Beer, D. O. Zakharov, J. Bresien, A. Schulz, *ChemPhysChem* **2021**, *22*, 813–817.
[102] E. Ramos-Cordoba, P. Salvador, E. Matito, *Phys. Chem. Chem. Phys.* **2016**, *18*, 24015–24023.
[103] E. Ramos-Cordoba, E. Matito, *J. Chem. Theory Comput.* **2017**, *13*, 2705–2711.
[104] T. Lu, F. Chen, *J. Comput. Chem.* **2012**, *33*, 580–592.

Manuscript received: February 25, 2022
Accepted manuscript online: April 21, 2022
Version of record online: May 19, 2022

6.3 Rational Design of a Phosphorus-centered Disbiradical

J. Rosenboom, F. Taube, L. Teichmeier, A. Villinger, M. Reinhard, S. Demeshko, M. Bennati, J. Bresien,* B. Corzilius,* A. Schulz*

Angew. Chem. Int. Ed. **2024**, 63, e202318210.

DOI: 10.1002/anie.202318210

How to cite: *Angew. Chem. Int. Ed.* **2024**, *63*, e202318210
doi.org/10.1002/anie.202318210

Radicals

Rational Design of a Phosphorus-Centered Disbiradical

Jan Rosenboom, Florian Taube, Leon Teichmeier, Alexander Villinger, Maik Reinhard, Serhiy Demeshko, Marina Bennati, Jonas Bresien, Björn Corzilius,* and Axel Schulz**

In memory of Edgar Niecke (1939–2023)

Abstract: Phosphorus-centered disbiradicals, in which the radical sites exist as individual spin doublets with weak spin-spin interaction have not been known so far. Starting from monoradicals of the type [•P(μ-NTer)$_2$P–R], we have now succeeded in linking two such monoradical phosphorus centers by appropriate choice of a linker. To this end, biradical [•P(μ-NTer)$_2$P•] (**1**) was treated with 1,6-dibromohexane, affording the brominated species {Br[P(μ-NTer)]$_2$}$_2$C$_6$H$_{12}$ (**3**). Subsequent reduction with KC_8 led to the formation of the disbiradical {•[P(μ-NTer)]$_2$}$_2$C$_6$H$_{12}$ (**4**) featuring a large distance between the radical phosphorus sites in the solid state and formally the highest biradical character observed in a P-centered biradical so far, approaching 100 %. EPR spectroscopy revealed a three-line signal in solution with a considerably larger exchange interaction than would be expected from the molecular structure of the single crystal. Quantum chemical calculations revealed a highly dynamic conformational space; thus, the two radical sites can approach each other with a much smaller distance in solution. Further reduction of **4** resulted in the formation of a potassium salt featuring the first structurally characterized P-centered distonic radical anion (**5**$^-$). Moreover, **4** could be used in small molecule activation.

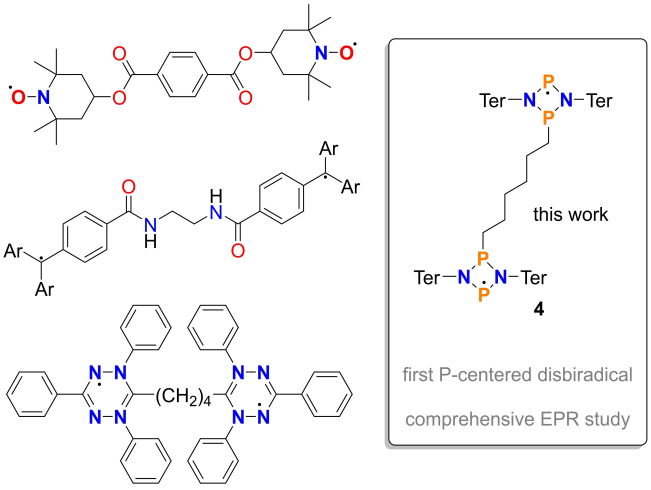

Figure 1. Left: Selected examples of O-, N-, and C-centered disbiradicals. Top: nitroxide[2]-, middle: trityl[4]- and bottom: verdazyl[5]-based disbiradicals. Right: Bis-*cyclo*-diphospha-diazene-diyl (**4**) featuring two phosphorus radical sites.

Biradicals are molecular entities with two unpaired electrons that can be classified by the interaction between the two electron spins (Figures 1 and 2),[1–3] which can be described by the electron exchange coupling constant J (note that throughout the paper the convention $\hat{H} = -2J\hat{\mathbf{S}}_1\hat{\mathbf{S}}_2$ will be used for the description of the isotropic exchange interaction). In case of $J \approx 0$, the interaction is negligible, the biradical is a two-doublet species, and has recently been termed a disbiradical.[1] Selected examples are shown in Figure 1. If $J \neq 0$ the species can be called a biradical(oid) and is either a singlet species ($J < 0$, antiferromagnetic coupling) or a triplet species ($J > 0$, ferromagnetic coupling, Figure 2). These different types of biradicals feature a different behavior in EPR experiments. While

[*] J. Rosenboom, F. Taube, L. Teichmeier, Dr. A. Villinger, Dr. J. Bresien, Prof. Dr. B. Corzilius, Prof. Dr. A. Schulz
Institut für Chemie, Universität Rostock
Albert-Einstein-Straße 3a, 18059 Rostock (Germany)
E-mail: jonas.bresien@uni-rostock.de
bjoern.corzilius@uni-rostock.de
axel.schulz@uni-rostock.de
Homepage: http://www.schulz.chemie.uni-rostock.de/
Prof. Dr. B. Corzilius, Prof. Dr. A. Schulz
Leibniz-Institut für Katalyse e.V.
Albert-Einstein-Straße 29a, 18059 Rostock (Germany)
M. Reinhard, Dr. S. Demeshko, Prof. Dr. M. Bennati
Georg-August-Universität Göttingen
Tammannstr. 4/6, 37077 Göttingen (Germany)
Prof. Dr. B. Corzilius
Department Life, Light & Matter, Universität Rostock
Albert-Einstein-Straße 25, 18059 Rostock (Germany)
M. Reinhard, Prof. Dr. M. Bennati
MPINAT, Research Group ESR Spectroscopy, Max Planck Institute for Multidisciplinary Sciences
Am Fassberg 11, 37077 Göttingen (Germany)

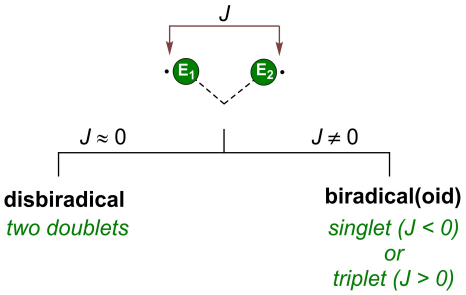

Figure 2. Classification of biradicals (E = any arbitrary atom containing an unpaired electron).

open-shell singlet biradicals like [•P(μ-NTer)$_2$P•] (**1**, Ter = 2,6-dimesitylphenyl) are EPR silent as their spin density is zero, triplet biradicals and disbiradicals show distinct EPR spectra. The form of an EPR signal associated with a disbiradical depends on the ratio between the electron-electron exchange interaction J and the hyperfine coupling A as illustrated in Figure 3.

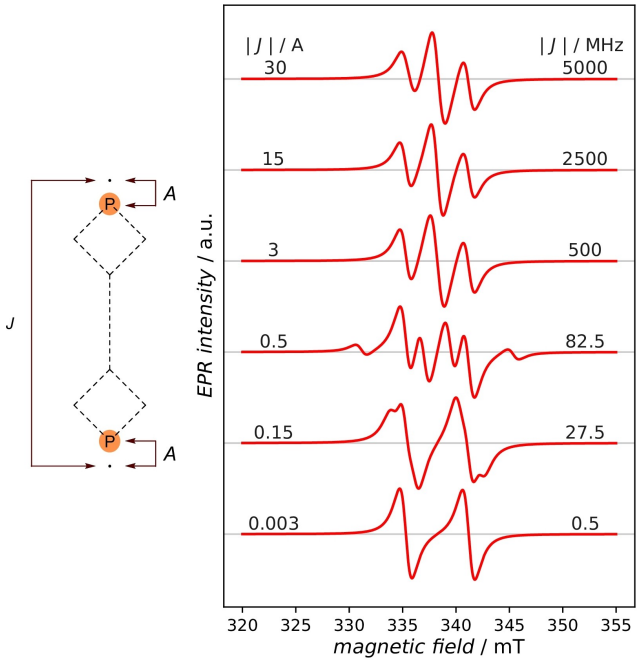

Figure 3. Comparison of simulated EPR signals arising from a symmetric P-centered disbiradical depending on the $|J|/A$ ratio ($g_{iso} = 2.0023$, $A_{iso}(^{31}P) = 165$ MHz, $S = 1/2$, $lw = 2$ mT (100 % LORENTZIAN, FWHM), $\omega_{\mu w} = 9.48$ GHz).

Figure 3 showcases the EPR signal form depending on various J/A ratios for a ^{31}P-centered biradical, with J varied and A held constant at 165 MHz. In the limiting case of a large J/A ratio, a three-line signal is visible. In case of a very small J/A ratio a two-line signal expected from a P-centered monoradical can be observed. Note that from a ratio $|J|/A > \approx 3$ no clear statement can be made about the strength of the J coupling. In this case ($|J| \gg A$), such a system can better be described by an effective spin $S = 1$, coupling with $A/2$ to two, in this specific case, equivalent nuclei without specification of the value of the J-coupling. This phenomenon was first described in copper acetate and also in other systems such as TSCHITSCHIBABIN type biradicals.[6,7]

Various classes of biradicals have been built up by combining two persistent monoradical units (nitroxides, verdazyls, triphenylmethyl (trityl) etc., Figure 1) with diverse conjugated and non-conjugated organic bridges.[1,8] The structural and electronic nature of the bridge results in a varying degree of interaction between the two unpaired electrons relevant for the usage as polarizing agents in DNP (Dynamic Nuclear Polarization) NMR spectroscopy.[4,9–11] Here we want to report on a novel phosphorus-centered disbiradical and its electronic and chemical properties.

Monoradicals of the type [•P(μ-NTer)$_2$P–R] can be prepared by addition of a bromoalkane, R–Br, to the well-known biradical [•P(μ-NTer)$_2$P•] (**1**) and subsequent reduction.[12] We now ask whether an analogous reaction with a dibromo-alkane would then lead to the desired disbiradical **4** (Schemes 1–3). For a sufficiently large distance between the radical centers to minimize their interaction, the alkane chain had to consist of at least a hexyl unit. Utilizing this bromoalkane route, it was indeed possible to add 1,6-dibromohexane to [•P(μ-NTer)$_2$P•] (**1**) in a 1:1 stoichiometry forming dibromo-precursor **2** in 52 % isolated yield (Scheme 1). When **2** was reacted with another equiv-

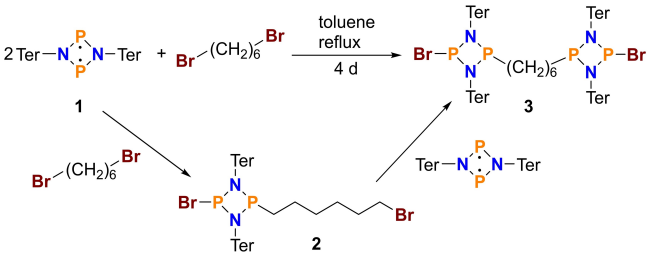

Scheme 1. Reaction between **1** and 1,6-dibromohexane forming **2** and bridged dibromo-precursor **3** depending on the used stoichiometry.

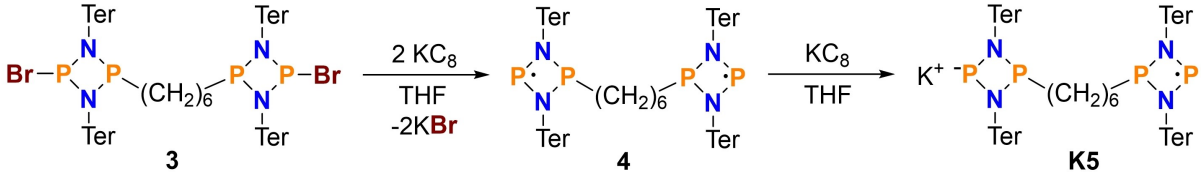

Scheme 2. Reduction of **3** with KC_8 yields disbiradical **4**. Overreduction leads to the formation of the potassium salt **K5** exhibiting a distonic radical anion **5**$^-$.

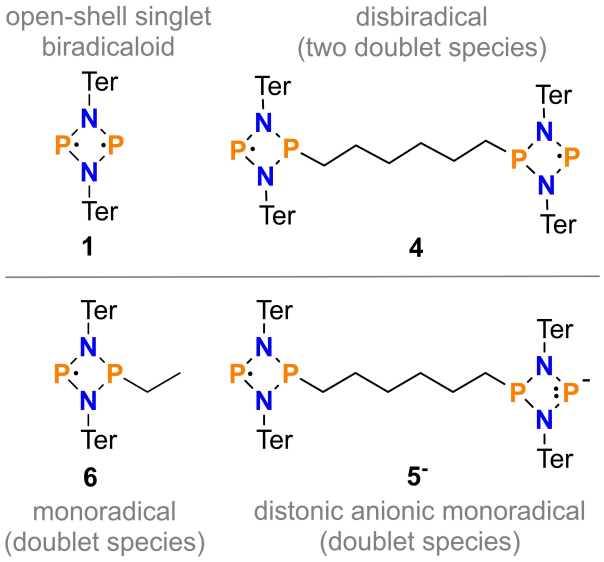

Scheme 3. Mono- and biradicals with a *cyclo*-diphospha-diaza-ring.

alent of **1** the desired bridged dibromo-substituted species **3** could be isolated. Compound **3** was also directly accessible on a gram scale when a 2:1 stoichiometry of **1** to 1,6-dibromohexane was applied from the beginning (yield = 68 %). Due to the large steric demand of the Ter substituents the reaction required high temperatures and long reaction times (111 °C over 4 d) compared to bromoalkanes with a smaller alkyl chain (minutes to days at RT).[12] Products **2** and **3** were fully characterized (see ESI, Figures S3–S6). Reduction of **3** with KC_8 in THF led to the formation of the desired disbiradical **4** in good yields (59 %, Scheme 2), which was immediately indicated by a color change to dark red.

It is important to know that the product distribution (purity) and yields depend strongly on the reaction control, especially on the stoichiometry. For example, when **3** and two equivalents of KC_8 were combined in the solid and then the solvent was added, over-reduction occurred due to the low solubility of **3** in THF, resulting in the partial formation of potassium salt **K5** bearing the distonic radical anion $\mathbf{5}^-$ (Scheme 2). However, when the KC_8 was added to a suspension of **3** in several small portions over a period of 15 min and the reaction mixture was then filtered over *celite*®, pure single-crystalline **4** could be obtained in moderate yields (50–60 %, Figures 4 and 5). The oxygen- and moisture-sensitive disbiradical **4** was long term stable when stored in a sealed ampoule under inert gas. Thermally, it decomposed at 200 °C while loss of solvent from the single crystals was already observed at 109 °C (for DSC data see Figure S7). As species **4** is paramagnetic, when crystals were dissolved in C_6D_6 and ^{31}P NMR spectra were recorded, no signals for **4** were detected, while in the ^1H NMR spectrum only signals of the co-crystallized THF molecules were visible. Dark red crystals of **4** crystallized from THF in the orthorhombic space group *Fddd* with eight formula units and six co-crystallized solvent molecules per cell. There are no close intermolecular contacts between molecules of **4** in

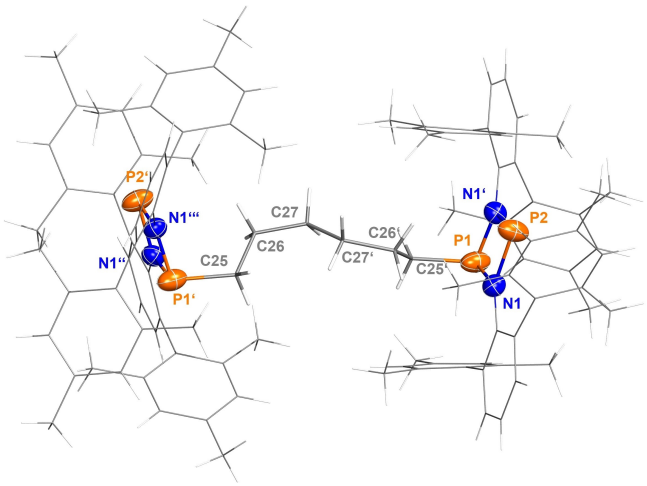

Figure 4. Molecular structure of the disbiradical **4** in the crystal. Thermal ellipsoids at 50 % probability (123 K). Ter substituents and alkyl bridge depicted as wireframe for clarity. Selected bond lengths (Å) and torsion angles [°]: N1–P1 1.749(4), N1′–P1 1.673(4), N1–P2 1.805(4), N1′–P2 1.683(4), P1–C25′ 1.85(1), P2···P2′ 10.913(6); P1–N1–N1′–P2 178.0(2), N1–P1–N1′–C25 101.2(4), N1′–P1–N1–C25 102.4(4).

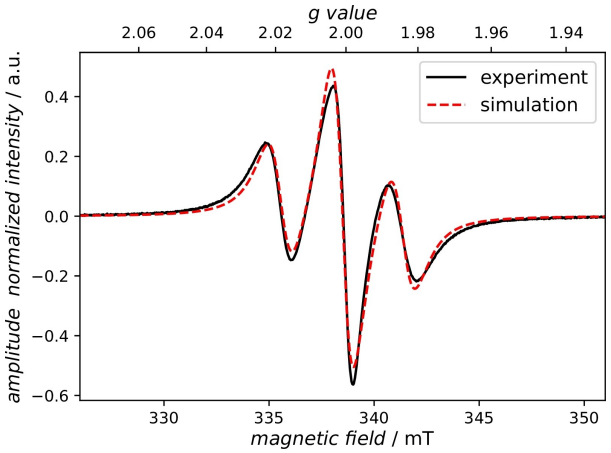

Figure 5. X-band (9.48 GHz) EPR spectrum of **4** in THF, $T = 293$ K ($S = 1$, $g_{iso} = 2.001$, $A_1(^{31}P)/2 = A_2(^{31}P)/2 = -40$ MHz, $A_3(^{31}P)/2 = 324$ MHz, $lw = 1.713$ mT (100 % Lorentzian, FWHM), $\tau_R = 0.035$ ns) (for details on simulation see below).

the crystal. The molecular structure is determined by its C_2 symmetry with an intersection of three C_2-axes resulting in a disorder over two molecule layers (overall D_2 symmetry, cf. Figure S1). Both radical phosphorus centers (P2/P2′), separated by 10.913(5) Å, sit in pockets that are well protected by the four bulky Ter substituents, as depicted in Figure 4. The most prominent structural feature of **4** is the two nearly planar P_2N_2 four-membered heterocycles bridged by a hexyl group (deviation from planarity < 2°). All four P–N distances are different (1.673(4)–1.805(4) Å) and are in the range of polar P–N single bonds (cf. Σr_{cov}(P–N) = 1.82 Å).[13]

As expected, computations of **4** confirm that it is a phosphorus-centered disbiradical (a two-doublet species).

The MULLIKEN spin density is mainly localized at the divalent P2 (≈0.75, cf. 0.70 [•P(μ-N–Ter)$_2$P–Et] (**6**), Scheme 3);[12] while only small values are computed for N1 (0.03) and N1′ (0.03), respectively (Figure S23). The large distance of 10.913(6) Å (calcd. 10.39 Å) between the two P atoms containing the unpaired electrons does not allow for any significant dipole-dipole interaction in the solid state (Figure 4 and Figure 6), and, additionally, the unconjugated hexyl linker leads to vanishing electron-electron exchange interaction by conjugation. It was all the more surprising that solution EPR experiments (Figure 5) with pure **4** yielded a spectrum with a 1:2:1 triplet (See Supporting Information section 5.1.4), typical of a biradical with a sizeable interaction between the two electrons. The line shape of the experimental spectra clearly indicates a *J*-coupling of >1 GHz when compared to simulations (Figure 3) and thus comes to the limit of what can be sensibly detected in X-band. From this observation, it was clear that the structure in solution must be subject to dynamics that cause the two radical P-atoms to approach each other.

Therefore, a conformer search using CREST[14,15] and CENSO[16] together with GFN-FF force field[17] and GFN2-xTB[18]//GFN-FF composite methods was performed. The screening of more than 60000 structures (500 conformers) revealed that in solution the most favorable structures are the ones with a much shorter P2···P2′ distance. The most energetically favorable and therefore dominant conformer in solution (T1, x=47 %, Figure 6; cf. Figure S21 for more details and other conformers) has a P2···P2′ distance of only 7.31 Å and is energetically stabilized with respect to the conformer observed in the solid state (T5, d(P2···P2′)= 10.39 Å) by 17 kJ/mol. Hence, the peculiar EPR signal of **4** in solution can be explained by exchange coupling of the two electrons not through the unconjugated CH_2-chain but "through space" in accord with computed EPR data (Table S6).

The EPR signal of **4** in solution was investigated at different temperatures (Figure 7) and with different microwave frequencies (X-band/Q-band). At higher temperatures, an increase in the amplitude of the outer transitions occurred which allows an investigation of dynamic effects within the system caused by partial averaging of the ***g***- and ***A***-anisotropies by rotational diffusion of the molecule.[19,20] A deviation of the spin system from the isotropic limit seems conceivable considering the high molar mass of M=1517 g/mol. To get access to the ***g***- and ***A***-tensors a spectrum of the Et-substituted monoradical **6** was recorded in frozen solution (See Supporting Information section 5.1.2) and evaluated. With this data, simulations were performed taking into account the isotropic rotation-correlation time τ_R which varies between 0.005 ns and 0.152 ns depending on the measurement temperature. These correlation times are at least an order of magnitude shorter than what is expected from the STOKES–EINSTEIN–DEBYE equation for a rigid spherical particle. Therefore, we conclude that internal conformational dynamics are allowing the radical moieties to reorient on a much faster timescale than the molecule as whole. The fact that all spectra can easily be reproduced considering a S=1 system coupling to two equivalent phosphorous atoms with $A(^{31}P)/2$ demonstrates that the resulting dynamically averaged J must still be much larger than the isotropic $A(^{31}P)$ and that isotropic (exchange) J is dominating over dipolar e–e interaction.

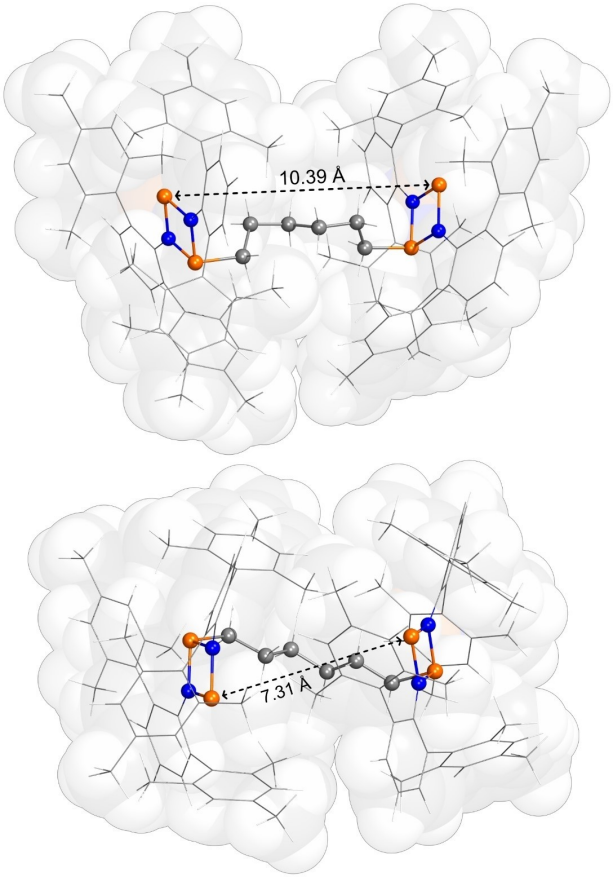

Figure 6. Comparison of the optimized molecular structures originating from the solid state data (T5, top) and most favorable conformer in toluene solution (T1, bottom; conformer search using CREST/CENSO, GFN2-xTB[18]//GFN-FF, optimization at B97–3c, solvent correction for toluene)

An EPR spectrum of a single crystal of **4** in the solid state was also measured. However, the intramolecular electron-electron interaction was not visible due to the high spin concentration causing a loss of all information about the (hyper−)fine structure and only one broad transition was observed (Figure S16). A Q-band EPR spectrum of **4** in solution could be simulated[21–23] using the parameters from the X-band series of Figure 7 (see Supporting Information section 5.1.5 for Q-band EPR spectrum and simulation), showing the consistency of our set of anisotropy parameters and correlation time at different field strengths.

In light of the definition of the term disbiradical ($J \approx 0$, vide infra), one could assume that a disbiradical is indeed present in the single crystal of species **4**, considering the expectedly small electron-electron interaction and the relatively larger ***A***–anisotropy. In contrast, in solution a dynamic conformational change occurs which gives rise to clear experimental evidence of an *EPR spectroscopically* significant electron-electron coupling dominating over the iso-

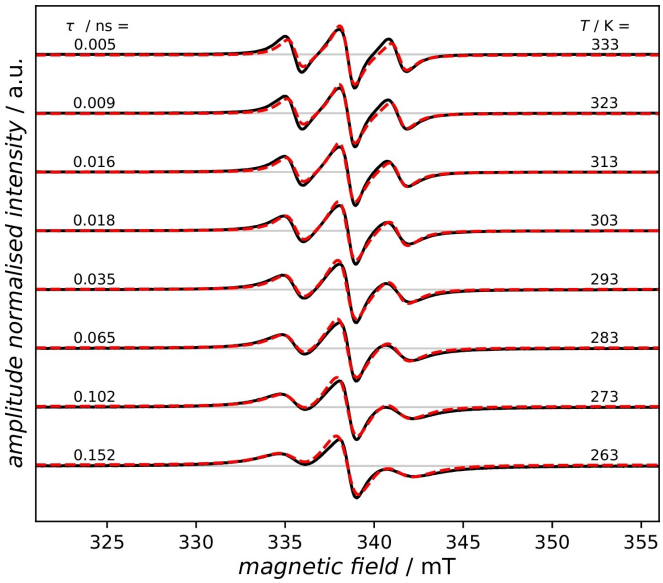

Figure 7. X-band (9.48 GHz) EPR spectra of **4** dissolved in THF at different temperatures. The hyperfine interaction tensor ***A*** determined from simulation of the experimental EPR spectrum of **6** at 100 K was kept constant for the different temperatures, varying only the rotational correlation time τ_R (See Supporting Information section 5.1.3 for further information and simulation parameters).

tropic EPR parameters. But the question now arises whether such a species can generally still be considered a disbiradical. This ultimately leads us to the dilemma to define at what magnitude of interaction the transition from a disbiradical to a biradical(oid) occurs, and it is worth noting that this transition is continuous, and also depends on the external conditions of the experiment (i.e., can the two doublet centers be spectroscopically distinguished with respect to their interaction). Equally interesting is the differing perspective from molecular chemists and spectroscopists about what is considered to be a significant interaction between the two unpaired electrons in a biradical. For example, the coupling constant J of >500 MHz as observed in the solution EPR spectrum equals a singlet-triplet energy gap (ΔE_{S-T}) of $>4.0\times10^{-4}$ kJ/mol which *from a chemical reactivity point of view* indicates virtually degenerate singlet and triplet states. Therefore, we refer to **4** as a disbiradical despite the observed three-line signal in the solution EPR spectrum.

The singlet-triplet energy gap was additionally estimated using magnetic susceptibility measurements on a SQUID magnetometer. Experimental data were modelled with the *julX* program[24] using a fitting procedure to the spin Hamiltonian $\hat{H} = -2J\hat{\mathbf{S}}_1\hat{\mathbf{S}}_2 + g\mu_B\mathbf{B}\left(\hat{\mathbf{S}}_1 + \hat{\mathbf{S}}_2\right)$. The coupling constant J amounted to $-0.19\ cm^{-1}$ equaling to a ΔE_{S-T} of $-0.38\ cm^{-1}$ or about -4.5×10^{-3} kJ/mol indicating a singlet ground state with a biradical character of virtually 100 % (see Figure S24). As intermolecular interactions also play a role in the solid compared to a low-concentrated sample in solution, this is to be considered as a maximum value and is thus in good agreement with the data obtained by EPR spectroscopy and computations ($\Delta E_{S-T} = -3.2\times10^{-3}$ kJ/mol, see Supporting Information section 6.2 for details).

After the synthesis of pure **4**, we also tried to reduce it further selectively to obtain the pure distonic radical anion $\mathbf{5}^-$ as potassium salt **K5** (Scheme 2). However, this proved to be very difficult. Even with long reaction times and a large excess of KC_8, it was impossible to obtain pure **K5**. Reaction EPR spectra and NMR data suggest overreduction of **5** towards a Ter-phosphide[25] while **4** was still detectable (Figure S12). Hence, only mixed single crystals of **4** and **K5** with varying ratios of both compounds could be isolated. As determined by single crystal XRD they crystallized very similarly to pure **4** in the orthorhombic space group *Fddd.* (See ESI for details). The molecular structure of **K5** is displayed in Figure 8. The mixed single crystals were also dissolved and an X-band EPR spectrum of the resulting mixture of **4** and **K5** (83 % to 17 %) was measured (Figure 9).

Due to the structural similarities, the *g*-factors and coupling constants A of the two compounds are virtually identical and therefore the two signals are superimposed. As in $\mathbf{5}^-$ only one unpaired electron is present (doublet species), this results in a two-line signal due to the coupling with one ^{31}P nucleus. As depicted in Scheme 3, the radical moiety of $\mathbf{5}^-$ is also structurally and electronically similar to the ethyl substituted monoradical **6** previously synthesized by our group.[12]

Therefore, it was possible to simulate[21–23] the EPR spectrum of a solution of **4**/**K5** mixed crystals by using the EPR parameters from pure **4** and the pure ethyl substituted monoradical **6**, magnetically virtually equivalent to $\mathbf{5}^-$, and applying the ratios derived from single crystal XRD of the same sample. By this procedure, it was possible to obtain

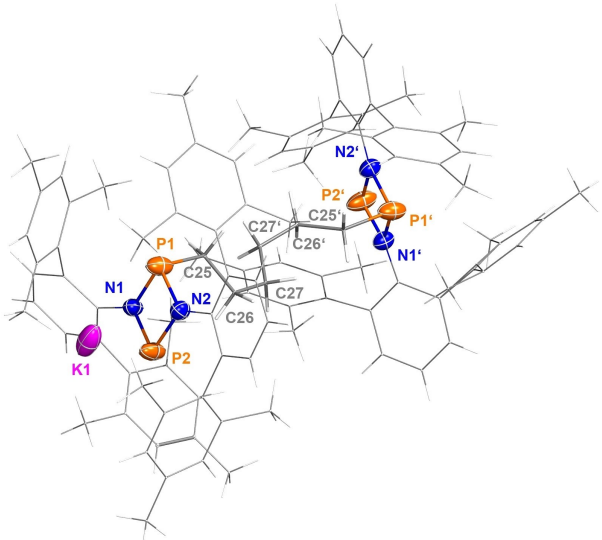

Figure 8. Molecular structures of the salt **K5** bearing the distonic radical anion $\mathbf{5}^-$ in the crystal. Thermal ellipsoids at 50 % probability (123 K). Ter substituents depicted as wireframe for clarity. Selected bond lengths (Å) and torsion angles [°]: N1–P1 1.70(1), N2–P1 1.771(9), N2–P2 1.74(1), N1–P2 1.71(1), P1–C25 1.879(7), K1–P2 2.810(7), P1–N1–N2–P2 179.1(7), N1–P1–N2–C25 97.6(5).

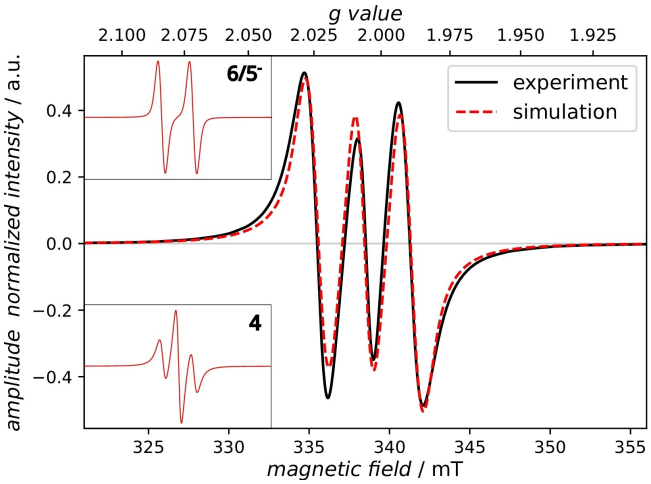

Figure 9. X-band (9.48 GHz) EPR spectrum and simulation of a mixture (83 : 17) of **4** and **K5** in toluene; simulated spectra of pure components are shown in inserts (magnetic field axis at same scale). EPR parameters for pure components in toluene: Monoradical: $S=1/2$, $g_{iso}=2.0011$, $A_{iso}(^{31}P)=164$ MHz, $lw=1.1$ mT : 1 mT (Gaussian : Lorentzian, FWHM); Biradical: $S=1$, $g_{iso}=2.001$, $A_1(^{31}P)/2=A_2(^{31}P)/2=-40$ MHz, $A_3(^{31}P)/2=324$ MHz, $lw=1.713$ mT (100% Lorentzian, FWHM), $\tau_R=0.044$ ns Simulation was done by using ratios obtained from single crystal XRD and EPR parameters of pure **4** and pure ethyl substituted monoradical **6**. See Supporting Information section 5.1.6. for details.

the simulated spectrum in Figure 9 despite the lack of a pure sample of **K5**, proving that EPR and XRD data are coherent. Although numerous P-centered monoradicals are known,[26–28] to the best of our knowledge there are no examples of structurally characterized P-centered distonic radical anions.[29–31]

Finally, first preliminary reactivity studies with **4** showed that it does not react with H_2 (1 atm, 60 °C, 3 h). However, when exposed to acetylene several new species were detected by ^{31}P NMR spectroscopy indicating poly-/oligomerization (Figure S18).

In summary, the synthesis of a phosphorus-based disbiradical **4** was achieved by introducing an innocent hexyl ligand (Scheme 3). **4** isomerizes in solution, forming conformers with significant shorter distances between the radical sites which can thereby interact weakly by partial overlap of the spin-carrying orbitals through space. Starting from brominated precursor **3**, a salt with a distonic monoradical anion was also synthesized by further reduction. In preliminary studies, **4** was used in small molecule activation chemistry and is to be applied as polarization transfer reagents in DNP NMR spectroscopy.

Supporting Information

The authors have cited additional references within the Supporting Information.[32–73] Deposition numbers 2304337 (for **2**), 2304336 (for **3**), 2304333 (for **4**), 2304334 (for **4**/**K5**), 2304335 (for **7**) contain the supplementary crystallographic data for this paper. These data are provided free of charge by the joint Cambridge Crystallographic Data Centre and Fachinformationszentrum Karlsruhe Access Structures service.

Acknowledgements

J.R. wants to thank the Konrad-Adenauer-Stiftung for financial and non-material support. Additionally, we thank Dr. Edgar Zander for help in the lab. We wish to thank the ITMZ at the University of Rostock for access to the cluster computer. This project received funding from the Deutsche Forschungsgemeinschaft (DFG; SCHU 1170/12-2, SFB TRR 386 TRR 386-A2). Purchase of the SQUID magnetometer was enabled by the Deutsche Forschungsgemeinschaft (DFG, German Research Foundation, project number INST 186/1329-1 FUGG) and the Niedersächsische Ministerium für Wissenschaft und Kultur (MWK); purchase of the EPR spectrometer was supported by the European Union through EFRE grant GHS-21-0005. Open Access funding enabled and organized by Projekt DEAL.

Conflict of Interest

The authors declare no conflict of interest.

Data Availability Statement

The data that support the findings of this study are available in the supplementary material of this article.

Keywords: Biradical · Diradical · Distonic Radical Anion · EPR Spectroscopy · Phosphorus Chemistry

[1] A. Hinz, J. Bresien, F. Breher, A. Schulz, *Chem. Rev.* **2023**, *123*, 10468–10526.
[2] M. Abe, *Chem. Rev.* **2013**, *113*, 7011–7088.
[3] J. Bresien, L. Eickhoff, A. Schulz, E. Zander, in *Comprehensive Inorganic Chemistry III* (Eds.: J. Reedijk, K. R. Poeppelmeier), Elsevier, Oxford, **2023**, pp. 165–233.
[4] S. Macholl, H. Jóhannesson, J. H. Ardenkjaer-Larsen, *Phys. Chem. Chem. Phys.* **2010**, *12*, 5804–5817.
[5] B. D. Koivisto, R. G. Hicks, *Coord. Chem. Rev.* **2005**, *249*, 2612–2630.
[6] B. Bleaney, K. D. Bowers, *Proc. R. Soc. London Ser. A* **1952**, *214*, 451–465.
[7] P. Ravat, M. Baumgarten, *Phys. Chem. Chem. Phys.* **2015**, *17*, 983–991.
[8] I. Ratera, J. Veciana, *Chem. Soc. Rev.* **2012**, *41*, 303–349.
[9] J. Soetbeer, P. Gast, J. J. Walish, Y. Zhao, C. George, C. Yang, T. M. Swager, R. G. Griffin, G. Mathies, *Phys. Chem. Chem. Phys.* **2018**, *20*, 25506–25517.
[10] R. Harrabi, T. Halbritter, F. Aussenac, O. Dakhlaoui, J. van Tol, K. K. Damodaran, D. Lee, S. Paul, S. Hediger, F. Mentink-Vigier, S. T. Sigurdsson, G. De Paëpe, *Angew. Chem. Int. Ed.* **2022**, *61*, e202114103.
[11] G. Menzildjian, J. Schlagnitweit, G. Casano, O. Ouari, D. Gajan, A. Lesage, *Chem. Sci.* **2023**, *14*, 6120–6148.

[12] J. Rosenboom, L. Chojetzki, T. Suhrbier, J. Rabeah, A. Villinger, R. Wustrack, J. Bresien, A. Schulz, *Chem. Eur. J.* **2022**, *28*, e202200624.
[13] P. Pyykkö, M. Atsumi, *Chem. Eur. J.* **2009**, *15*, 186–197.
[14] S. Grimme, *J. Chem. Theory Comput.* **2019**, *15*, 2847–2862.
[15] P. Pracht, F. Bohle, S. Grimme, *Phys. Chem. Chem. Phys.* **2020**, *22*, 7169–7192.
[16] S. Grimme, F. Bohle, A. Hansen, P. Pracht, S. Spicher, M. Stahn, *J. Phys. Chem. A* **2021**, *125*, 4039–4054.
[17] S. Spicher, S. Grimme, *Angew. Chem. Int. Ed.* **2020**, *59*, 15665–15673.
[18] C. Bannwarth, S. Ehlert, S. Grimme, *J. Chem. Theory Comput.* **2019**, *15*, 1652–1671.
[19] E. G. Bagryanskaya, D. N. Polovyanenko, M. V. Fedin, L. Kulik, A. Schnegg, A. Savitsky, K. Möbius, A. W. Coleman, G. S. Ananchenko, J. A. Ripmeester, *Phys. Chem. Chem. Phys.* **2009**, *11*, 6700–6707.
[20] S. Stoll, D. Goldfarb, *EPR Spectroscopy: Fundamentals and Methods*, Wiley, Hoboken, **2018**.
[21] M. Schröder, T. Biskup, **2023**, https://doi.org/10.5281/ZENODO.8150469.
[22] M. Schröder, T. Biskup, *J. Magn. Reson.* **2022**, *335*, 107140.
[23] S. Stoll, A. Schweiger, *J. Magn. Reson.* **2006**, *178*, 42–55.
[24] E. Bill, *julX*, *Program for Simulation of Molecular Magnetic Data*, Max-Planck Institute for Chemical Energy Conversion, Mülheim/Ruhr, **2008**.
[25] A. Hinz, A. Schulz, A. Villinger, *Angew. Chem. Int. Ed.* **2015**, *54*, 668–672.
[26] B. Das, A. Makol, S. Kundu, *Dalton Trans.* **2022**, *51*, 12404–12426.
[27] Y. Su, X. Zheng, X. Wang, X. Zhang, Y. Sui, X. Wang, *J. Am. Chem. Soc.* **2014**, *136*, 6251–6254.
[28] P. P. Power, *Chem. Rev.* **2003**, *103*, 789–810.
[29] B. F. Yates, W. J. Bouma, L. Radom, *J. Am. Chem. Soc.* **1984**, *106*, 5805–5808.
[30] K. M. Stirk, L. K. M. Kiminkinen, H. I. Kenttamaa, *Chem. Rev.* **1992**, *92*, 1649–1665.
[31] D. M. Tomazela, A. A. Sabino, R. Sparrapan, F. C. Gozzo, M. N. Eberlin, *J. Am. Soc. Mass Spectrom.* **2006**, *17*, 1014–1022.
[32] C. H. Butzlaff, A. X. Trautwein, E. Winkler, *Metallobiochemistry*, *Pt. D: Physical and Spectroscopic Methods for Probing Metal Ion Environments in Metalloproteins*, Academic Press, New York, **1993**, pp. 412–437.
[33] E. Bill, *mpView.1.4.1*, *Program for Viewing and Data Import for Files from MPMS3 SQUID Magnetometer*, Max-Planck Institute for Chemical Energy Conversion, Mülheim/Ruhr, **2021**.
[34] F. Neese, F. Wennmohs, U. Becker, C. Riplinger, *J. Chem. Phys.* **2020**, *152*, 224108.
[35] F. Neese, *Wiley Interdiscip. Rev.: Comput. Mol. Sci.* **2022**, *12*, e1606.
[36] C. Bannwarth, E. Caldeweyher, S. Ehlert, A. Hansen, P. Pracht, J. Seibert, S. Spicher, S. Grimme, *Wiley Interdiscip. Rev.: Comput. Mol. Sci.* **2021**, *11*, e01493.
[37] J. G. Brandenburg, C. Bannwarth, A. Hansen, S. Grimme, *J. Chem. Phys.* **2018**, *148*, 064104.
[38] S. Grimme, J. Antony, S. Ehrlich, H. Krieg, *J. Chem. Phys.* **2010**, *132*, 154104.
[39] S. Grimme, S. Ehrlich, L. Goerigk, *J. Comput. Chem.* **2011**, *32*, 1456–1465.
[40] F. Weigend, R. Ahlrichs, *Phys. Chem. Chem. Phys.* **2005**, *7*, 3297.
[41] A. Hellweg, C. Hättig, S. Höfener, W. Klopper, *Theor. Chem. Acc.* **2007**, *117*, 587–597.
[42] W. Haberditzl, *Angew. Chem. Int. Ed.* **1966**, *5*, 288–298.
[43] G. A. Bain, J. F. Berry, *J. Chem. Educ.* **2008**, *85*, 532.
[44] G. M. G. M. Sheldrick, *SADABS*, University Of Göttingen, Germany, University of Göttingen, Germany, **2004**.
[45] T. Biskup, **2023**, https://doi.org/10.5281/zenodo.4717937.
[46] Origin(Pro), Version 2023. OriginLab Corporation, Northampton, MA, USA.
[47] G. M. Sheldrick, *Acta Crystallogr. Sect. A* **2015**, *71*, 3–8.
[48] J. Popp, T. Biskup, *Chem. Methods* **2022**, *2*, e202100097.
[49] F. Neese, *Wiley Interdiscip. Rev.: Comput. Mol. Sci.* **2012**, *2*, 73–78.
[50] S. Ehlert, M. Stahn, S. Spicher, S. Grimme, *J. Chem. Theory Comput.* **2021**, *17*, 4250–4261.
[51] S. Grimme, *J. Comput. Chem.* **2006**, *27*, 1787–1799.
[52] A. V. Marenich, C. J. Cramer, D. G. Truhlar, *J. Phys. Chem. B* **2009**, *113*, 6378–6396.
[53] F. Neese, *J. Chem. Phys.* **2001**, *115*, 11080–11096.
[54] F. Neese, *J. Chem. Phys.* **2003**, *118*, 3939–3948.
[55] F. Neese, *J. Chem. Phys.* **2005**, *122*, 34107.
[56] F. Neese, *eMagRes* **2017**, *6*, 1–22.
[57] B. A. Heß, C. M. Marian, U. Wahlgren, O. Gropen, *Chem. Phys. Lett.* **1996**, *251*, 365–371.
[58] J. P. Perdew, K. Burke, M. Ernzerhof, *Phys. Rev. Lett.* **1996**, *77*, 3865–3868.
[59] J. P. Perdew, K. Burke, M. Ernzerhof, *Phys. Rev. Lett.* **1997**, *78*, 1396–1396.
[60] C. Adamo, V. Barone, *J. Chem. Phys.* **1999**, *110*, 6158–6170.
[61] F. Neese, F. Wennmohs, A. Hansen, U. Becker, *Chem. Phys.* **2009**, *356*, 98–109.
[62] D. Hegarty, M. A. Robb, *Mol. Phys.* **1979**, *38*, 1795–1812.
[63] R. H. A. Eade, M. A. Robb, *Chem. Phys. Lett.* **1981**, *83*, 362–368.
[64] H. B. Schlegel, M. A. Robb, *Chem. Phys. Lett.* **1982**, *93*, 43–46.
[65] F. Bernardi, A. Bottoni, J. J. W. McDouall, M. A. Robb, H. B. Schlegel, *Faraday Symp. Chem. Soc.* **1984**, *19*, 137.
[66] P. E. M. Siegbahn, *Chem. Phys. Lett.* **1984**, *109*, 417–423.
[67] M. A. Robb, U. Niazi, in *Reports in Molecular Theory, Vol. 1* (Eds.: H. Weinstein, G. Náray-Szabó), CRC Press, Boca Raton, **1990**, pp. 23–55.
[68] M. J. Frisch, I. N. Ragazos, M. A. Robb, H. B. Schlegel, *Chem. Phys. Lett.* **1992**, *189*, 524–528.
[69] N. Yamamoto, T. Vreven, M. A. Robb, M. J. Frisch, H. B. Schlegel, *Chem. Phys. Lett.* **1996**, *250*, 373–378.
[70] M. Klene, M. A. Robb, M. J. Frisch, P. Celani, *J. Chem. Phys.* **2000**, *113*, 5653–5665.
[71] F. Weigend, *Phys. Chem. Chem. Phys.* **2006**, *8*, 1057.
[72] T. Soda, Y. Kitagawa, T. Onishi, Y. Takano, Y. Shigeta, H. Nagao, Y. Yoshioka, K. Yamaguchi, *Chem. Phys. Lett.* **2000**, *319*, 223–230.
[73] J.-P. Malrieu, G. Trinquier, *J. Phys. Chem. A* **2012**, *116*, 8226–8237.

Manuscript received: November 29, 2023
Accepted manuscript online: December 20, 2023
Version of record online: January 19, 2024

Der zugehörige Lebenslauf ist aus Datenschutzgründen ausschließlich in der Druckversion dieser Arbeit verfügbar.